A STUDY OF LATERAL DIFFUSION IN THIN FILM COUPLES OF GOLD AND SILVER

William Allen Watkins

Doctor of Philosophy

December 1972

A STUDY OF LATERAL DIFFUSION IN THIN FILM COUPLES OF GOLD AND SILVER

A Thesis

Submitted to the Faculty

of

Purdue University

by

William Allen Watkins

In Partial Fulfillment of the

Requirements for the Degree

of

Doctor of Philosophy

December 1972

Dedicated

To Sandy, David, Sean and Katrice

ACKNOWLEDGMENTS

The author expresses sincerest appreciation to Professor Samuel J. Hruska for this guidance, interest and patience during the course of this research. The author also wishes to thank Professors Mysore A. Dayananda and Gerald L. Liedl for the many thoughtful hours of discussion during this work.

The author wishes to thank the United States Navy, whose permission allowed this author to continue his education, and the Advanced Research Projects Agency of the Department of Defense for their financial support.

The author expresses special thanks to Mr. Robert Staley for his many hours of assistance in the designing of the experimental apparatus, and to Mr. David McCabe for his assistance on the Electron Microscope and Scanning Electron Microprobe.

The author thanks his wife, Sandy, for her encouragement and help during the final composition of this thesis.

TABLE OF CONTENTS

LIST OF TABLES

LIST OF FIGURES

Figure Page

Figure Page

Figure Page

Appendix
Figure

ABSTRACT

Watkins, William Allen. Ph.D., Purdue University, December 1972. A Study of Lateral Diffusion in Thin Film Couples of Gold and Silver. Major Professor: Samuel J. Hruska.

An experimental deposition technique was developed to model a thin film couple after the standard bulk diffusion sandwich couple. The initial region of mixing between the two sides of the thin film couple was less than 2 microns.

An empirical conversion parameter, following the bulk procedures of Ziebold and Ogilvie, was determined for thin films of gold and silver between 500 and 2,000 Å. X-ray intensity data from the electron microprobe were converted, through use of the parameter, to units of mass concentration. Pure and alloy films of gold and silver exhibited linearity between the microprobe x-ray intensity and film thickness up to 2,000 Å. The maximum error in alloy film composition using the conversion parameter was shown to be 10 atomic % at 500 Å.

Thin film couples of pure silver and gold annealed above 500°C, and at 416°C for times greater than 72 hours, exhibited dewetting on the pure gold side. The dewetting of the gold film was shown to be in accord with Mullin's theory of grain boundary grooving. For Ag-Au couples annealed below 500°C

a zone of porosity occurred, increasing with time and temperature of anneal, leading to film separation near the pure silver side of the original region of mixing. The porosity formation was similar to that reported by investigators of bulk sandwich couples of pure Au and pure Ag.

Incremental thin film couples with initial concentration differences of 20 atom% did not exhibit the zone of porosity which again was in agreement with investigators using bulk couples with small concentration differences. The diffused concentration profiles were compared with numerical solutions of the initial profile. The numerical technique was based on an approximate solution to Fick's second law for one dimensional diffusion.

A series of apparent diffusion coefficients was determined for temperatures between 200 and 416°C. A plot of ln D versus 1/T was linear with a coefficient of correlation of 0.99. The data fit the following relationship

$$D = 1.9 \times 10^{-7} \exp(-10{,}900/RT) \text{ cm}^2\text{sec}^{-1}$$

An apparent diffusion coefficient was also determined for a series of pure Ag and Au couples annealed at 416°C and compared favorably with the incremental couples' diffusion coefficient at the same temperature.

Two models were considered in order to attribute the apparent diffusivity to a single transport mechanism. The surface diffusion model was refuted because of the low reported value of activation energy (10.9 kcal/mole), in

comparison with what was theoretically expected and experimentally reported by other investigators. A model attributing the apparent diffusivity to transport along the film's grain boundaries was considered to be likely, if the grain boundaries could be assumed in a high state of disorder.

INTRODUCTION

Diffusion in thin (< 5,000 Å) vacuum deposited metallic films is a phenomenon which has received significant attention only during the last ten years. This is largely due to the increasing use of thin films in electronics either as complete thin film circuits, or more commonly as interconnections and contacts in integrated circuits.

Until the last two years, the majority of thin film diffusion studies had been done with multilayer films. Multilayer films are produced by the successive deposition of material stacked layer by layer, one on top of the other, as shown in Figure 1. In a layered film, deposited in high vacuum (< 10^{-5}torr), each interface region will be nearly perfect. For example, there will be atomic contact between any two superimposed deposits. Diffusion occurs in one direction only, and the limiting boundaries of the system are perpendicular to the direction of the highest concentration gradient. Several investigators have devised experimental methods to detect the subsequent diffusion over the extremely short distances relative to that of bulk diffusion. Two comprehensive and fully referenced review articles have been written by C. Weaver [1, 2] and bring the reader up through 1970 in all work related to diffusion in thin films.

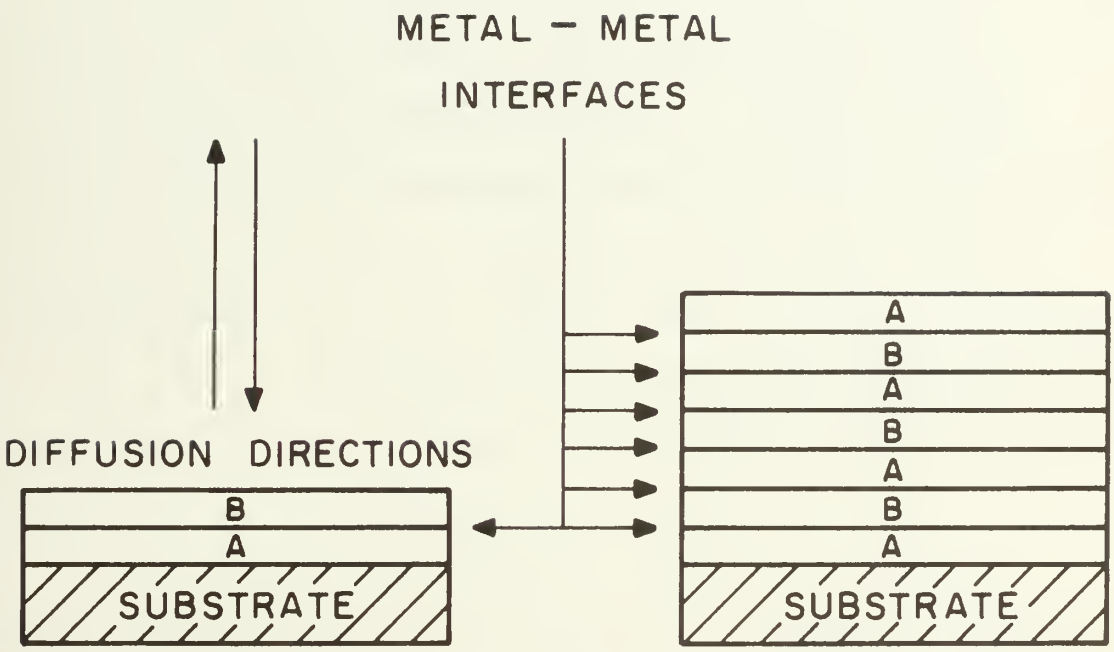

Figure 1

Multilayer Film Geometry Using Alternating

Films of Metal A and Metal B

Interconnections and contacts in integrated circuitry made of dissimilar materials have a possible mode of atomic transport which cannot be modeled using the multilayer film technique. A thin film (< 2,000 Å) couple made of two films side by side on a suitable substrate has an increase in the surface to volume ratio of approximately 10^5 relative to a standard size bulk diffusion couple. Atomic transport across the film surface-vapor interface could significantly contribute to the rate of homogenization, especially at temperatures below $\frac{1}{2}$ the melting point of the pure components of the couple. Film-substrate interactions and surface morphology changes for various annealing times and temperatures can also be studied.

Lateral diffusion, diffusion along the length of a binary thin film couple parallel to the substrate, has not had the same degree of attention as that of diffusion normal to the substrate (multilayer films). Only four investigators [3, 4, 5 and 6] have developed experimental techniques to investigate lateral diffusion. Three authors [3, 4 and 5] used the overlapping film technique. This method consists of alternating film deposition onto a suitable substrate intervened by a mask shift parallel to the substrate. The resultant film-substrate geometry used by all four investigators is shown in Figure 2.

After film deposition, each investigator gave the binary thin film couples an anneal in vacuo. The overlap

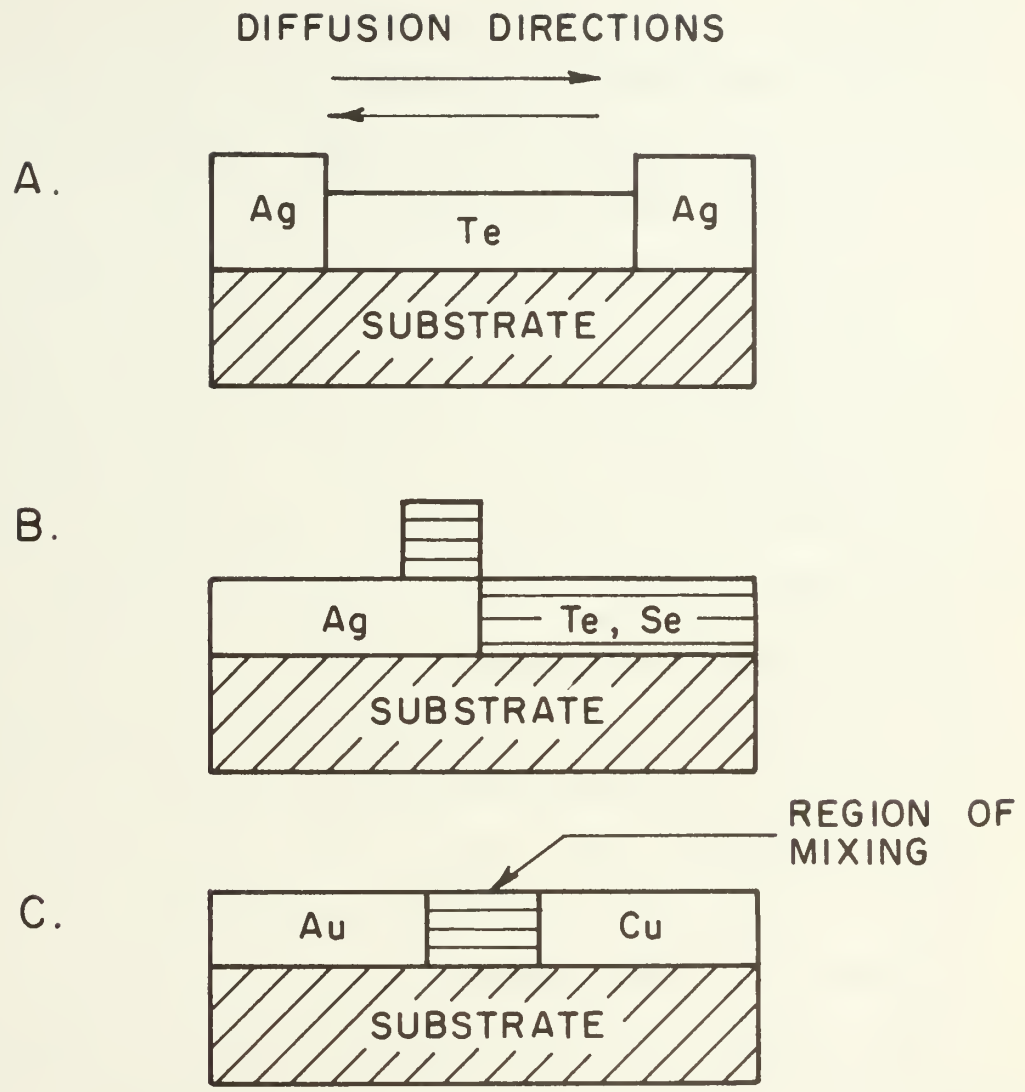

Figure 2

Film Geometry for Previous Lateral Diffusion Studies;

A. Monch [3] B. Pines et al. [4] and Johnson and Brown [5]

C. Smallen [6]

indicated by A. & B. in Figure 2, homogenizes rapidly due to the short diffusion distance perpendicular to the substrate. Two of the four investigators [3, 4] overlapped films of Ag with Te and Se, respectively. Another author [5] studied diffusion in both sets of binary systems. Both Ag-Te and Ag-Se have an intermetallic Ag_2X_3 reported [7] in studies of their equilibrium phase system. All three authors [3, 4, 5] reported rapid formation of the intermetallic compound in the overlap region. Further, each of these investigators studied the subsequent lateral growth of the intermetallic after homogenization of the overlap region. High rates of diffusion with low activation energies, relative to bulk diffusion values, were reported. [3, 4] attributed these results to transport along grain boundaries, and [5] to diffusion along the film surface-vapor interface. In all these three independent studies, the experimental results were strongly dependent on the subsequent film geometry. Variations in either of both of the film's thicknesses caused variations of two orders of magnitude in the reported diffusion rates. In [5], the Ag had to be deposited first on the substrate in order for lateral diffusion to occur at all.

Smallen's work [6] in the gold-copper system provided the major impetus for the present study. Using the method of simultaneous deposition of the gold and copper onto a suitable substrate, he reported rates of diffusion both

parallel and perpendicular to the substrate. Smallen reported rates of diffusion in the lateral direction almost seven orders of magnitude faster than in the perpendicular direction. An associated activation energy was reported and was almost $\frac{1}{2}$ that of the previously reported bulk value.

A study of the Bi-Te system, which also has a reported [8] intermetallic compound in its equilibrium phase system, was undertaken by this author. In order to more closely approximate the sandwich couple, so as to compare more favorably with the initial conditions of the bulk, it was decided to try to improve the experimental methods of [3, 4, 5 and 6].

An experimental method was devised and reported [9] in order to reduce the overlap region of [3, 4, 5 and 6] from the order of 10^{-2} meters, to 10^{-5} meters, and minimize the thickness variation in the lateral direction. The new geometry for a thin film diffusion couple used in the author's work is shown in Figure 3. Note that the overlap region of Figure 2 is now called a region of mixing, which more closely represents the physics of the new experimental deposition process [9].

The formation of an intermetallic compound in the region of mixing was observed in couples made of pure bismuth and tellurium. However, after formation of the intermetallic compound, no lateral diffusion was observed. A summary of the work accomplished on this system, with

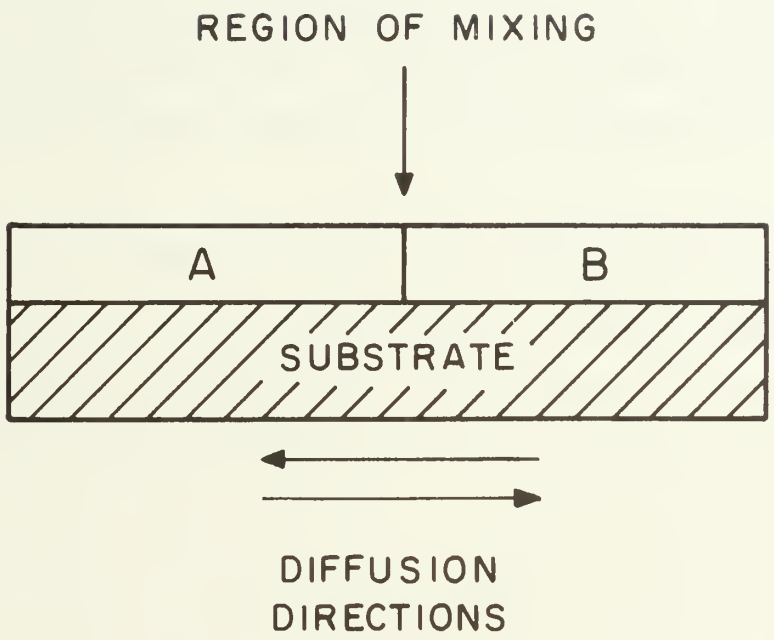

Figure 3

Geometry for Thin Film Couples Used in Present Study

the experimental results, and a discussion of the same, is found in Appendix A.

A second study was undertaken in the Ag-Au system, which is entirely miscible throughout the entire composition range. In this study, the region of mixing was further reduced to the order of 10^{-6} meters as the experimental procedure was further improved. (See Experimental Procedure section.)

The initial phase of the second study involved couples of pure Au and Ag. During the anneals surface morphology changes occurred in the couple. The changes were similar to those previously reported in studies of bulk Ag-Au couples, however they occurred to a greater extent and interrupted the continuity of the couple. Because of the film separation, quantitative rates of diffusion could not be determined as anticipated. However, similarities between the concentration profiles for various annealing times led to an alternate technique; this allowed values of diffusivity to be determined.

Johnson [38], using bulk Ag-Au couples with small initial concentration differences, did not observe these morphology changes. Accordingly, an experimental procedure was devised to make thin couples with an initial concentration difference of 20 atomic %. As with Johnson's results, no morphology changes were observed in the present study.

A numerical technique was devised to treat experimentally determined initial concentration profiles. The numerical solutions were compared with the experimental concentration profiles after various times and temperatures of anneal. Values of chemical diffusivity were determined as a function of annealing temperature. From the comparison of the numerical solutions with the diffused concentration profiles, an equation for the apparent diffusivity for the couple was determined. Possible atomic transport mechanisms were investigated over the working range of the present study.

Lastly, a calibration study, involving the fabrication and use of Ag-Au thin film standards was undertaken.

Empirical working curves over the entire composition range were determined so that electron micro-analysis could be directly applied to deduce mass concentration variations in the diffusion studies.

BACKGROUND AND LITERATURE SURVEY

Two separate investigations into the literature had to be undertaken in order to carry out the experimental work of this author.

The first investigation focused on a method to analyze the annealed thin film couple and from this, deduce mass concentration variations as a function of lateral distance, time, and temperature of anneal.

The second involved an investigation into the previous diffusion studies in the Ag-Au system in order to compare with the experimental results of the present thin film study.

Empirical Method for Thin Film Analysis

The experimental method of [3, 4, 5] involved the optical observation of the growth of the diffusion zone as a function of time and temperature. In all three cases, the diffusion zone was an intermetallic compound with a significant reflectivity difference relative to the pure components. Smallen [6], however, worked in the gold-copper system which is completely miscible throughout the composition range. In order to determine atomic concentration profiles in his couples he used the electron microprobe. By scanning his samples, under the electron beam, he generated x-ray

intensity data as a function of lateral distance. In order to convert the x-ray spectrometric data to atomic concentration, he made the rather crude assumption that the relative x-ray intensity, corrected for background, was proportional to atomic concentration.

Due to the similar work in miscible systems by Smallen [6], and to the present work of this author, the electron microprobe was used to determine mass concentration changes as a function of lateral distance, time, and temperature of anneal. However, an investigation was necessary to determine the relationships between the x-ray spectrometric data generated from a thin film sample, under the electron beam, and the specimen's mass concentration.

The important variables relating the emitting x-ray intensity to the chemical composition of the beam target, were first reported by Castaing [17]. The full correction for the measured relative intensity in the bulk is

$$K_A = \frac{I_{alloy}}{I_{pure\ A}} = \left[\frac{f(x)}{f^0(x)}\right]\left[1 + K_f\right]\left[\frac{Rp}{R^0p^0}\right] C_A \qquad (1)$$

where $[f(x)/f^0(x)]$ is the absorption correction factor

$[1 + K_f]$ is the correction for secondary fluorescence

$\left[\frac{Rp}{R^0p^0}\right]$ is the backscatter-ionization correction

C_A is the weight fraction A in A-B alloy

I_{alloy} is the measured x-ray intensity of the characteristic line for element A (corrected for background) of the A-B alloy

$I_{pure\ A}$ is the measured x-ray intensity of the characteristic line for element A (corrected for background) of a sample of pure A.

Ziebold and Ogilvie [18] made a series of experimental observations between K_A and C_A in 17 different binary systems, including the Ag-Au system. They found that their experimental data in all 17 systems displayed linearity when plotted in the form of C_A/K_A, versus C_A. The analytical straight line function is written

$$C_A/K_A = a_{AB} + (1 - a_{AB})C_A. \qquad (2)$$

The single parameter needed to describe the empirical working curves of [18] is the limiting value of C_A/K_A, when C_A goes to zero. The subscript, AB, indicates that the conversion parameter applies to the measurement of characteristic x-rays of element A in binary A-B alloys.

Rearrangement of equation (2) gives a more symmetrical form:

$$\frac{1-K_A}{K_A} = a_{AB}\ \frac{1-C_A}{C_A}. \qquad (3)$$

Figures 4 and 5 show the experimentally determined bulk relationships of [18] between K and C in the silver-gold system. A hand calculation of the values of the three correction parameters of equation (1), as a function of composition, was made using semi-theoretical formulae, based on the three correction factors of equation (1). An operating voltage of 25 kv of the electron microprobe, with a 52.5° spectrometer takeoff angle, (parameters used in the present experimental work) was assumed in the calculation. In Figure 6, the results of the hand calculation are plotted in terms of the variables of equation (3).

In the case of thin film analysis, if the linear analytical function of equation (2) is assumed to hold for thin films in the Ag-Au system, then the empirical conversion parameters (a_{AgAu}, a_{AuAg}) must be determined separately from the previously reported bulk values.

Hutchins [19] showed that the thin film x-ray intensity, normalized with respect to a bulk sample of the film material, can be expressed as three factors:

$$\frac{I_{(FS)}}{I_{bulk}} = (S)\ (I_F)\ \left(\frac{1}{I_{bulk\ exc.}\ f(x)}\right) \qquad (4)$$

where I_{FS} = the measured intensity for the film on a particular substrate

I_{bulk} = the measured intensity for an infinitely thick film (with respect to the electron beam)

S = substrate correction

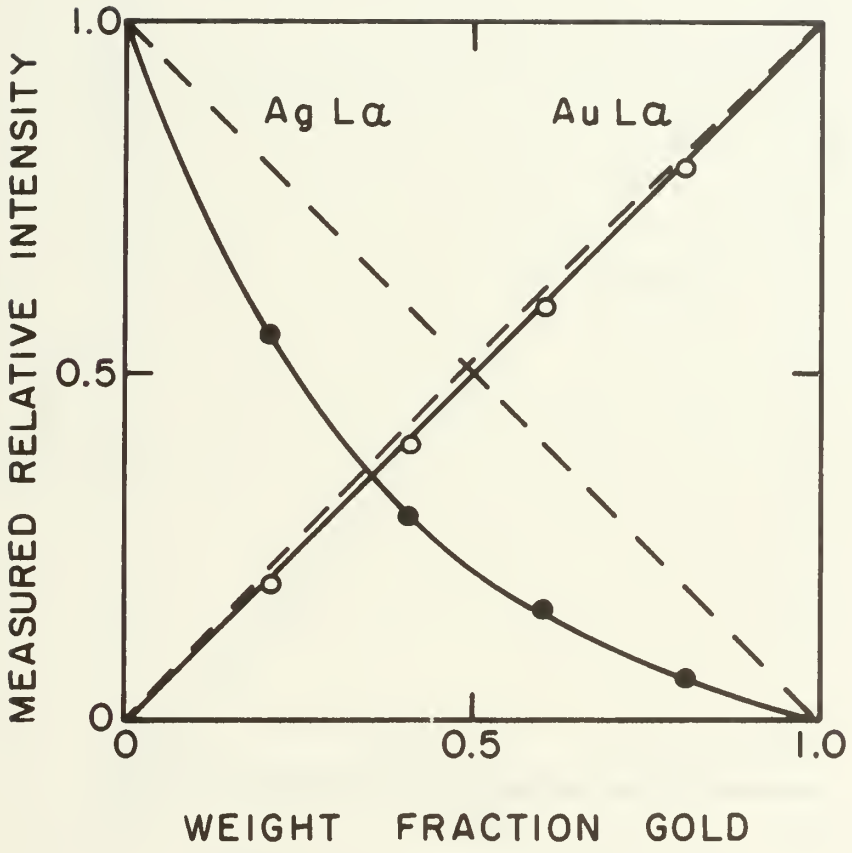

Figure 4

Experimental Microprobe Calibration Data for the Bulk Silver-Gold System at 30 kv and 15.5° Spectrometer Takeoff Angle.

Zeibold and Ogilvie [18]

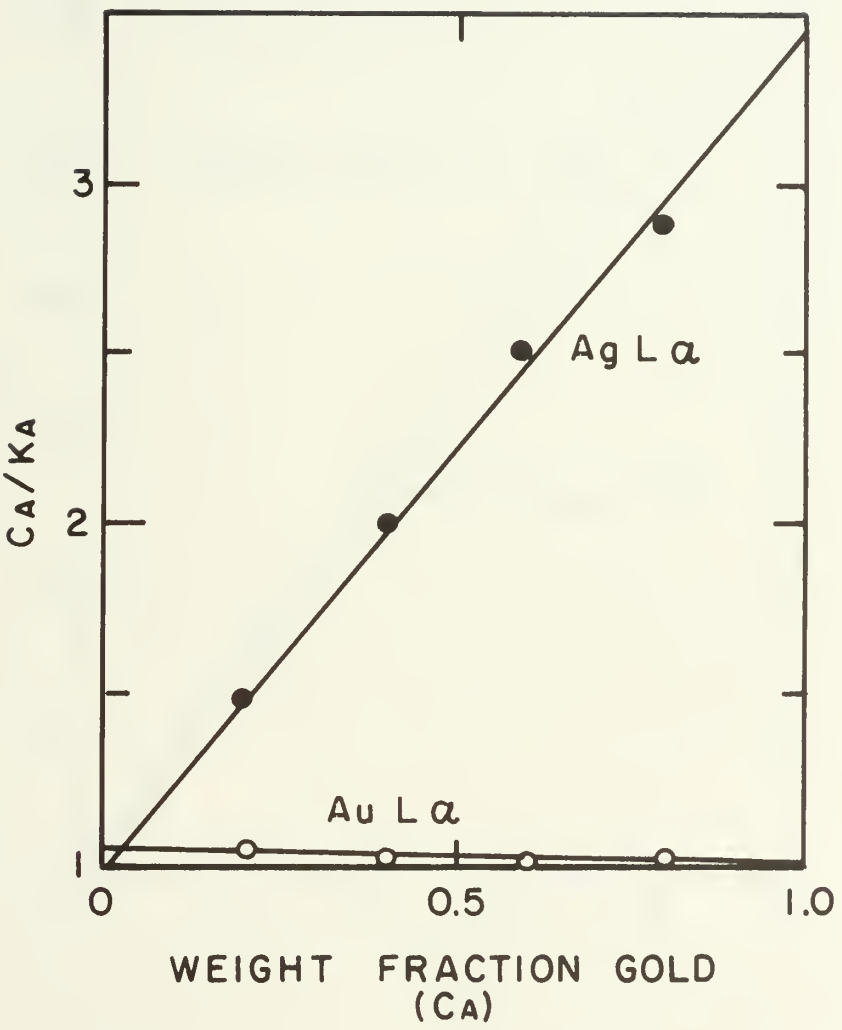

Figure 5

Functions C_A/K_A for Bulk Silver-Gold System.

Microprobe at 30 kv and 15.5° Spectrometer

Takeoff Angle.

Zeibold and Ogilvie [18]

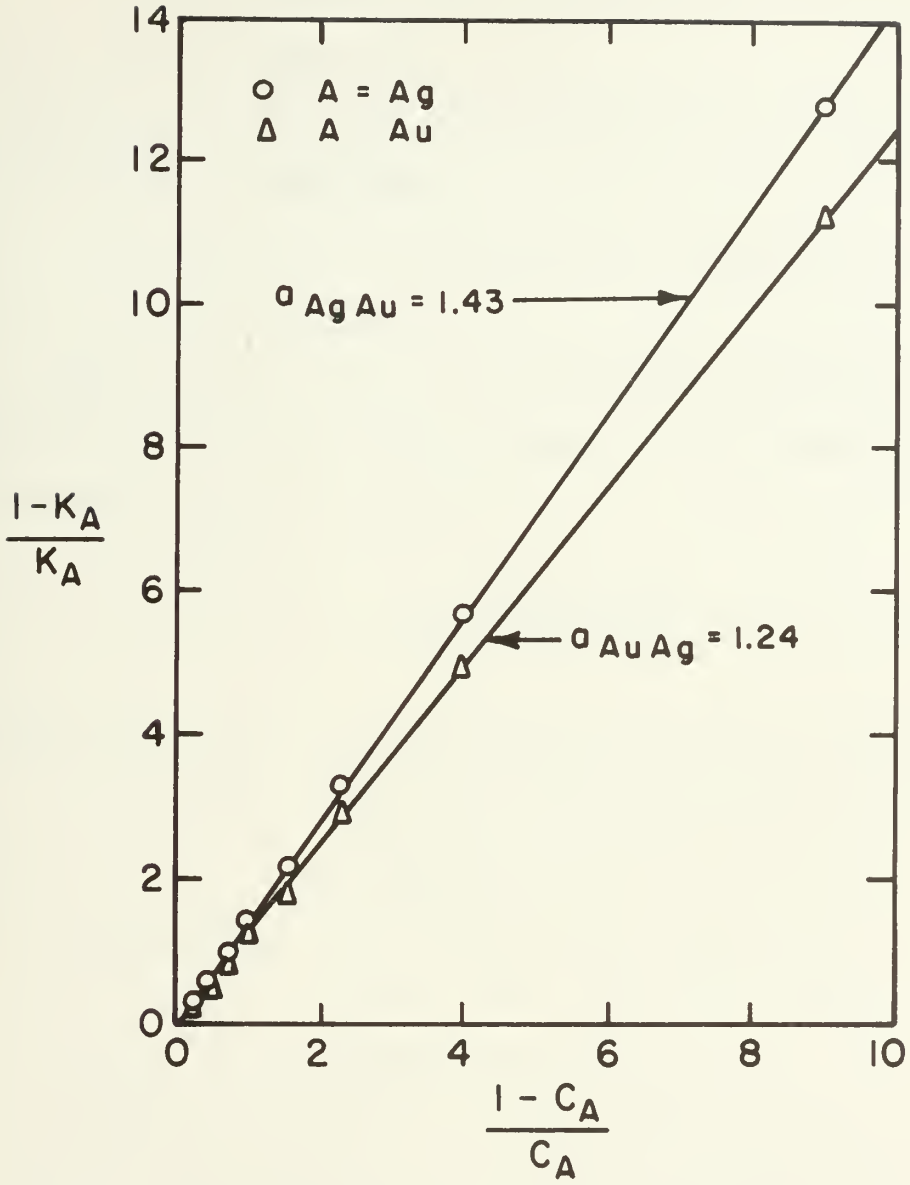

Figure 6

Results of Hand Calculation Using Semi-Theoretical Formulae, Based on Equation (1) Plotted in Form of Equation (3). Microprobe at 25 kv with 52.5° Spectrometer Takeoff Angle.

I_F = the measured intensity for the film without a substrate

$I_{\text{bulk exc.}}$ = the excited intensity for an infinitely thick film

$f(x)$ = the x-ray absorption correction for film thickness, t.

For a particular set of operating conditions of the electron probe and film thickness, t, the measured relative intensity can be written as

$$K_A = \frac{I_{\text{alloy(FS)}}}{I_{\text{pure A(FS)}}} , \tag{5}$$

where $I_{\text{alloy(FS)}}$ = the measured intensity for an A-B alloy film on a particular substrate at a film thickness t

$I_{\text{pure A(FS)}}$ = the measured intensity for a film of pure A on a particular substrate at a film thickness t.

Solving equation (4) for I_{FS}, and substituting into the numerator and denominator of equation (5) with appropriate subscripts

$$K_A(\text{film thickness t}) = \left[\frac{I_{\text{alloy(F)}}}{I_{\text{pure A(F)}}}\right] \cdot \left[\frac{I_{\text{pure A bulk exc.}}\ f(x)_P}{I_{\text{alloy bulk exc.}}\ f(x)_A}\right]\left[\frac{I_{\text{bulk alloy}}}{I_{\text{bulk pure A}}}\right] \tag{6}$$

Ziebold and Ogilvie [18] were unable to justify their experimental observations leading to equation (2) on the theoretical grounds of the bulk relationship of equation (1). This author will likewise make no claim to the prediction of a linear relationship in the present thin film data plotted in the form of equation (2), based on equation (6). A straight line relationship, within the limits of the reproducibility of the experimental data, between the variables of equations (2) or (3) will justify the use of the empirical conversion parameter to deduce weight fraction composition from the measured relative intensity of the electron microprobe.

To convert from weight fraction composition (C_A) to mass concentration involves knowledge of the density variation of gold-silver alloys across the entire composition range.

In Figure 7, the Vegard's law deviation is shown for the silver-gold system. Using the lattice parameter data of Sachs and Werts [20], and the relationship derived in Barrett and Massalski [22] for the density in a substitutional alloy system,

$$\rho(AgAu) = n\bar{A}/VN \qquad (7)$$

where N = Avagadro's number

V = volume of the unit cell

N = number of atoms/unit cell

$\bar{A}$ = mean atomic weight,

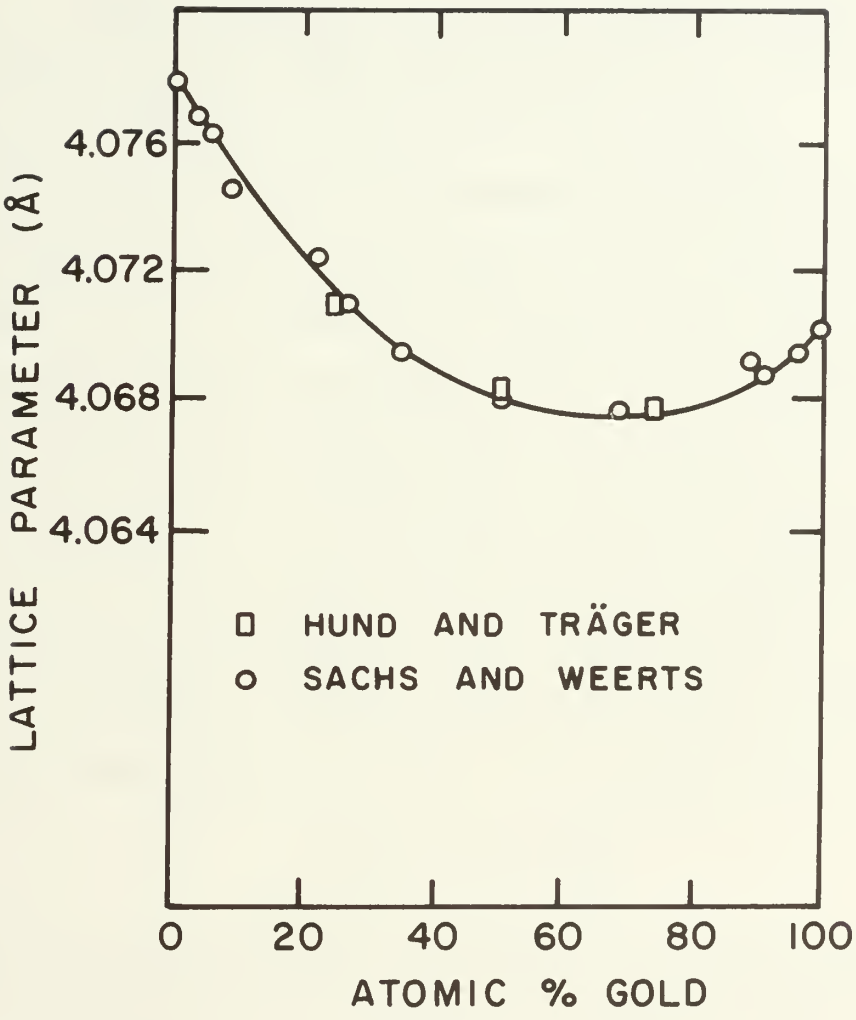

Figure 7

Variation in Lattice Parameter of Bulk Alloys in the Silver-Gold System Using Experimental Data of Hund and Trager [21] and Sachs and Weerts [20].

the density of gold-silver alloys as a function of atomic concentration was determined and is shown in Figure 8.

Bulk Diffusion in the Gold-Silver System

At the present time there has been no reported study of thin film diffusion in the gold-silver system.

The initial studies of chemical bulk diffusion in the silver-gold system was undertaken by [23, 24 and 25]. In all three works, the method of chemical etch limit was used to determine average diffusion coefficients over the entire composition range. Johnson [38], who doubted the validity of the chemical etch limit method, studied chemical diffusion in the silver-gold system using sandwich couples with initial concentration differences of less than 20 atomic %. Concentration-penetration profiles were determined by the now accepted method of sectioning. Using Fick's Second Law,

$$\frac{\partial C}{\partial t} = \frac{\partial}{\partial x}\left(D \frac{\partial C}{\partial x}\right). \tag{8}$$

Johnson assumed that, due to the use of couples with small initial-concentration gradients, D was not a function of composition over the working range of his couples. Therefore he wrote

$$\frac{\partial C}{\partial t} = D \frac{\partial^2 C}{\partial x^2} \tag{9}$$

and solved equation (8) using the standard initial and boundary conditions,

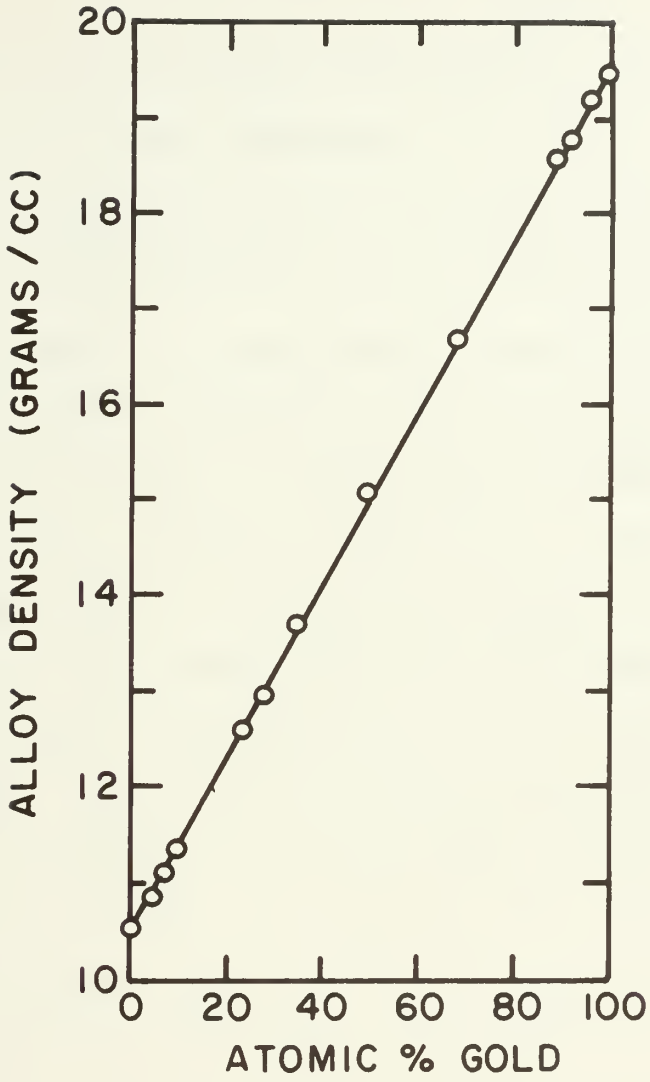

Figure 8

Variation of Alloy Density for Bulk Alloys in Gold-Silver System Using Relationship Derived in Barret and Massalski [22]

$$\frac{C - C_0}{C_1 - C_0} = \frac{1}{2}\left[1 - \operatorname{erf}\left(\frac{x}{2\sqrt{D_t}}\right)\right] \qquad (10)$$

where C = concentration, after time t, at a distance x from the interface

C_1 = concentration at $t = 0$, for $x < 0$

C_0 = concentration at $t = 0$, for $x > 0$

Johnson compared his experimental profiles with those of equation (10) to determine D, and also plotted his results on probability paper to justify his assumption of $D \neq f(C)$. Figure 9 shows Johnson's results for an alloy containing 49.2 atomic % gold, along with the results of [23, 24 and 25]. Jost's [25] data, taken at lower temperatures, were extrapolated by Johnson [38] up to his experimental temperature range. The data of an investigator named Braune are reported in Johnson's work and shown in Figure 9, however, he does not reference him in his paper. The straight line through Johnson's data can be represented by the following equation,

$$D_C = 0.14 \exp\left(\frac{-41,700}{RT}\right) \text{ cm}^2\text{sec}^{-1}. \qquad (11)$$

Included in his work were determinations of the gold and silver self diffusion coefficients using radioactive tracers. Over the same temperature range they are represented by the following equations,

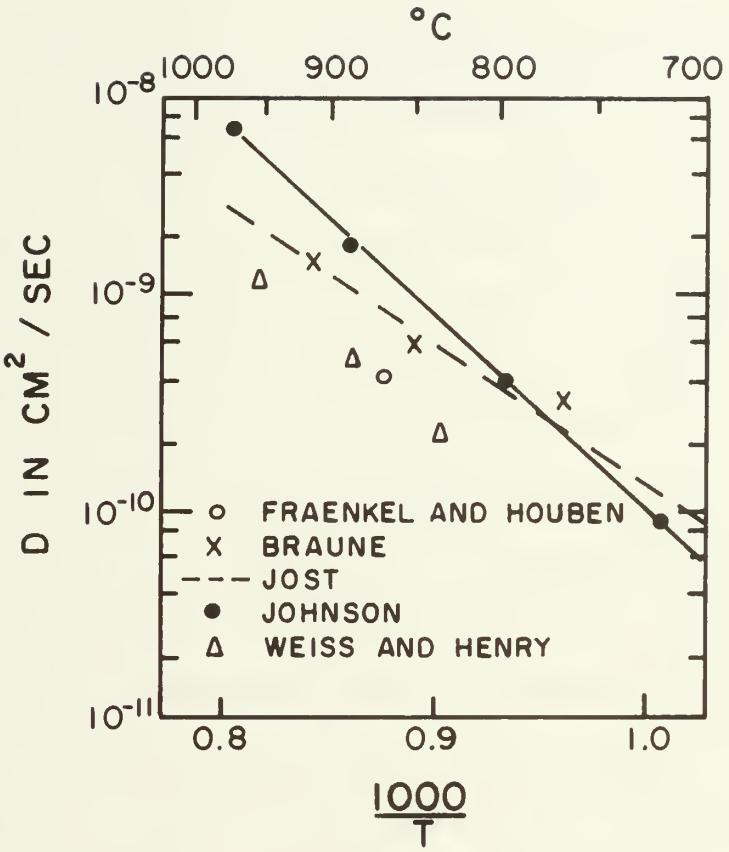

Figure 9

Chemical Diffusivity as a Function of Temperature for Bulk Sandwich Couples in the Silver-Gold System. Johnson [38]

$$D_{Ag} = 0.39 \exp\left(\frac{-44,700}{RT}\right) \text{ cm}^2\text{sec}^{-1} \quad (12)$$

$$D_{Au} = 0.12 \exp\left(\frac{-44,100}{RT}\right) \text{ cm}^2\text{sec}^{-1} \quad (13)$$

A very extensive study of self diffusion in silver-gold solid solutions was done by Mallard et al. [26], also using radioactive tracer sectioning techniques. They reported that the silver tracer moved between 2 and 3 times faster than the gold tracer, across the entire composition range. They also report a variation of less than $\frac{1}{2}$ of an order of magnitude in the diffusivities of both the gold and silver tracers across the entire composition range.

Baluffi and Seigle [27] studied diffusion in bi-metal vapor-solid couples of zinc-alpha brass, copper-nickel and gold-silver. In their investigations of vapor-solid couples of gold-silver they observed the formation of 13% volume porosity, by lineal analysis, in the diffusion zone after 93 hours at 940°C. In order to elucidate the cause of the porosity formation, they made an additional study of pure gold-pure silver sandwich couples. The porosity again appeared in the sandwich couple and its formation was evident at times as early as 1 hour, increasing with time up to 50 volume %. Similar observations on gold-silver sandwich couples were made by Seitz and Kotterman [28]. Both investigators [27, 28] observed the porosity formation on the pure silver side of the couple. Baluffi and Seigle [27] made corrections to account for the observed volume

porosity to determine diffusivities by the Matano method. Seitz and Kotterman did not make corrections and therefore, their data are suspect. Baluffi and Seigle took Laue back reflection x-ray photograms of the diffusion zone. They observed multiple spots and attributed this to polygonization of the diffusion zone.

In his earlier work, Baluffi [29] determined that silver atoms diffuse into gold more rapidly than gold diffuses out, causing a volume increase, with expansion in all three directions. Using the theoretical calculations of Huntington and Seitz [31], he speculated that diffusion by vacancy mechanism coupled with the unequal diffusion rates, could account for the observed volume increase.

Barnes [30] used multiple sandwich couples of thin interleaved sheets of copper and nickel to accentuate any observed volume increase due to diffusion. He reported that there was an increase of volume in the diffusion zone as a result of atomic diffusion in the copper-nickel and copper-zinc systems that he studied, each system having unequal rates of the two diffusing species. He also showed that this volume increase is associated with the formation in the diffusion zone of voids with faceting. These voids appear near the original interface and on that side from which there is a net loss of atoms (net gain of vacancies). He also conducted an experiment which showed the presence of strain in the diffusion zone and another experiment to

attribute this strain to diffusion. He conducted an x-ray investigation like that of Baluffi and Seigle [27], and again concluded the presence of polygonization in the diffusion zone. Barnes [30] speculated that the difference in atomic fluxes of the two diffusing species was compensated by a vacancy flux in the direction of the smaller flux. The generation and annihilation of vacancies on opposite sides of the couple cause strain in the couple. He suggested that the voids forming as a result of diffusion, imply that some of the large number of vacancies involved in the diffusion zone condense out of the lattice. He postulated generation and annihilation sites such as grain boundaries, polygon boundaries and on the edge component of dislocations.

He, however, did not discuss the magnitude of the deviation of the equilibrium number of vacancies present in the diffusion zone during the anneal. He explained that the growth of the void could be explained by diffusion and absorption of some of the excess numbers of vacancies on void surfaces.

Seitz [34] postulated that the process of porosity formation is precipitation of supersaturated vacancies caused by the unequal diffusion current and occurs by heterogeneous nucleation. He calculated a value of 10^{11} for the lifetime number of vacancy jumps in the diffusion zone by using the porosity observations of Barnes and an arbitrary

value of 1 for the critical relative excess vacancy concentration to form holes.

Baluffi [32] supported Seitz's postulate of heterogeneous nucleation to form voids from a supersaturated solution. Baluffi, however, pointed out that the high value of supersaturation expected by Seitz could not be compatible with the experimental results of parabolic Kirkendall marker shifts with time. He considered the problem with an improved mathematical treatment, and his results indicated that the relative excess vacancy concentration for void formation to be < 0.01 (1%).

Barnes and Mazey [33] using sandwich couples of Cu and Ni under a hydrostatic pressure reaffirmed Baluffi's [32] conclusion of 1% relative excess vacancy concentration necessary to form holes, and also showed experimental evidence that void formation was by heterogeneous nucleation, probably foreign particles or inclusions at the weld interface. A more recent and complete mathematical treatment of the vacancy flux contribution during diffusion and Kirkendall shift in binary alloys, is given by Manning [37].

During an experimental investigation of the Kirkendall shift in the gold-silver system, Ruth [35] observed the formation of a zone of small protrusions of the pure gold side of the couple. He reported that the growth law of the width of this zone is a secondary effect of diffusion. The protrusions were observed to form in the vicinity of

intersections with crystal surfaces of <112> lines in {110} planes. He explained the observations by proposing that a $\frac{1}{2}$ [110] edge dislocation, which has a [112] direction, acting as a diffusion pipe. The excess silver atoms, caused by the unequal diffusion rates, should migrate along the dislocation line to the surface.

There are no reported studies of grain boundary diffusion in bulk silver-gold alloys. Hoffman and Turnbull [36], however, studied lattice and grain boundary self diffusion in silver. Over the temperature range of their study (250-500°C) they reported the grain boundary diffusion coefficient times the grain boundary thickness fit the equation,

$$D'_{GB} = D_{GB}\gamma = 1.5 \times 10^{-9} \exp\left(\frac{-20,200}{RT}\right) \text{ cm}^2\text{sec}^{-1} \qquad (14)$$

where $\gamma = 5 \times 10^{-8}$cm

Grain sizes for their specimens varied from 21-60 microns.

DESIGN AND CONSTRUCTION OF EQUIPMENT

The successful deposition of thin films in vacuum requires a working understanding of vacuum technology. The experimental apparatus must be maintained in an environment suitable for the selective transport of mass over a distance, using materials which maintain this environment during all the operating conditions of the experiment. In order to give the reader insight into the many criteria which had to be satisfied in order to successfully create the three thin film geometries, and carry out the required experimental conditions for the study of atomic diffusion, detailed explanation is given in the following sections.

The discussion of this author's experimental equipment is broken into three sections: the vacuum system, the experimental apparatus in vacuo, and the associated external equipment.

Vacuum System

The environment for the generation of both binary thin film couples and thin film standards was a vacuum chamber capable of maintaining residual gas pressures of 10^{-7}torr. Primary pumping was obtained using a 4 inch oil diffusion pump in conjunction with a mechanical roughing pump.

Auxiliary pumping, located in a stainless steel base separated from the diffusion pump by a high vacuum valve, included a Varian tri-filament titanium sublimation pump and a liquid nitrogen cooled cyrogenic baffle. Residual gas pressure was measured using a Granville-Phillips dual tungsten filament ionization gauge tube with an associated Series 260 controller.

A 12" Varian, all stainless steel, spool piece was placed on top of the base, using viton gaskets to maintain vacuum integrity. Integral to the spool piece are ten $2\frac{3}{4}$" Conflat® ports for insertion of necessary feedthroughs to maintain electrical and mechanical connectivity between the evacuated apparatus and the external test and monitoring equipment. An 18" high pyrex glass bell jar, also sealed with a viton gasket, was placed on top of the spool piece completing the vacuum system described above. A sketch of the vacuum system with its important components labeled is shown in Figure 10. Photographs of the exterior and interior of the vacuum system are displayed in Figures 11 and 12 respectively.

Experimental Apparatus in vacuo

The substrate holder, two sources, and associated monitoring and shielding mechanisms were constructed entirely within the 12" diameter spool piece. OFHC copper, type 303 and 304 stainless steel, aluminum, and 96% polycrystalline dense alumina, were used exclusively in the construction of the

Figure 10

Schematic of the Vacuum System Used in the Present Study

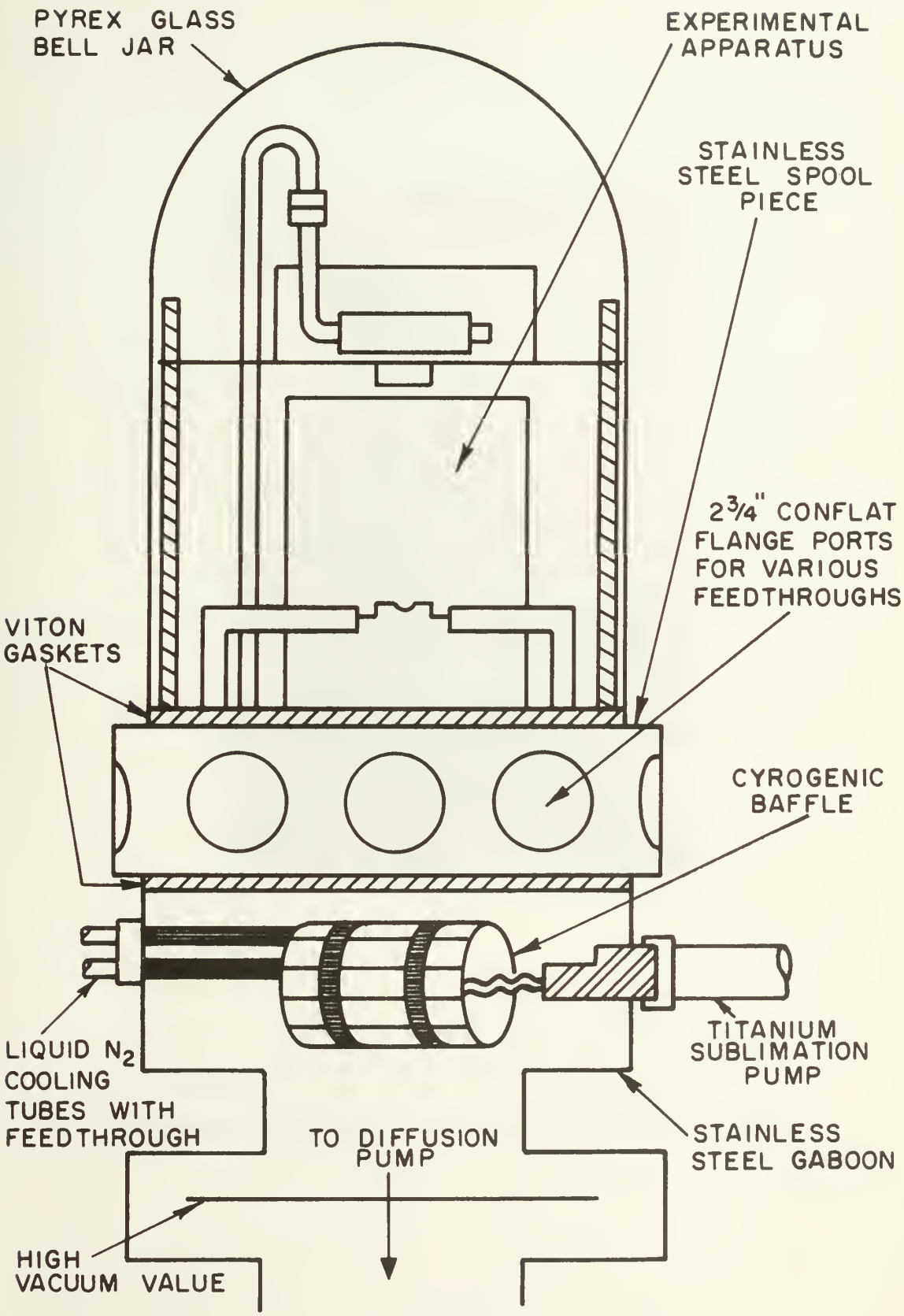
PYREX GLASS BELL JAR
EXPERIMENTAL APPARATUS
STAINLESS STEEL SPOOL PIECE
2¾" CONFLAT FLANGE PORTS FOR VARIOUS FEEDTHROUGHS
VITON GASKETS
CYROGENIC BAFFLE
LIQUID N_2 COOLING TUBES WITH FEEDTHROUGH
TITANIUM SUBLIMATION PUMP
TO DIFFUSION PUMP
STAINLESS STEEL GABOON
HIGH VACUUM VALUE

Figure 10

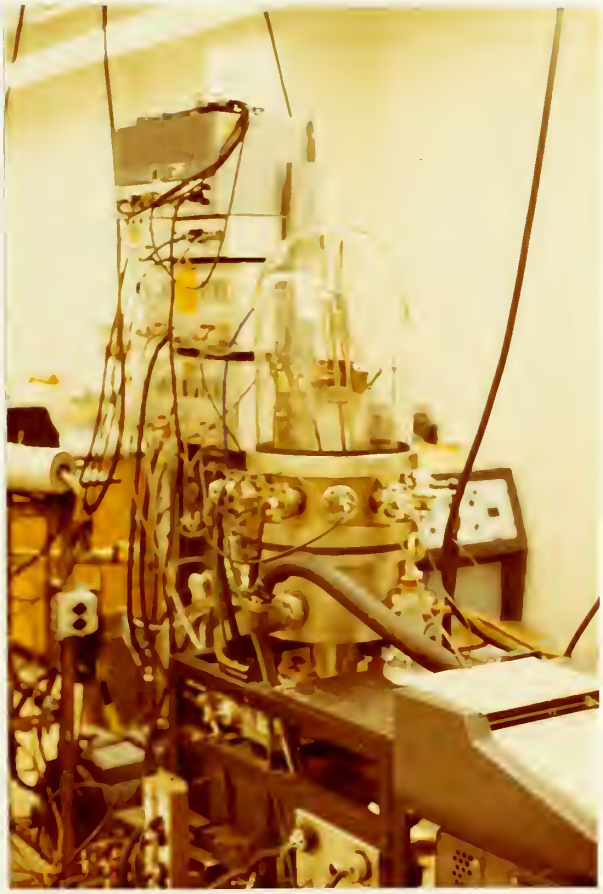

Figure 11

Photograph of the Vacuum System and Associated External Equipment Used in the Present Study

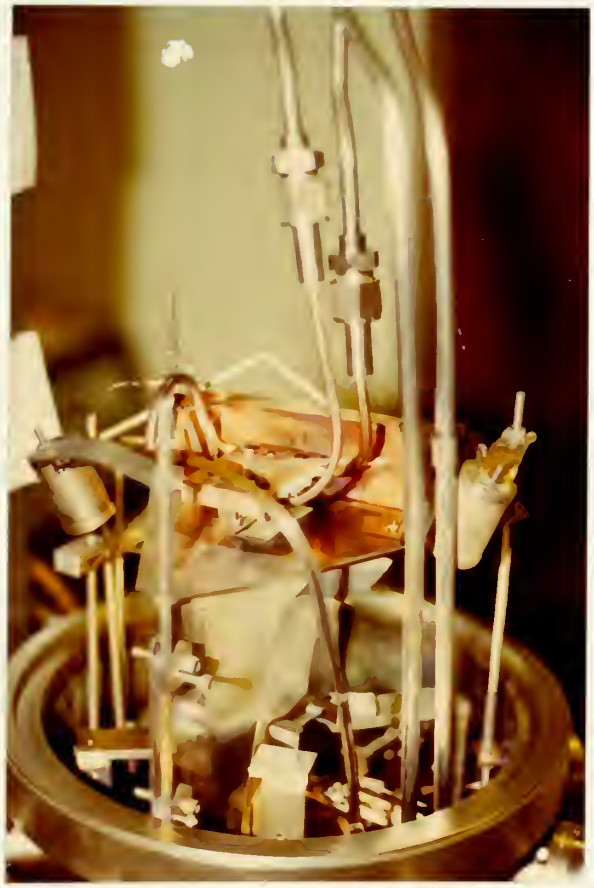

Figure 12

Photograph of the Experimental Apparatus in vacuo

experimental apparatus. These materials have reported [10] low ($< 10^{-9}$torr) vapor pressures at the operating temperatures of the vacuum system (-192°C to 600°C). In addition, wherever possible, leak paths were provided for all fastened assemblies to minimize the outgassing of virtual leaks.

The substrate holder, a sketch of which is shown in Figure 13, was made from a 3" × 2" × $\frac{1}{2}$" block of OFHC copper. Both large faces of the copper block were milled to within .001". Two similarly milled copper restraining plates were used to hold the substrate uniformly against the copper block. All materials, except the heater and insulating tubes, which will be described later, were constructed out of OFHC copper. The use of copper exclusively on the substrate holder eliminated differential stress buildup during heating of the block, maintaining the critical alignment between the various support mechanisms both on and off the substrate holder.

A copper quench tube, making two passes through the substrate holder, was connected to two stainless steel Swagelock fittings. The fittings completed the quench line, through attachment to two stainless steel quench gas delivery tubes connected externally to the gas source by a stainless steel dual tube feedthrough. In addition, the fittings allowed removal of the substrate holder, by sealing together through the use of replaceable copper gaskets. The razor blade support mechanism was made of two sets of two small

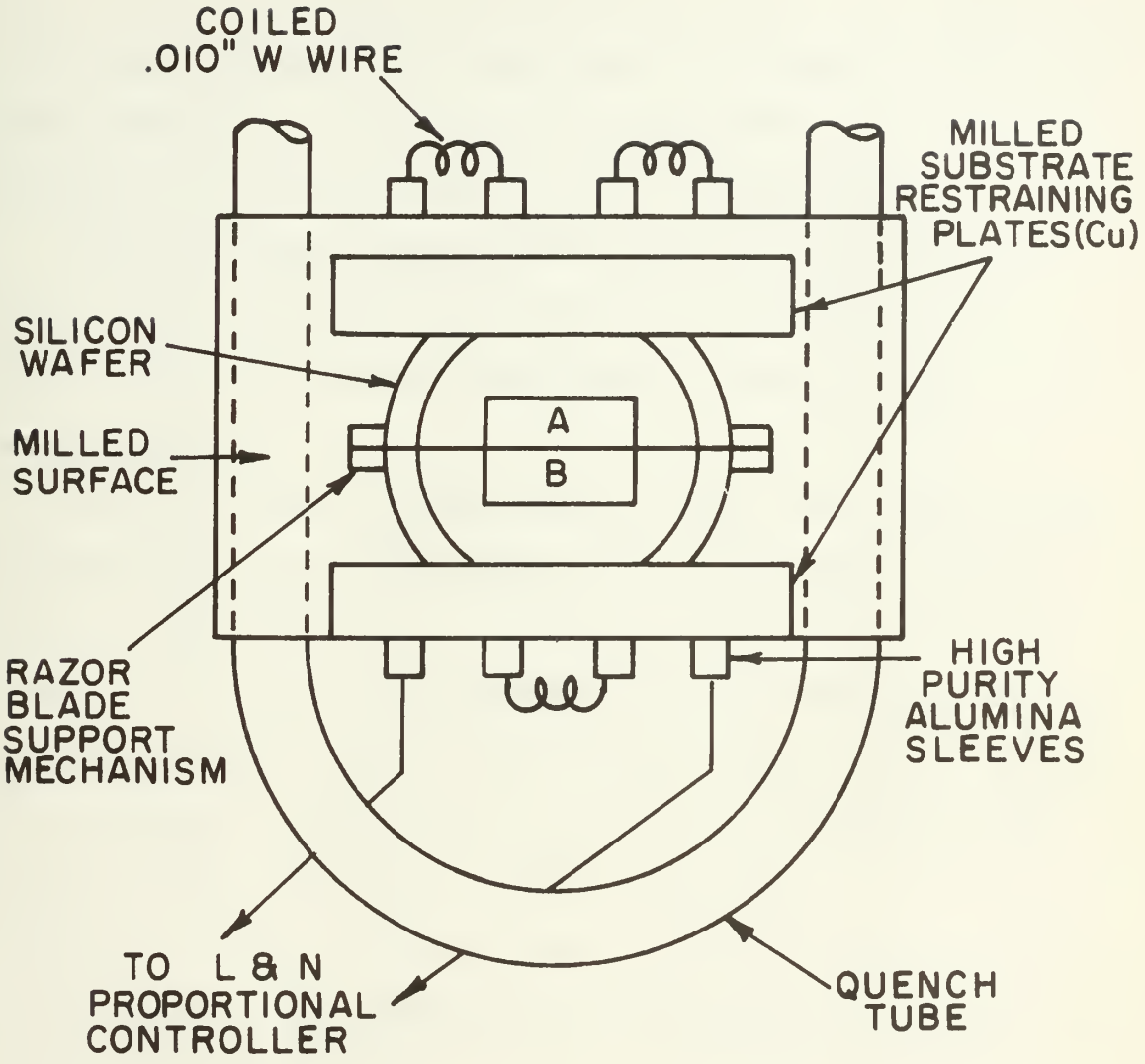

Figure 13

Schematic of Bottom View of the Substrate Holder with Substrate and Razor Blade Mounted in Place

copper blocks, squared true to the substrate holder's milled face. In each set where the faces held the razor blade, a .002" reset was milled on each face to accommodate the razor blade thickness. Copper screws held together the two sets of blocks in each set, and as a unit to the substrate holder.

Chromel-alumel thermocouples used to record the substrate temperature were press fit by screw heads onto the surface of the substrate away from the line of sight of the two sources.

Four (4) tubes, symmetrically placed above and through the substrate and copper block respectively, were filled with sleeves of 99.7 wt. % alumina of 96% polycrystalline density. The sleeves provided electrical insulation between the copper block and the .010" coiled tungsten wire, which was interwoven between the four sleeves, providing a heat source to the substrate. Alumina of lesser density was found to absorb water vapor readily at atmospheric pressure and subsequently outgas heavily during heatup in vacuum.

The deposition of gold and silver was carried out in two independently controlled resistance heated boats purchased from the R. D. Mathis Company. A .010" molybdenum boat with a .010" coating of alumina was used for the gold deposition, and a .010" tantalum boat was used for the silver. The tungsten boat more commonly used for gold deposition in flash evaporation systems was found to be partially wet by

the gold, giving erratic rates of deposition, and possible stratification of the deposited film.

Figure 14 is a sketch of the approximate orientation relationships between the sources, substrate holder, shutter mechanism, and crystal mass deposition monitors.

The shutter mechanism moves, according to the plane of the sketch in and out of the paper, on two aluminum tracks fastened to the spool piece. The shutter was designed with the winged contour to provide, simultaneously, controlled interruption of the gold and silver vapor to the substrate, continuous monitoring of each vapor flux by the respective crystal monitors, and vibrationless transit with respect to the substrate-razor blade-flux barrier alignment.

As indicated in Figure 14, the flux barrier between the two sources is completed by a stainless steel sheet. In order to compensate for expansion of the substrate holder during heating, and adjustment of the edge of the sheet true to the edge of the razor blade, the flux barrier is adjustable vertically and horizontally, respectively.

The radiant transfer of heat to the vacuum chamber walls and surrounding apparatus during heating of the substrate holder assembly was minimized by the construction of a two piece (for disassembly) copper box surrounding the substrate holder on three sides (open side facing sources). The addition of the copper shroud served a dual purpose. It maintained the internal surfaces of the vacuum surfaces

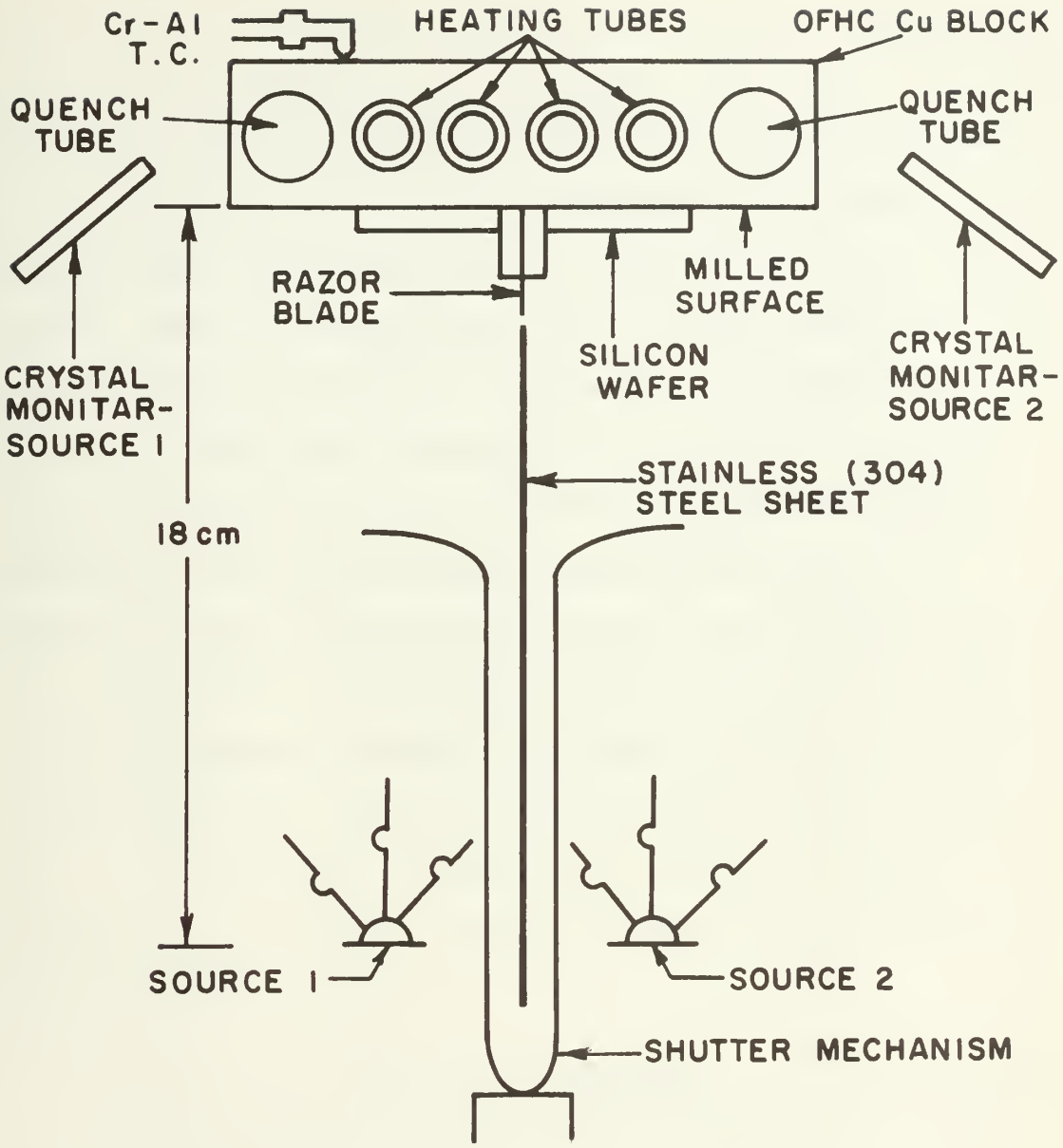

Figure 14

Sketch of the Approximate Orientation Relationships between the Sources, Substrate Holder, Shutter Mechanism and Crystal Mass Deposition Monitors

below 100°C, preventing outgassing of the same reducing the low pressure capability of the system. Secondly, it assisted in maintaining an isothermal condition for the substrate.

Two Sloan water cooled ultra-high vacuum remote crystal holders were rigidly mounted in line of sight, one to each source. Five (5) MC gold and silver coated quartz, AT cut round crystals were used in the holder for monitoring the gold and silver source respectively. Each crystal gives thickness monitoring up to 60,000 Å of aluminum or mass equivalent. The round crystals used were found to be superior to the square crystals used in early experimentation. The uniform stress pattern generated in the round crystal during mass deposition eliminated false (unrelated to mass deposited) frequency shifts common to the square type. A radiant heat shield placed around the crystal minimized false frequency shifts of the crystals due to induced thermal stress.

External Equipment

Automatic deposition control was achieved using two Sloan Omni II Deposition Control Monitors. While each source was controlled to give the preset deposition rate, the rate and thickness output was continuously monitored by 4 Rustrak chart recorders.

Substrate temperature was monitored by a Leeds and Northrup millivolt potentiometer, Sargent Model SRG chart

recorder and a Leeds and Northrup M Line Model C-1, C.A.T. controller.

In conjunction with the C.A.T. controller, a Leeds and Northrup M Line Model C-2 low level set point unit, silicon controlled rectifier, and tungsten heating element in the substrate holder assembly was used to control the substrate temperature during the anneals to within ± 1°C.

A variac auto transformer fed by 115 VAC from a constant voltage transformer was used for initial heatup and outgassing of the substrate and was switched in or out of the heating circuit with a DPDT high current switch.

The bottled helium quench gas was of commercial purity, regulated, and provided to the appropriate feedthrough, maintaining the substrate holder assembly, by tygon tubing.

SUBSTRATE

When studying the physical phenomena in thin films, the substrate or restraining medium on which the films are created is of signal importance. The substrate in many cases may determine whether or not a particular physical phenomena in the film or films occurs. It was with this in mind that this author has written this section, and divided it into two parts, the selection of the substrate, and the subsequent substrate preparation prior to actual film deposition.

Substrate Selection

Single crystal silicon wafers grown in the [111] from the melt were purchased from the General Diode Corporation. The wafers were 1.5" in diameter and 10-15 mills in thickness. As received, one side was mechanically polished, the other etched.

The selection of the silicon wafer as a substrate for all experimental work in the silver-gold system was based on the following criteria: Firstly, the substrate must have a surface flatness and roughness so to consistently reproduce the desired film geometry with respect to the region of mixing and uniform thickness. Deviations from

flatness in the substrate leads to variations in the distance between the razor blade edge and substrate. This coupled with the intrinsic variations in the razor blade edge height can lead to umbra effects resulting in formation of a gap in lieu of a region of mixing between the two films. The surface roughness of a substrate leads to surface protrusions of high frequency. The subsequent decay by surface self diffusion is considered an undesirable variable for the present experimental method. Doctors Anderson and Neudeck [11] compared nine common substrate materials and found the mechanically polished silicon wafer to exhibit a flatness on the order of 0.1 part/thousand, and a surface roughness on the order of, or below, the resolution limit (≈ 50 Å) of the measuring instrument [12].

Secondly, the thickness of the substrate was to be minimized as much as possible to reduce the temperature gradient maintained between the substrate holder where the temperature was measured and the surface of the substrate supporting the films. A 1.6 mm thick soft glass substrate clamped to the smooth face of a copper block held at 90°C, exhibited a 20°C temperature difference across the substrate thickness [13]. The silicon wafer, with 1,500 Å of SiO_2 grown on the surface, is almost an order of magnitude thinner than soft microscope glass. A temperature difference of 1°C, or less, across the wafer's thickness was experimentally observed by this author when the substrate holder

was held at 416°C, and uniform clamping pressure by the Cu restraining plates was applied.

Thirdly, a substrate with a low average atomic number was desirous for quantitative thin film measurement by electron probe microanalysis. High energy electrons backscattered from the substrate and the continuous spectrum of the substrate, will enhance the characteristic (Au and Ag), x-ray intensity produced by the primary electron beam. Both the backscattered electron fraction and continuous spectrum intensity increase with atomic number [15]. The enhancement of the background intensity limits the theoretical limit of detection of trace elements. Campbell [14], using fluorescent x-ray spectrographic analysis defined the minimum detectable limit as "that concentration or amount required to give a line intensity above background for counting times of 10 minutes." For smaller counting times, since the standard deviation is a square root function, the loss in sensitivity goes as a square of the factor decrease in counting time. Birks [16], comparing the methods of Campbell with the electron probe, showed that due to the smaller counting rates of the probe the limits of detectability are 2 orders of magnitude higher (1 ppm vs. 100 ppm).

An additional consideration for electron microanalysis of thin films is the presence of materials in the substrate which cause fluorescence excitation by line radiation. Tin and thorium generate a high fluorescent yield for Ag and Au

respectively, however these materials are not found as major constituents in most common substrate materials.

Fourthly, the linear coefficient of expansion of the substrate must be as close as possible to those of Ag and Au to prevent shivering or crazing to develop in the film, during the quench to room temperature at the conclusion of the anneal. Silicon, while not an ideal match, with a linear coefficient of expansion of 7.3 microinch/inch°C, vice 14.2 and 19.7 for the gold and silver respectively, gave no experimental observations of shivering or crazing for quenches up to 500°C.

The above criteria are all satisfied by the selection of a silicon crystal wafer as a substrate. Individual criteria may be met to a greater degree by a different type of substrate, however none was found that satisfied all four criteria to the degree as that of the silicon wafer.

Two criteria were not met by the silicon wafer; however, they were satisfied by the growth of a thin film of SiO_x* by means of oxidation of the wafer.

The growth of the amorphous layer of SiO_x allowed the deposition of polycrystalline thin films. Secondly, it acts as a diffusion barrier, allowing negligible diffusion perpendicular to the substrate for the times and temperatures of this work.

---

* The oxidized layer contains molecules of SiO, SiO_2, and loosely bonded oxygen radicals.

Substrate Preparation

All substrates were cleaned by immersion in hot sulfuric and nitric acid for 15 and 10 minutes respectively. A rinse in deionized water was followed by several rinses in reagent grade acetone and trichloroethylene. The substrates were then placed into a constant temperature zone of a tubular furnace fed with dry oxygen at 1,000°C, where 1,500 Å of SiO_x were grown onto the silicon wafer. From the sensitive color change due to selective light absorption of the oxidized layer, its thickness was visually determined to be uniform over the wafer to well within 100 Å.

The wafers were then masked and placed into a MRC sputtering chamber, where a 5,000 Å thick annulus of tantalum with an inner and outer diameter of 1" and 1.5" respectively, was sputtered onto the oxidized silicon wafer. The sputtering parameters were as follows:

System Base Pressure	10^{-5}torr
Sputtering Gas	Argon
Sputtering Gas Pressure	8×10^{-2}torr (pressure controlled)
Cathode Voltage	4 kv D.C. (regulated)
Current	90 milliamps
Deposition Rate	250 Å/minute

The 5,000 Å thick annulus maintained a fixed distance between the razor blade edge resting on the tantalum surface and the SiO_x surface. This fixed distance for each experimental run gave a reproducible region of mixing in the resultant film geometry. Figure 15 shows the top and edge view of the substrate after the preparation process described above.

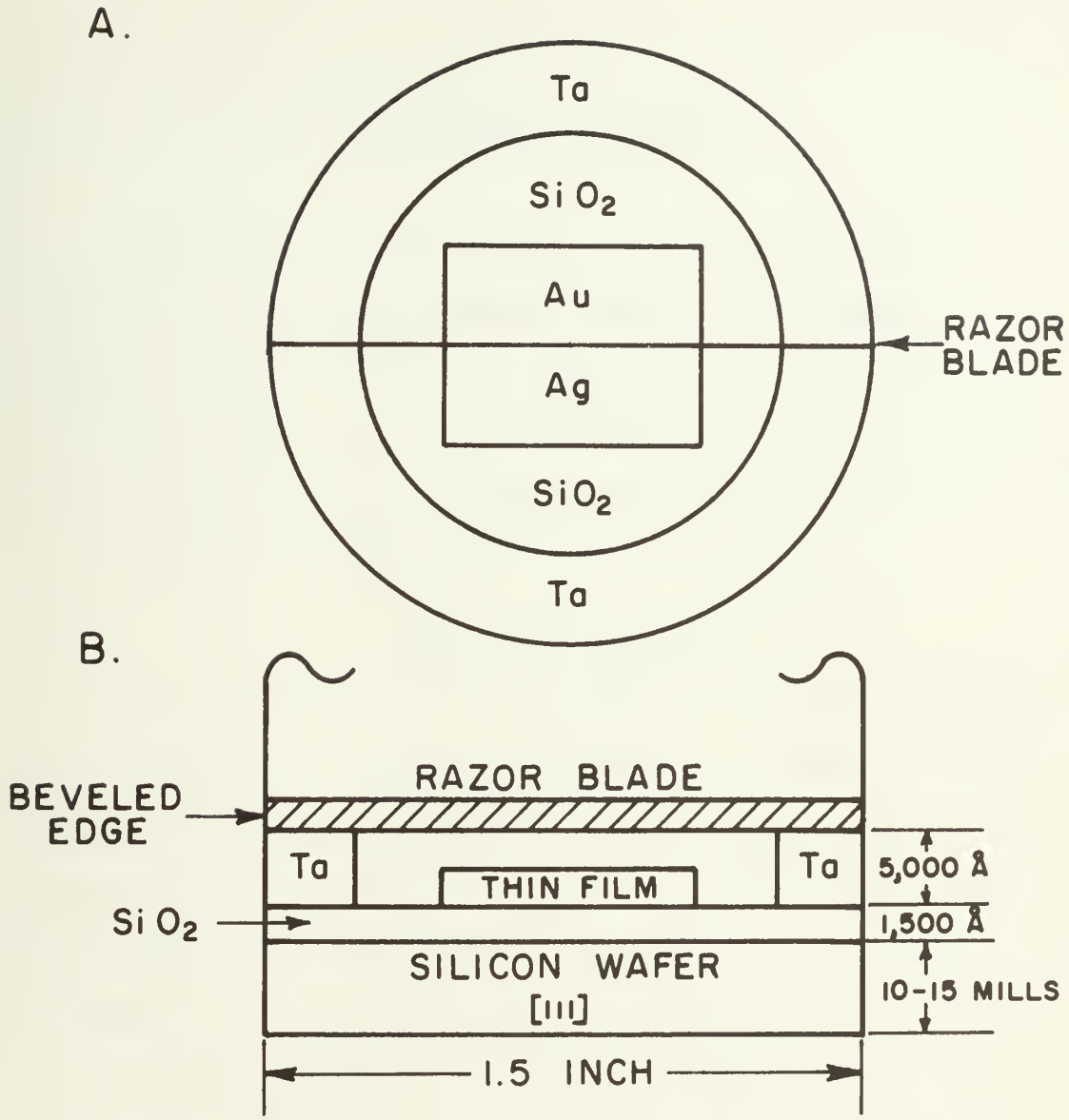

Figure 15

Orientation Relationships between Silicon Wafer and Associated Films. A. Top View of Substrate B. Cross Sectional View of Substrate with Razor Blade in Place

EXPERIMENTAL PROCEDURE

Three different film deposition methods were used during the course of the experimental work of this author. The procedures used for the vacuum deposition of thin film standards, thin film couples, of pure gold and silver, and an incremental couple with an initial concentration difference of 20 atomic %, will be described in three subsections.

Thin Film Standards

Oxidized Silicon wafers, with no Ta annulus sputtered on the surface, were used as substrates. The 1.5" wafers were cut into small sections using a diamond scribe, and mounted onto the substrate holder. The available area of deposition was further reduced by masking with a thin .010" Ta sheet. This provided a sharp edge for thickness measurement, and a negligible variation in thickness over the film area. The razor blade was not used and the stainless steel barrier was lowered away from the substrate holder, its only use was to provide a line of sight barrier between the two sources to prevent cross contamination. The system was then evacuated to 5×10^{-7}torr while the substrate was outgassed by heating to 150°C, driving off adsorbed water and other volatile impurities on the surface.

The sources were heated slowly over a period of 5 minutes, followed by a 2 minute soak cycle just below deposition temperature to bring each source to a uniform temperature prior to deposition.

Deposition was carried out simultaneously, the rates (Å/sec) of each source adjusted, prior to opening the shutter, by the control monitors, so that the time of deposition for both sources was equal, and yet still maintaining the necessary mass ratio to give the film concentration desired. Films of 500, 1,000, 1,500 and 2,000 Å in thickness, each with compositions of 0, 20, 40, 60 and 100 atomic %, were deposited. A detailed explanation of the method of achieving film composition is given in Appendix B.

Gold and silver of 99.99% purity were used as source material for deposition of thin film standards.

Film thickness was measured by a Dektak. Four (4) measurements of the edge height were taken on each film, with the average thickness reported.

X-ray emission data were taken with the ARL-AMX Electron Microprobe. Intensity measurements were obtained with the electron microprobe, operated with an emission current of 100 μamps, beam current of 0.5 μamps, and an operating voltage of 25 kv. The intensities of the gold and silver Lα lines were measured with a LiF and ADP crystal, respectively. Two (2) measurements for a fixed time count of 10 seconds were taken at five different locations on each film.

Background measurements were taken by moving the spectrometers off the peak position.

Thin-Film Couple (Ag-Au)

Oxidized Silicon wafers with the Ta annulus sputtered onto the surface were used as substrates. The substrates were mounted onto the substrate holder and clamped firmly into place by the copper restraining plates. A Personna 74 double edge razor blade, with its commercial stamping removed, was cleaned by ultrasonic agitation in reagent grade acetone and trichloroethylene. A small strip of .009 mm aluminum foil was spot welded onto the razor blade to cover the center slot design. The final assembly was cleaned further in solvents and then placed into the razor blade support mechanism. The substrate holder was placed into the vacuum system. The source barrier was then adjusted horizontally to be true to the razor blade edge, and vertically so that as the substrate was heated and expansion occurred, the vertical height between the top of the barrier and the razor blade edge was as small as possible.

The vacuum system was pumped down to 5×10^{-7}torr while the substrate was heated by the variac to the annealing temperature. The sources were preheated as described above.

While the substrate was held above room temperature, helium quench gas was slowly passed through the quench tubes. The small flow rate was monitored by terminating the gas

line in a flask filled with distilled water. This prevented oxidation of the inner surfaces of the copper quench tubes, which were exposed to 1 atm. pressure.

When the substrate was at the annealing temperature, the Leeds and Northrup proportional counter was switched into the heating circuit, controlling the temperature of the substrate to within ± 1°C.

Deposition of the gold and silver, while the substrate was held at the annealing temperature, was carried out simultaneously. The rates (5 Å/sec) of each source were adjusted equally by the crystal monitors, prior to opening the shutter, so that the time of deposition and film thickness of the gold and silver were the same. Silver and gold of 99.99% and 99.9999% purity, respectively, were used as source material for deposition.

At the conclusion of the film deposition, the anneal was begun. The anneal was terminated by removing the flask from the terminus of the gas line and then forcing helium gas at a pressure of 12 lbs./sq. inch through the quench tubes. The cooling curves were exponential in character, representing quench rates of approximately 75-100°C per minute, down to substrate temperatures of around 60°C. The quench rate lowered to approximately 50°C per minute for the two low temperature anneals.

The substrates were then removed from the vacuum system for further analysis.

Film thickness of both the pure gold and pure silver portion of the couple and thickness variation across the region of mixing were measured by Dektac.

X-ray emission data were taken with the ARL-AMX Electron Microprobe. Intensity measurements were obtained with the electron microprobe operating as described above in the subsection on thin film standards. Intensity profiles as a function of distance were determined by recording the characteristic x-ray intensity while the sample was moved under the electron beam at a rate of 4 microns/minute. Fixed time counts of 10 seconds were taken as the sample was scanned.

Photomicrographs of the film surface were taken on a Leitz orthoplan microscope and a JSM-U3 Scanning Electron Microscope. The scanning electron microscope was operated at 27 kv with a sample current of 1.89×10^{-10} amps. Limited x-ray emission data were also taken with the scanning electron microscope, taking advantage of the small spot size of the electron beam, and will be noted as the data are reviewed.

Grain sizes of the films were determined using the transmission mode of a Siemens Elmiskop 101 electron microscope operating at 100 kv, with beam currents of 10 and 60 microamps.

Incremental Couple (Au-20% Ag)

Oxidized Silicon wafers with the Ta annulus sputtered onto the surface were again used as substrates. The thin film deposition was carried out in two steps.

Initially the substrate, mounted onto the substrate holder, was placed into the vacuum system without the razor blade. The substrate was heated to the annealing temperature, and then a layer of gold film was deposited across the entire substrate surface. After cooling to room temperature, the substrate holder was removed from the vacuum system where the razor blade was mounted into the support mechanism. After alignment of the razor blade with the barrier mechanism, as in the case of the Ag-Au couple, the system was again evacuated. The substrate was again heated to the annealing temperature, and films of gold and silver were deposited over the initial gold underlayer, in the manner of the Ag-Au couple described in the previous subsection.

Film thickness, x-ray emission data, photomicrographs and grain size determinations were taken in the same manner as described in the previous subsection.

RESULTS

Thin Film Standards

The determination of the thin film empirical conversion parameter between the measured relative intensity of the microprobe and thin film composition, involved the fabrication of twenty-four (24) different films. Gold-silver films of 0, 20, 40, 60, 80, 100 atomic % silver were each made of 4 different approximate thicknesses, 500, 1,000, 1,500 and 2,000 Å. Each film thickness was measured on the Dektac where the accuracy of measurement is ± 50 Å. Two plots of measured characteristic x-ray intensity versus measured film thickness, were made for each film composition. The two plots were of the characteristic x-ray data of the Lα lines taken from the gold and silver spectrometers. A linear least squares fit was made on each intensity versus thickness plot.

From the resultant linear analytical equation for each plot, the film x-ray intensity was determined for numerical thicknesses of 500, 1,000, 1,500 and 2,000 Å. K_{Ag} and K_{Au} for each composition and film thickness, in the form of equation (1), were determined after correcting both the pure and alloy films for their respective backgrounds.

The backgrounds of the pure Au and Ag films were determined by moving the spectrometers off each side of the characteristic Lα peak of the Au and Ag line respectively, and averaging the two values. The alloy background was determined by the following relationship:

$$B_{alloy} = B_{pure\ Au}\ \overline{C}_{Au} + B_{pure\ Ag}\ \overline{C}_{Ag}. \qquad (15)$$

where B_{alloy} = the background of an alloy film of thickness, t.

$B_{pure\ A}$ = the background of a pure A film of thickness, t.

$\overline{C}$ = atomic fraction.

The values of K_{Ag}, K_{Au} and C_{Ag}, C_{Au} respectively, were plotted in the form of equation (3), where another linear least squares fit was made, the slope representing the value of the empirical conversion parameter, a_{AgAu} and a_{AuAg} respectively. The process was repeated for each film thickness. In addition, a linear least squares fit was made for all the data of each spectrometer to determine an average value of the empirical conversion parameter for film thicknesses between 500 and 2,000 Å.

The statistical calculations discussed above were accomplished by the computer program in Appendix C. Tables 1 and 2 are the direct computer output printed on the Gould electrostatic printer, displaying the results of the calibration data taken off the silver and gold spectrometer respectively.

TABLE 1. CALIBRATION DATA TAKEN OFF THE SILVER SPECTROMETER

BACKGROUND INTENSITY OF PURE SILVER FILMS

INTENSITY	FILM THICKNESS *
177.000000	550.000000
256.000000	1125.000000
376.000000	1670.000000
556.000000	2200.000000

EQUATION OF LINE IS..... INTENSITY = A0 + A1 X THICKNESS.....

INTERCEPT (A0) = 25.27911

SLOPE (A1) = .22793

STANDARD ERROR OF THE ESTIMATE = 27.87330

SUM SQUARES DEVIATION OF Y = 142.80297

COEFFICIENT OF CORRELATION = .98077

(ATOMIC FRACTION SILVER)
COMPOSITION = 1.00

INTENSITY	FILM THICKNESS *
158.000000	0.000000
2380.000000	550.000000
5084.000000	1125.000000
7009.000000	1670.000000
9449.000000	2200.000000

EQUATION OF LINE IS..... INTENSITY = A0 + A1 X THICKNESS.....

INTERCEPT (A0) = 152.15723

SLOPE (A1) = 4.20545

STANDARD ERROR OF THE ESTIMATE = 124.27736

SUM SQUARES DEVIATION OF Y = 3285.62999

COEFFICIENT OF CORRELATION = .99928

(ATOMIC FRACTION SILVER)
COMPOSITION = 0.00

INTENSITY	FILM THICKNESS *
158.000000	0.000000
246.000000	500.000000
363.000000	1125.000000
393.000000	1400.000000
459.000000	2000.000000

EQUATION OF LINE IS..... INTENSITY = A0 + A1 X THICKNESS.....

INTERCEPT (A0) = 169.46382

SLOPE (A1) = .15357

STANDARD ERROR OF THE ESTIMATE = 13.75257

SUM SQUARES DEVIATION OF Y = 107.83951

COEFFICIENT OF CORRELATION = .99183

* ± 50 Å

Table 1. (Cont'd.)

(ATOMIC FRACTION SILVER)
COMPOSITION = .80

INTENSITY	FILM THICKNESS *
158.000000	0.000000
1992.000000	580.000000
3376.000000	1160.000000
5472.000000	1760.000000
6528.000000	2100.000000

EQUATION OF LINE IS..... INTENSITY = A0 + A1 X THICKNESS....

INTERCEPT (A0) = 134.02150

SLOPE (A1) = 3.00998

STANDARD ERROR OF THE ESTIMATE = 128.39483

SUM SQUARES DEVIATION OF Y = 2302.86069

COEFFICIENT OF CORRELATION = .99844

(ATOMIC FRACTION SILVER)
COMPOSITION = .60

INTENSITY	FILM THICKNESS *
158.000000	0.000000
1292.000000	520.000000
2502.000000	1125.000000
3916.000000	1650.000000
4669.000000	2195.000000

EQUATION OF LINE IS..... INTENSITY = A0 + A1 X THICKNESS....

INTERCEPT (A0) = 191.18882

SLOPE (A1) = 2.10948

STANDARD ERROR OF THE ESTIMATE = 132.57346

SUM SQUARES DEVIATION OF Y = 1652.48753

COEFFICIENT OF CORRELATION = .99678

(ATOMIC FRACTION SILVER)
COMPOSITION = .40

INTENSITY	FILM THICKNESS *
158.000000	0.000000
932.000000	525.000000
1855.000000	1100.000000
2565.000000	1650.000000
3241.000000	2180.000000

EQUATION OF LINE IS..... INTENSITY = A0 + A1 X THICKNESS....

INTERCEPT (A0) = 198.39180

SLOPE (A1) = 1.42237

STANDARD ERROR OF THE ESTIMATE = 52.98806

SUM SQUARES DEVIATION OF Y = 1104.70981

COEFFICIENT OF CORRELATION = .99885

* ± 50 Å

Table 1. (Cont'd.)

[illegible] EVAPORATION SILVER
[illegible] 20

INTENSITY	FILM THICKNESS *
158.000000	0.000000
642.000000	613.000000
903.000000	1115.000000
1477.000000	1520.000000
1577.000000	2000.000000

EQUATION OF LINE IS . INTENSITY = A0 + A1 X THICKNESS. .

INTERCEPT (A0) = 67.97303

SLOPE (A1) = .72599

STANDARD ERROR OF THE ESTIMATE = 54.12734

SUM SQUARES DEVIATION OF Y = 525.27518

COEFFICIENT OF CORRELATION = .99428

FILM THICKNESS = 500.00

1-K/K	1-C/C
.755932	.456566
1.463639	1.210402
2.715738	2.284155
7.822900	7.700417

INTERCEPT (A0) = 0.00000

SLOPE (A1) = 1.07539

STANDARD ERROR OF THE ESTIMATE = .19292

SUM SQUARES DEVIATION OF Y = 7.82576

COEFFICIENT OF CORRELATION = .99762

FILM THICKNESS = 1000.00

1-K/K	1-C/C
.623600	.456705
1.177475	1.210402
2.424776	2.284155
6.610625	7.700417

INTERCEPT (A0) = 0.00000

SLOPE (A1) = .90058

STANDARD ERROR OF THE ESTIMATE = .10098

SUM SQUARES DEVIATION OF Y = 5.61879

COEFFICIENT OF CORRELATION = .99909

* ± 50 Å

Table 1. (Cont'd.)

FILM THICKNESS = 1500.00

1/K	T/L
.05629	.05626
1.00617	1.01405
2.00559	2.02413
6.01630	7.04117

INTERCEPT (B0) = 0.00000

SLOPE (B1) = .85079

STANDARD ERROR OF THE ESTIMATE = .07803

SUM SQUARED DEVIATION OF Y = 5.06485

COEFFICIENT OF CORRELATION = .90940

FILM THICKNESS = 2000.00

1/K	T/L
.04944	.04962
1.00034	1.01402
2.00188	2.02772
6.00624	7.04117

INTERCEPT (B0) = 0.00000

SLOPE (B1) = .82729

STANDARD ERROR OF THE ESTIMATE = .06249

SUM SQUARED DEVIATION OF Y = 4.81712

COEFFICIENT OF CORRELATION = .90951

LINEAR LEAST SQUARES FIT FOR ALL DATA

INTERCEPT (B0) = 0.00000

SLOPE (B1) = .91349

STANDARD ERROR OF THE ESTIMATE = .10265

SUM SQUARED DEVIATION OF Y = 5.92574

COEFFICIENT OF CORRELATION = .90623

TABLE 2 CALIBRATION DATA TAKEN OFF THE GOLD SPECTROMETER

BACKGROUND INTENSITY OF SOME GOLD FILMS

INTENSITY	FILM THICKNESS *
690.000000	500.000000
1030.000000	1125.000000
1260.000000	1400.000000
1428.000000	2000.000000

EQUATION OF LINE IS..... INTENSITY = A0 + A1 X THICKNESS. ...

INTERCEPT (A0) = 549.48851

SLOPE (A1) = .44200

STANDARD ERROR OF THE ESTIMATE = 102.51018

SUM SQUARED DEVIATION OF Y = 259.43918

COEFFICIENT OF CORRELATION = .91863

(ATOMIC FRACTION SILVER)
COMPOSITION = 0.00

INTENSITY	FILM THICKNESS *
240.000000	0.000000
470.000000	500.000000
1040.000000	1125.000000
1240.000000	1400.000000
1820.000000	2000.000000

EQUATION OF LINE IS..... INTENSITY = A0 + A1 X THICKNESS. ...

INTERCEPT (A0) = 308.34895

SLOPE (A1) = 9.12463

STANDARD ERROR OF THE ESTIMATE = 198.37946

SUM SQUARES DEVIATION OF Y = 6358.31857

COEFFICIENT OF CORRELATION = .99951

(ATOMIC FRACTION SILVER)
COMPOSITION = 1.00

INTENSITY	FILM THICKNESS *
240.000000	0.000000
294.000000	550.000000
349.000000	1125.000000
494.000000	1670.000000
457.000000	2400.000000

EQUATION OF LINE IS..... INTENSITY = A0 + A1 X THICKNESS. ...

INTERCEPT (A0) = 239.46777

SLOPE (A1) = .09137

STANDARD ERROR OF THE ESTIMATE = 4.34419

SUM SQUARES DEVIATION OF Y = 71.46859

COEFFICIENT OF CORRELATION = .99815

* ± 50 Å

Table 2. (Cont'd.)

(ATOMIC FRACTION SILVER)
COMPOSITION = .20

INTENSITY	FILM THICKNESS *
240.000000	0.000000
4173.000000	613.000000
8166.000000	1115.000000
11720.000000	1630.000000
14865.000000	2000.000000

EQUATION OF LINE IS . INTENSITY = A0 + A1 X THICKNESS .

INTERCEPT (A0) = 22.29339

SLOPE (A1) = 7.22218

STANDARD ERROR OF THE ESTIMATE = 203.11756

SUM SQUARES DEVIATION OF Y = 5409.24856

COEFFICIENT OF CORRELATION = .99824

(ATOMIC FRACTION SILVER)
COMPOSITION .40

INTENSITY	FILM THICKNESS *
240.000000	0.000000
3136.000000	525.000000
6092.000000	1100.000000
9572.000000	1650.000000
13152.000000	2180.000000

EQUATION OF LINE IS . . . INTENSITY = A0 + A1 X THICKNESS . . .

INTERCEPT (A0) = -16.44151

SLOPE (A1) = 5.99096

STANDARD ERROR OF THE ESTIMATE = 261.57327

SUM SQUARES DEVIATION OF Y = 4577.52840

COEFFICIENT OF CORRELATION = .99337

(ATOMIC FRACTION SILVER)
COMPOSITION .60

INTENSITY	FILM THICKNESS *
240.000000	0.000000
1836.000000	520.000000
3875.000000	1125.000000
5853.000000	1650.000000
7996.000000	2195.000000

EQUATION OF LINE IS . . . . . INTENSITY = A0 + A1 X THICKNESS . . . .

INTERCEPT (A0) = 96.89299

SLOPE (A1) = 3.52851

STANDARD ERROR OF THE ESTIMATE = 141.56437

SUM SQUARES DEVIATION OF Y = 2758.43177

COEFFICIENT OF CORRELATION = .99886

* ± 50 Å

Table 2. (Cont'd.)

[illegible] ILLUMINATION SILVER
[illegible] CONCENTRATION 80

INTENSITY	FILM THICKNESS *
[illegible]	0.000000
[illegible]	580.000000
[illegible]	1160.000000
[illegible]	1760.000000
[illegible]	2100.000000

EQUATION OF LINE IS. . . . INTENSITY = A0 + A1 X THICKNESS. . . .

INTERCEPT (A0) = 256.40921

SLOPE (A1) = 1.76856

STANDARD ERROR OF THE ESTIMATE = 82.50263

SUM SQUARES DEVIATION OF Y = 1753.49539

COEFFICIENT OF CORRELATION = .99814

FILM THICKNESS = 500.00

1-K/K	1-C/C
.687619	.136904
1.092398	.265076
2.671813	.821471
5.541159	2.190457

INTERCEPT (A0) = 0.00000

SLOPE (A1) = 2.63989

STANDARD ERROR OF THE ESTIMATE = .32832

SUM SQUARES DEVIATION OF Y = 3.64777

COEFFICIENT OF CORRELATION = .98511

FILM THICKNESS = 1000.00

1-K/K	1-C/C
[illegible]	.136904
[illegible]	.265076
1.958436	.821471
4.728470	2.190457

INTERCEPT (A0) = 0.00000

SLOPE (A1) = 2.18440

STANDARD ERROR OF THE ESTIMATE = .10588

SUM SQUARES DEVIATION OF Y = 2.90361

COEFFICIENT OF CORRELATION = .99807

* ± 50 Å

Table 2. (Cont'd.)

FILM THICKNESS = 1500.00

1-K/K	1-C/C
.326917	.136904
.636869	.365076
1.784711	.821421
4.506660	2.190457

INTERCEPT (A0) = 0.00000

SLOPE (A1) = 2.06492

STANDARD ERROR OF THE ESTIMATE = .07706

SUM SQUARES DEVIATION OF Y = 2.71208

COEFFICIENT OF CORRELATION = .99890

FILM THICKNESS = 2000.00

1-K/K	1-C/C
.293810	.136904
.594943	.365076
1.706431	.821421
4.403519	2.190457

INTERCEPT (A0) = 0.00000

SLOPE (A1) = 2.00980

STANDARD ERROR OF THE ESTIMATE = .07533

SUM SQUARES DEVIATION OF Y = 2.62443

COEFFICIENT OF CORRELATION = .99892

LINEAR LEAST SQUARES FIT FOR ALL DATA

INTERCEPT (A0) = 0.00000

SLOPE (A1) = 2.22476

STANDARD ERROR OF THE ESTIMATE = .34502

SUM SQUARES DEVIATION OF Y = 3.05982

COEFFICIENT OF CORRELATION = .98036

Incremental Couple (80%Au-Au)

Table 3 summarizes the experimental runs completed during the study of chemical diffusion in the incremental couples. The couples consisted of a pure gold film layered side by side to an alloy film of equal thickness, and with a composition of 80 and 20 atomic % gold and silver, respectively. The film thickness for all the runs was approximately 1,500 Å; actual measurements made on each film using the Dektac are reported in Table 3.

Five (5) couples were annealed for 24 hours at temperatures of 200, 250, 300, 350 and 416°C. Two additional couples were annealed at 416°C for 12 and 48 hours.

One (1) couple (Run 227) was not annealed and represents the initial (time = 0) concentration profile. Figure 16 shows the concentration-distance profile generated from the computer plotting program of Appendix D. The computer program reads in the x-ray intensity data from the microprobe as a function of lateral distance (Stepsize 0.8 microns), calculates the measured relative intensity corrected for background, and converts K_{Ag} to units of mass concentration (grams Ag/cc) through the empirical conversion parameter and appropriate value of alloy density.

Figures 17 through 23 show the concentration-distance profiles, generated from the same computer program, of the annealed couples. In order to compare the annealed profiles with the initial profile, and thus determine values of

Table 3. Summary of Experimental Conditions for Runs 224-232

Incremental Couples (80Au-Au)

Run No.	Temperature of Anneal (°C)*	Time of Anneal (hrs)	Film Thickness† (Å)	Comments
224	416	24.0	1500‡	No interface contact
225	300	24.0	1480	
226	350	24.0	1525	
227	25	0.0	1490	
228	416	24.0	1480	
229	416	48.0	1440	
230	250	24.0	1525	
231	416	12.0	1530	
232	200	24.0	1500	

* ± 1°C

† ± 50 Å

‡ not measured

Figure 16

Concentration versus Relative Distance for Incremental Thin Film Couple Deposited at Room Temperature with no Anneal. (t = 0 Profile used for Generation of Numerical Solutions)

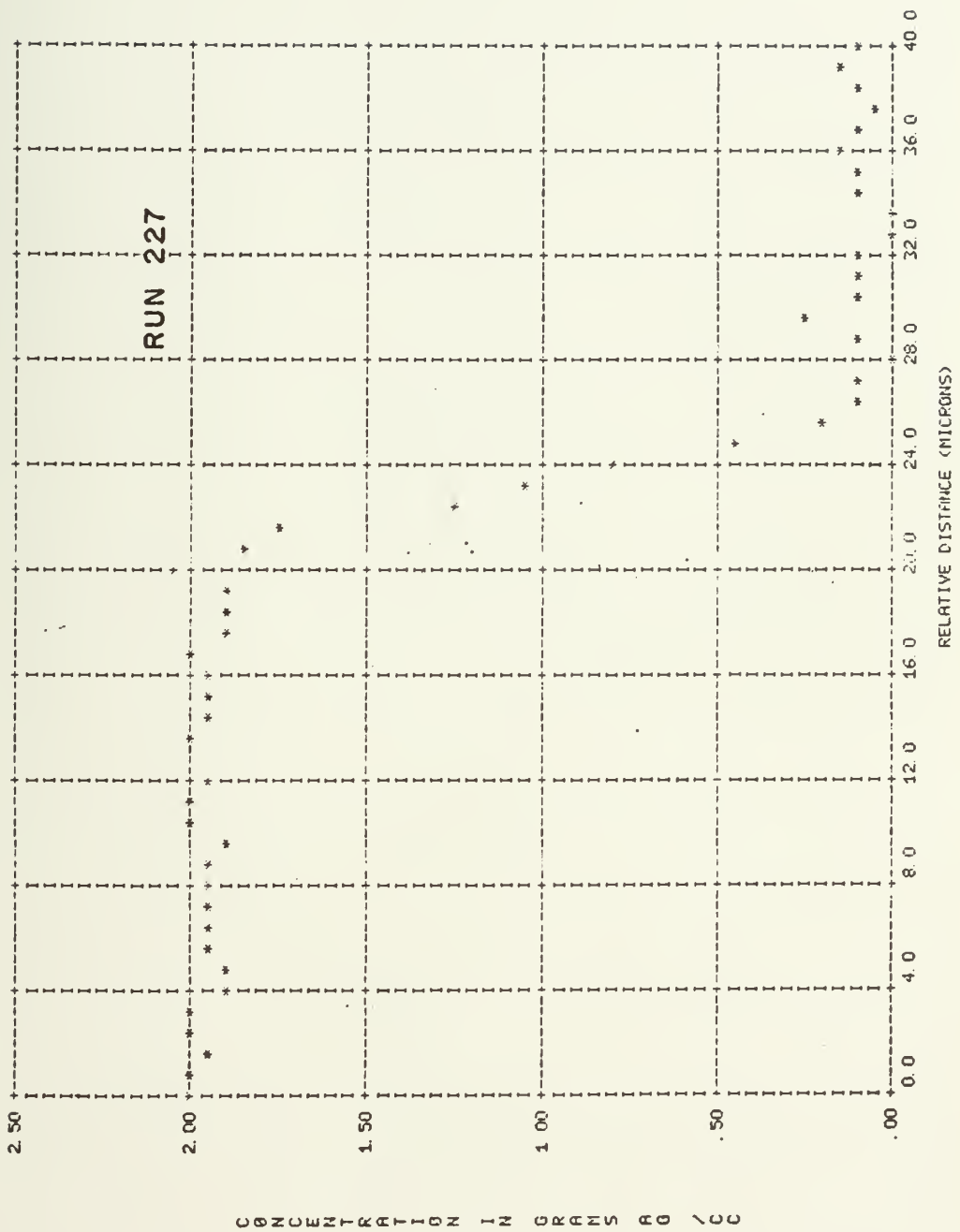
RUN 227
CONCENTRATION IN GRAMS AG /CC
2.50
2.00
1.50
1.00
.50
.00
0.0
4.0
8.0
12.0
16.0
20.0
24.0
28.0
32.0
36.0
40.0
RELATIVE DISTANCE (MICRONS)

Figure 16

Figure 17

Comparison of the Numerical and Experimental Concentration Profiles for an Incremental Thin Film Couple Annealed at 200°C for 24 Hours.

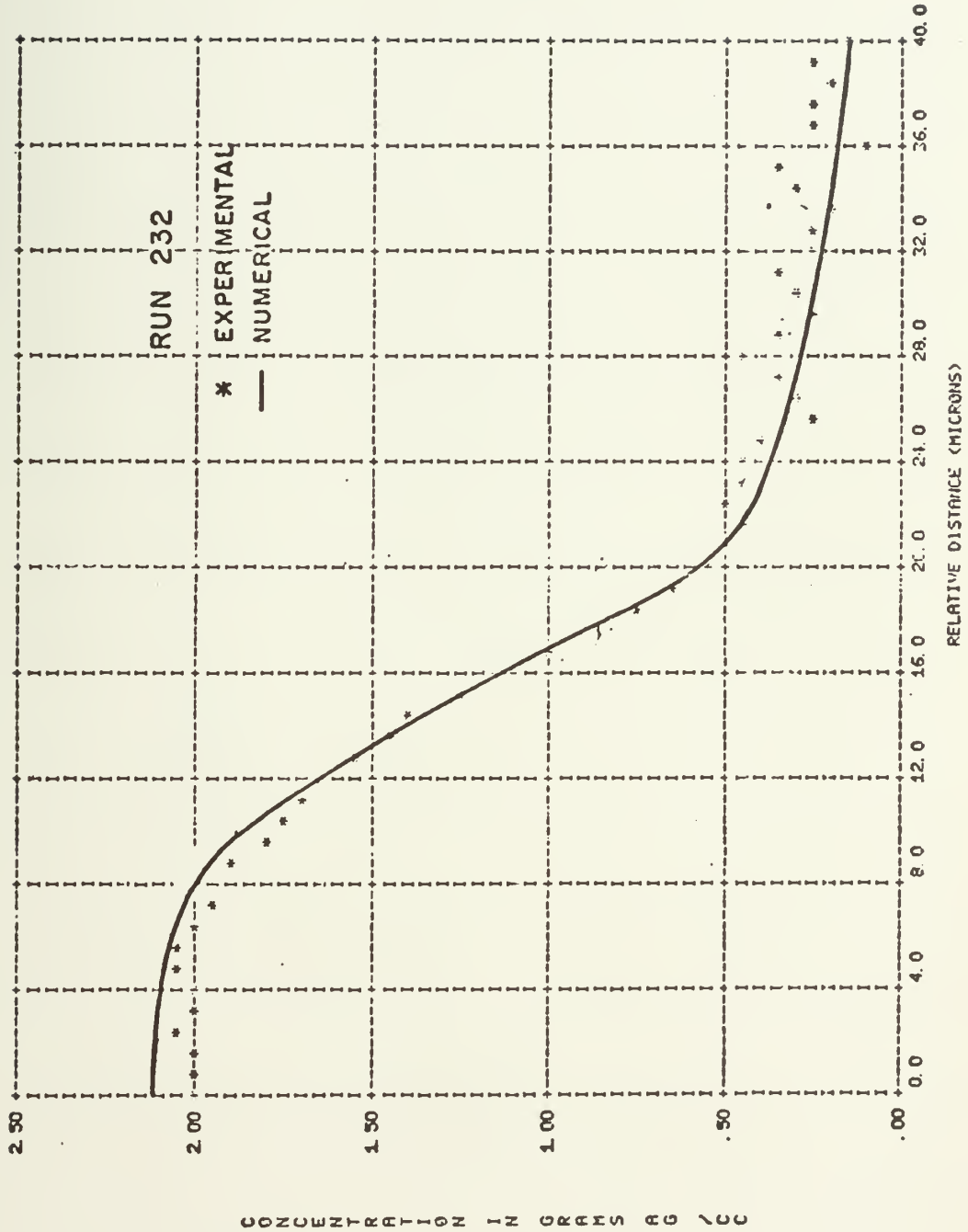
RUN 232
* EXPERIMENTAL
— NUMERICAL
CONCENTRATION IN GRAMS AG /CC
2.50
2.00
1.50
1.00
.50
.00
0.0
4.0
8.0
12.0
16.0
20.0
24.0
28.0
32.0
36.0
40.0
RELATIVE DISTANCE (MICRONS)

Figure 17

Figure 18

Comparison of the Numerical and Experimental Concentration Profiles for an Incremental Thin Film Couple Annealed at 250°C for 24 Hours.

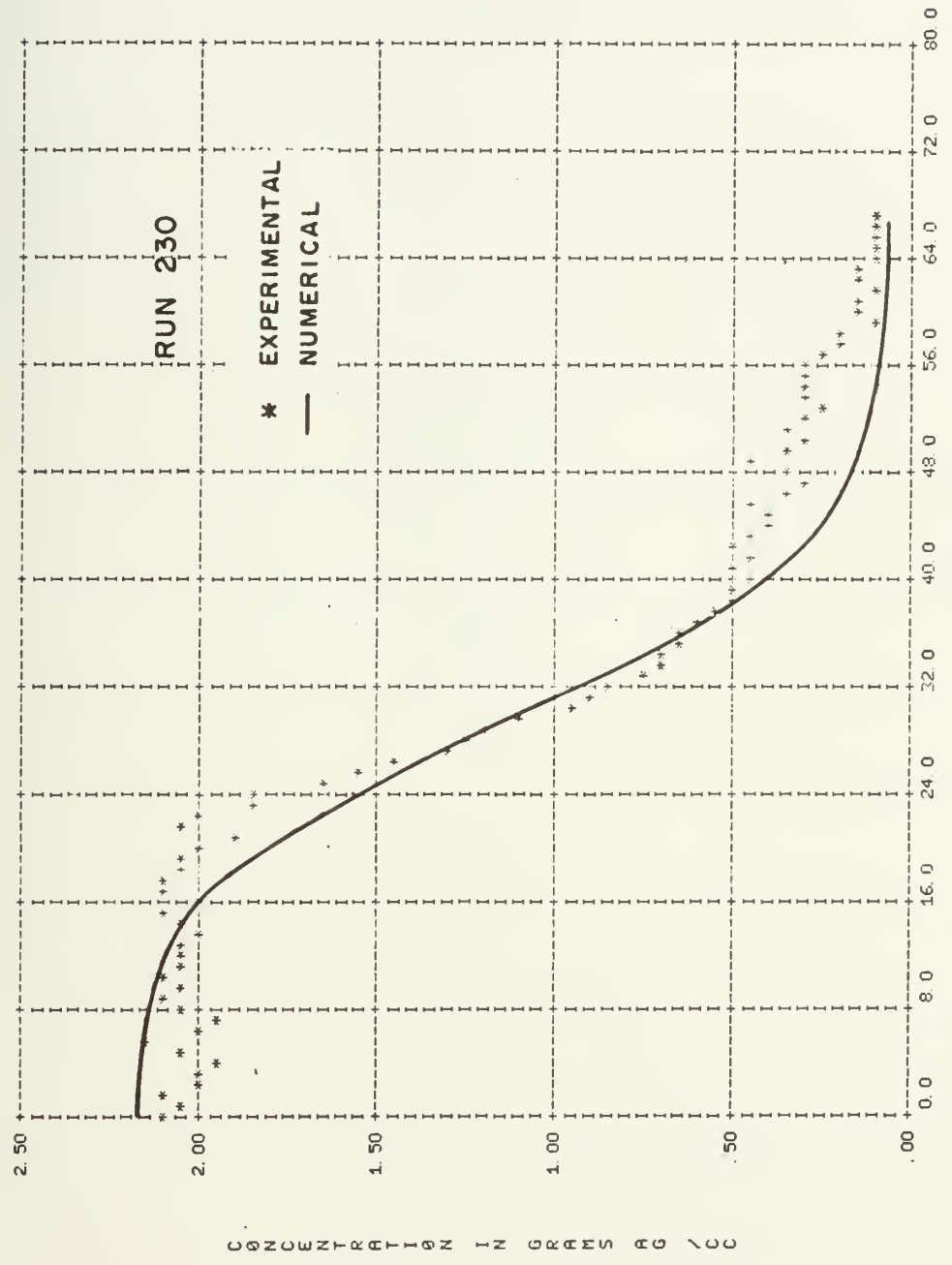
RUN 230
* EXPERIMENTAL
— NUMERICAL
CONCENTRATION IN GRAMS AG /CC
2.50
2.00
1.50
1.00
.50
.00
0.0
8.0
16.0
24.0
32.0
40.0
48.0
56.0
64.0
72.0
80.0
RELATIVE DISTANCE (MICRONS)

Figure 18

Figure 19

Comparison of the Numerical and Experimental Concentration Profiles for an Incremental Thin Film Couple Annealed at 300°C for 24 Hours.

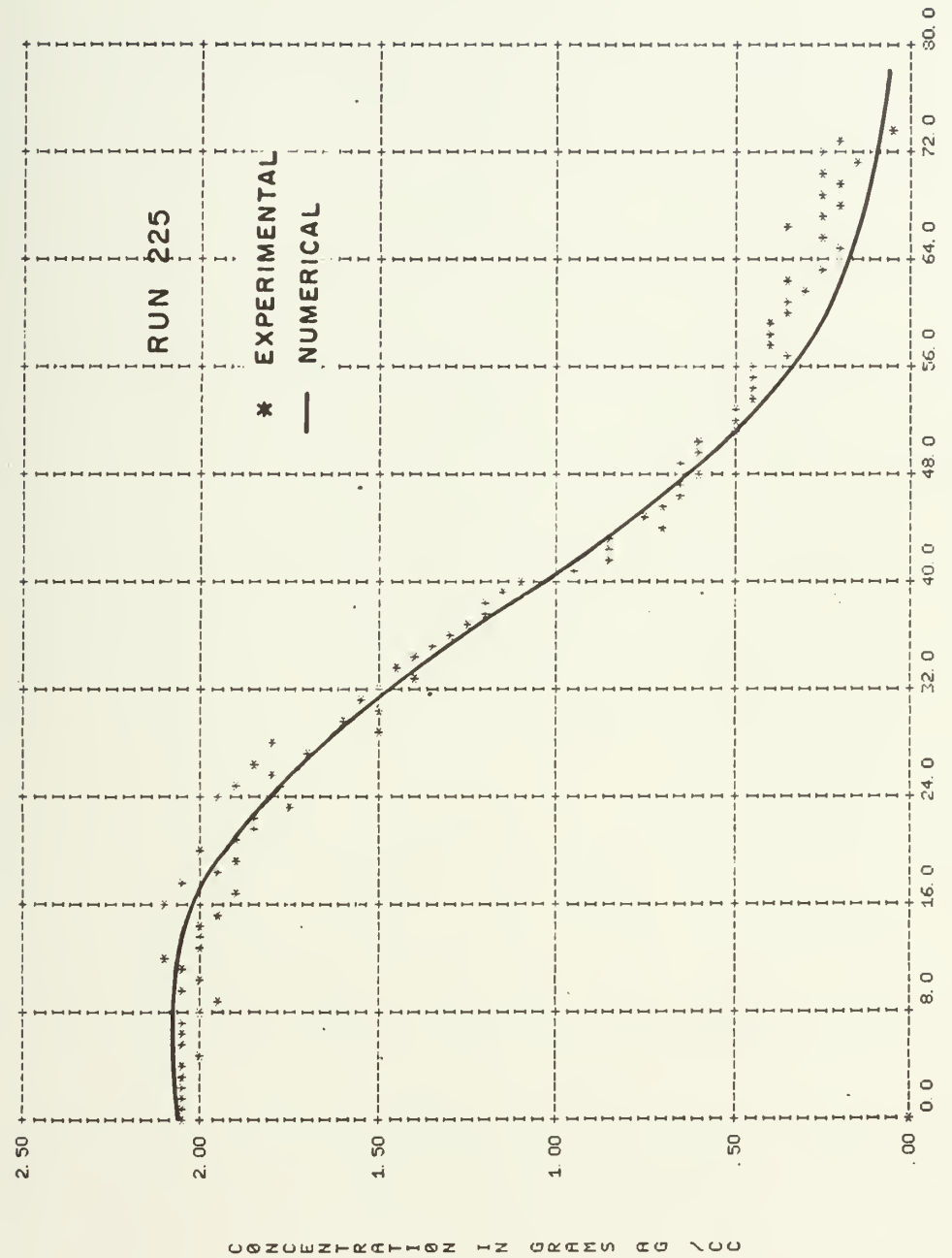
RUN 225
* EXPERIMENTAL
— NUMERICAL
CONCENTRATION IN GRAMS AG /CC
2.50
2.00
1.50
1.00
.50
.00
0.0
8.0
16.0
24.0
32.0
40.0
48.0
56.0
64.0
72.0
80.0
RELATIVE DISTANCE (MICRONS)

Figure 19

Figure 20

Comparison of the Numerical and Experimental Concentration Profiles for an Incremental Thin Film Couple Annealed at 350°C for 24 Hours.

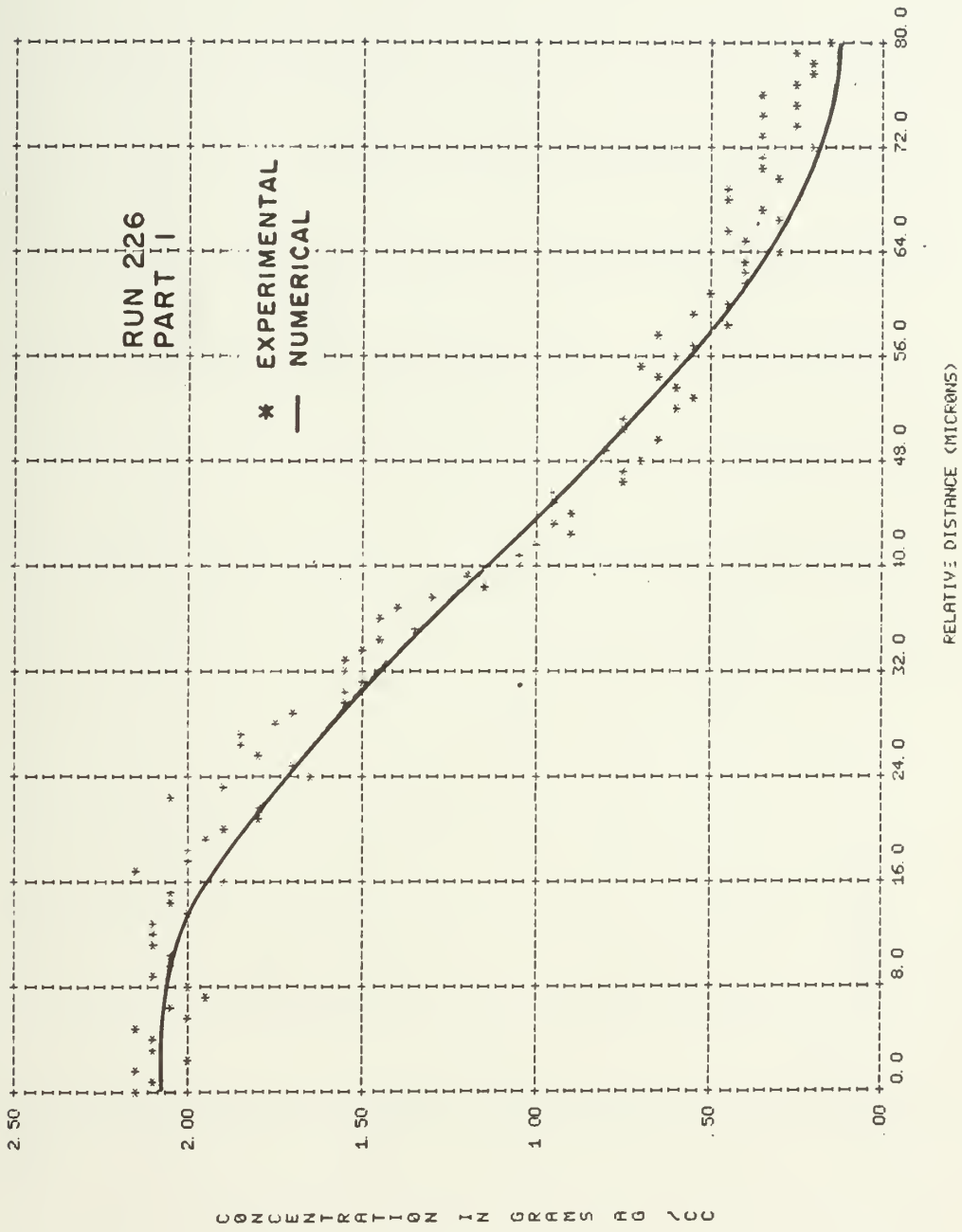
RUN 226
PART I
* EXPERIMENTAL
— NUMERICAL
CONCENTRATION IN GRAMS AG /CC
2.50
2.00
1.50
1.00
.50
.00
0.0
8.0
16.0
24.0
32.0
40.0
48.0
56.0
64.0
72.0
80.0
RELATIVE DISTANCE (MICRONS)

Figure 20

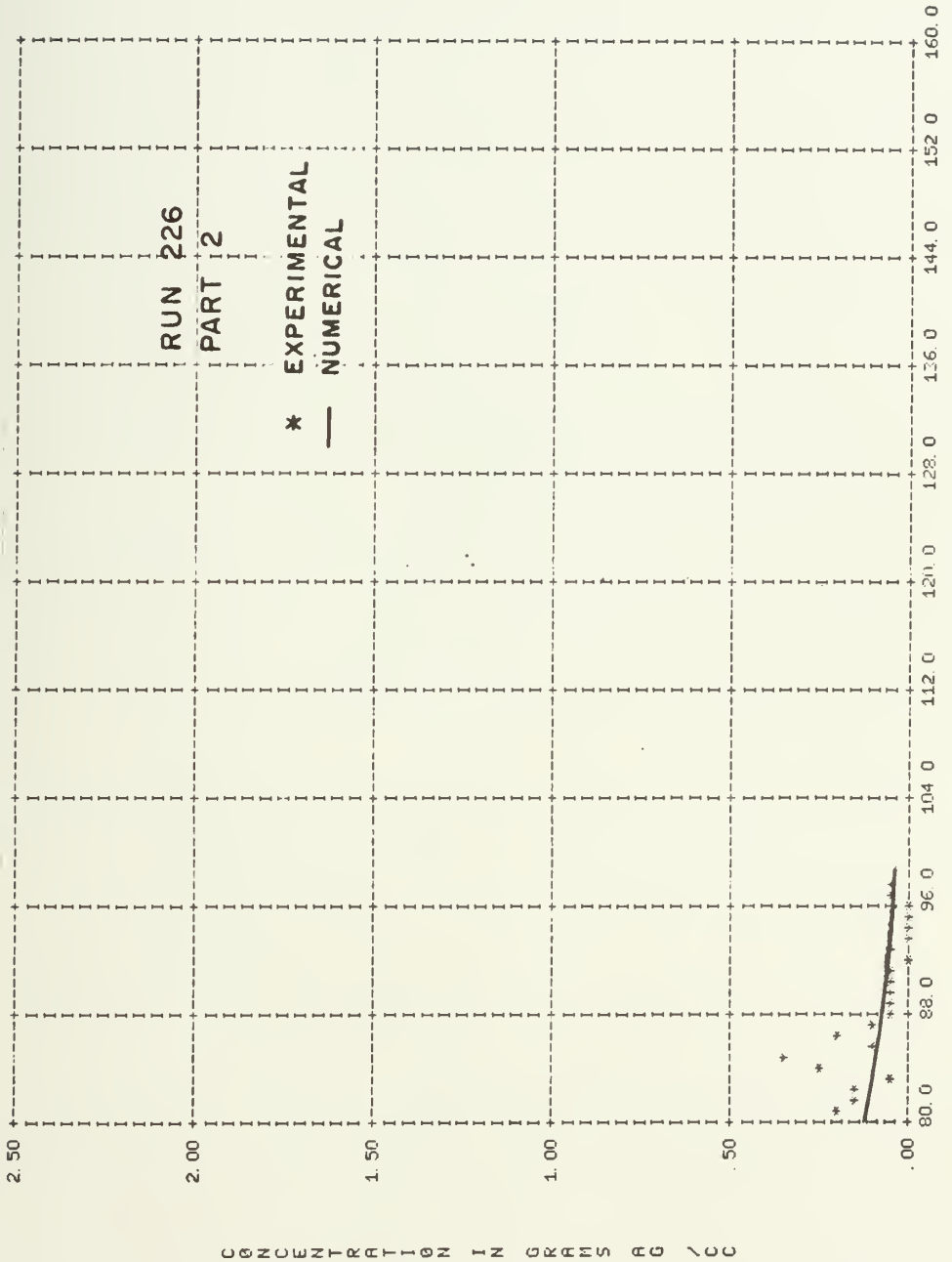

Figure 20 (Cont'd.)

Figure 21

Comparison of the Numerical and Experimental Concentration Profiles for an Incremental Thin Film Couple Annealed at 416°C for 24 Hours.

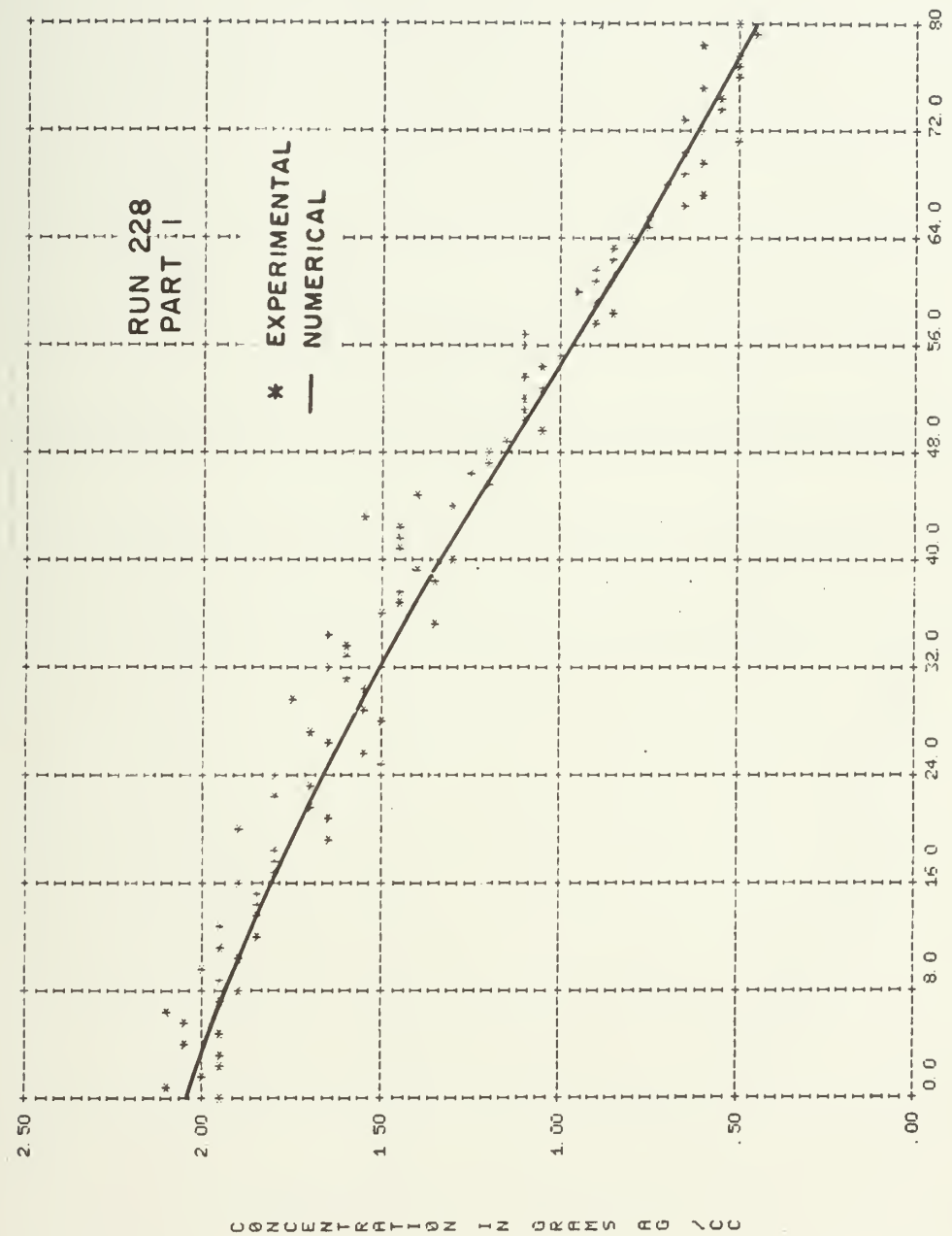
RUN 228
PART II
* EXPERIMENTAL
— NUMERICAL
CONCENTRATION IN GRAMS AG /CC
RELATIVE DISTANCE (MICRONS)
2.50
2.00
1.50
1.00
.50
.00
0.0
8.0
16.0
24.0
32.0
40.0
48.0
56.0
64.0
72.0
80.0

Figure 21

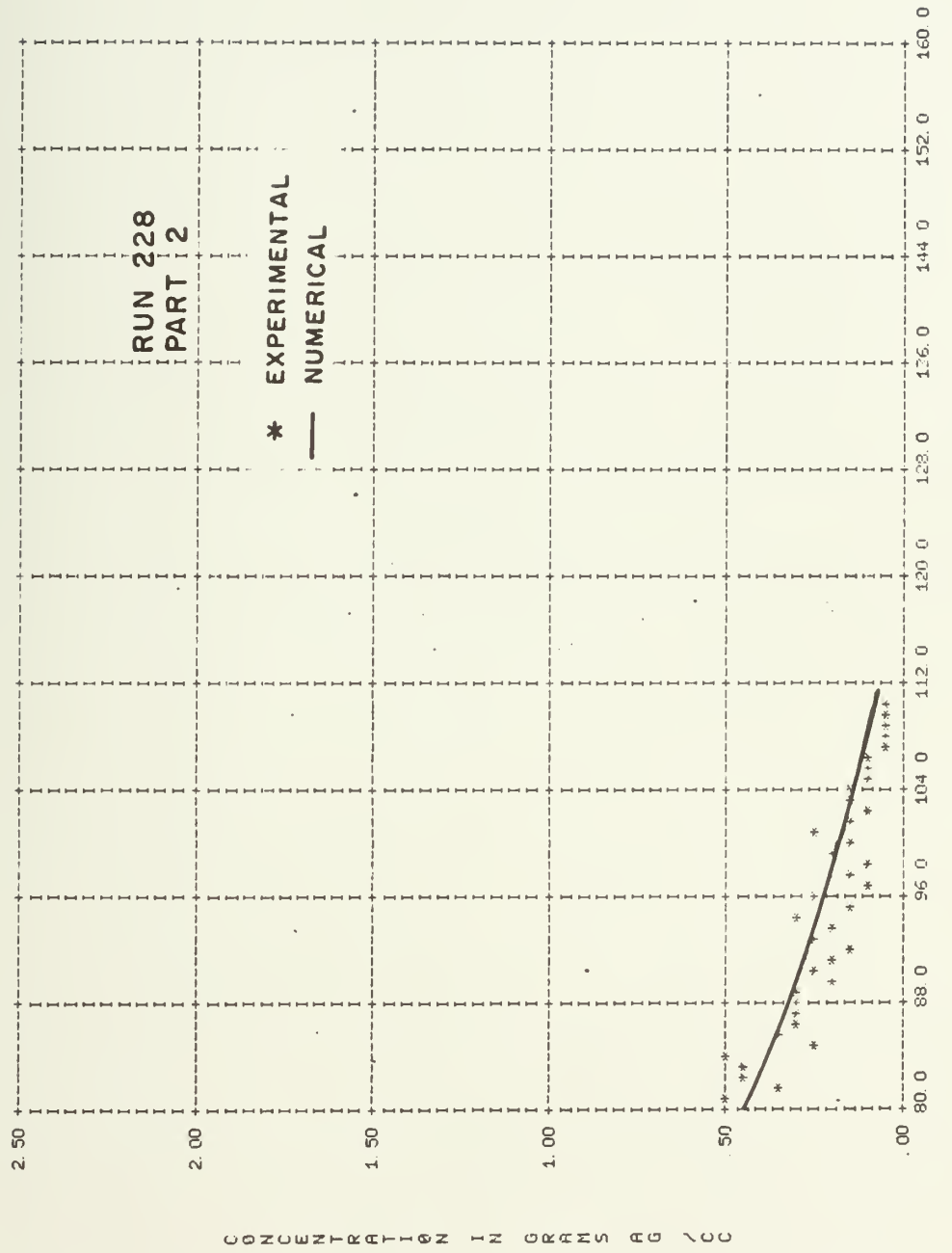

Figure 21 (Cont'd.)

Figure 22

Comparison of the Numerical and Experimental Concentration Profiles for an Incremental Thin Film Couple Annealed at 416°C for 12 Hours.

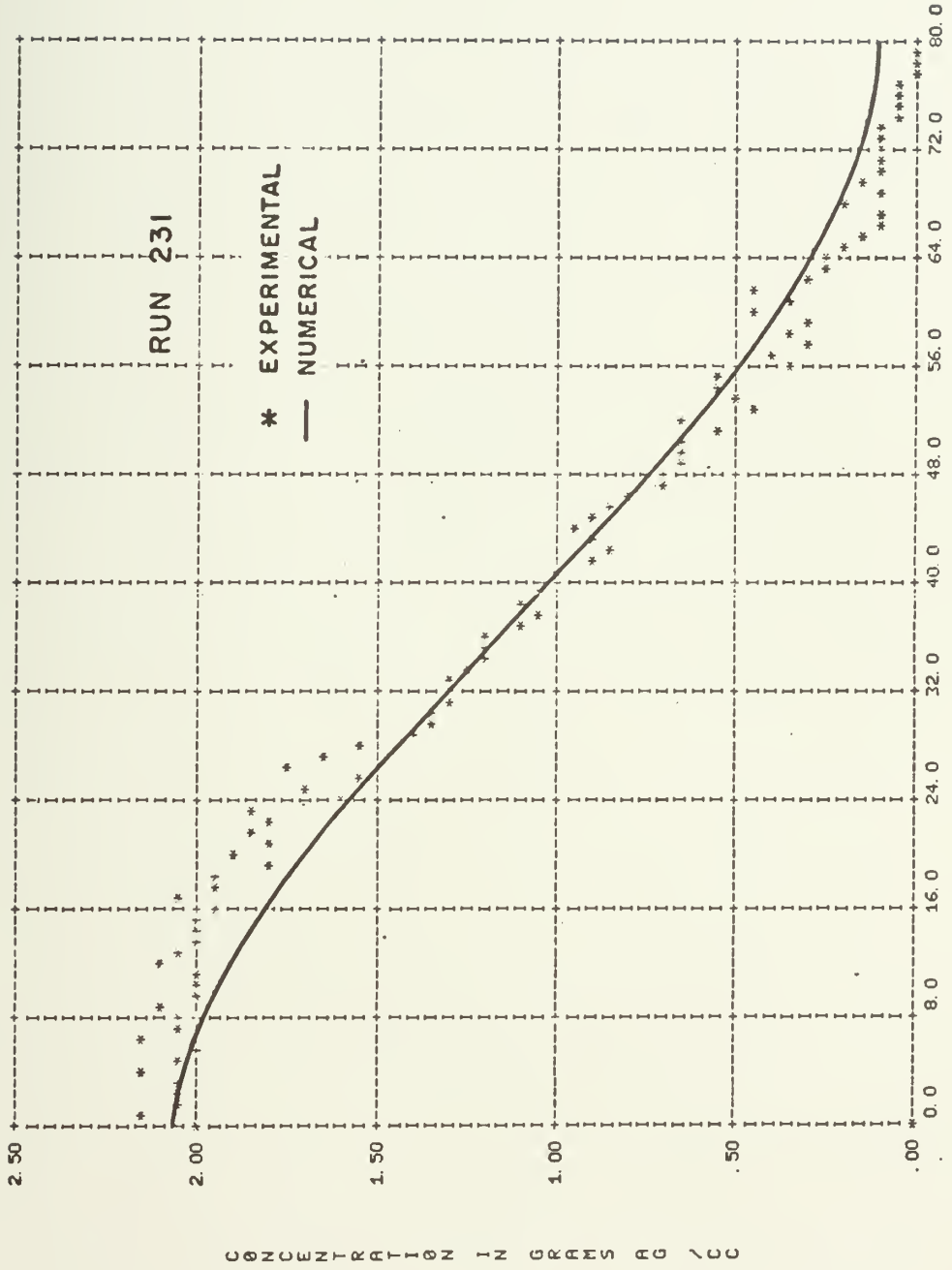
RUN 231
* EXPERIMENTAL
— NUMERICAL
CONCENTRATION IN GRAMS AG /CC
2.50
2.00
1.50
1.00
.50
.00
0.0
8.0
16.0
24.0
32.0
40.0
48.0
56.0
64.0
72.0
80.0
RELATIVE DISTANCE (MICRONS)

Figure 22

Figure 23

Comparison of the Numerical and Experimental Concentration Profiles for an Incremental Thin Film Couple Annealed at 416°C for 48 Hours.

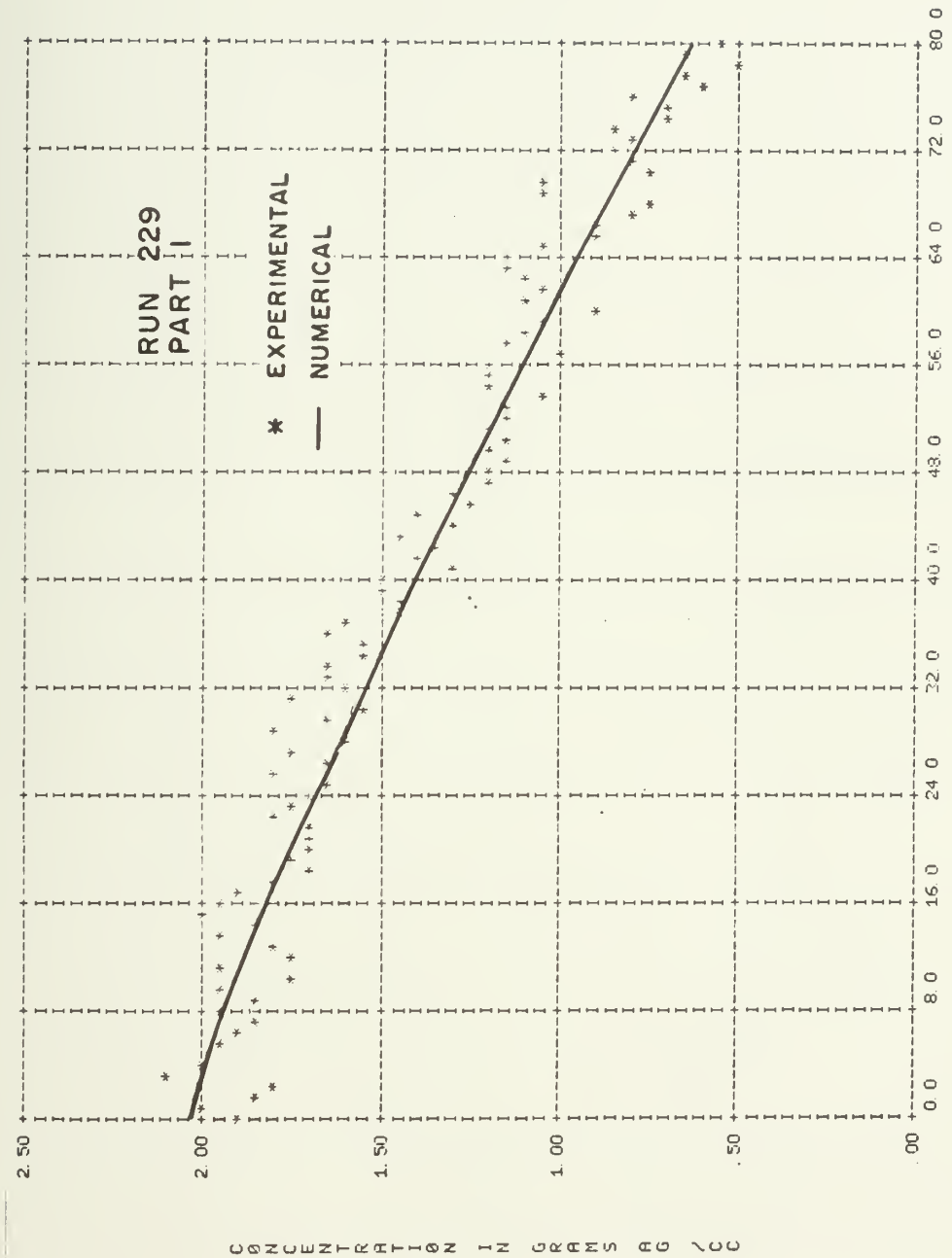
RUN 229
PART I
* EXPERIMENTAL
— NUMERICAL
CONCENTRATION IN GRAMS AG /CC
2.50
2.00
1.50
1.00
.50
.00
0.0
8.0
16.0
24.0
32.0
40.0
48.0
56.0
64.0
72.0
80.0
RELATIVE DISTANCE (MICRONS)

Figure 23

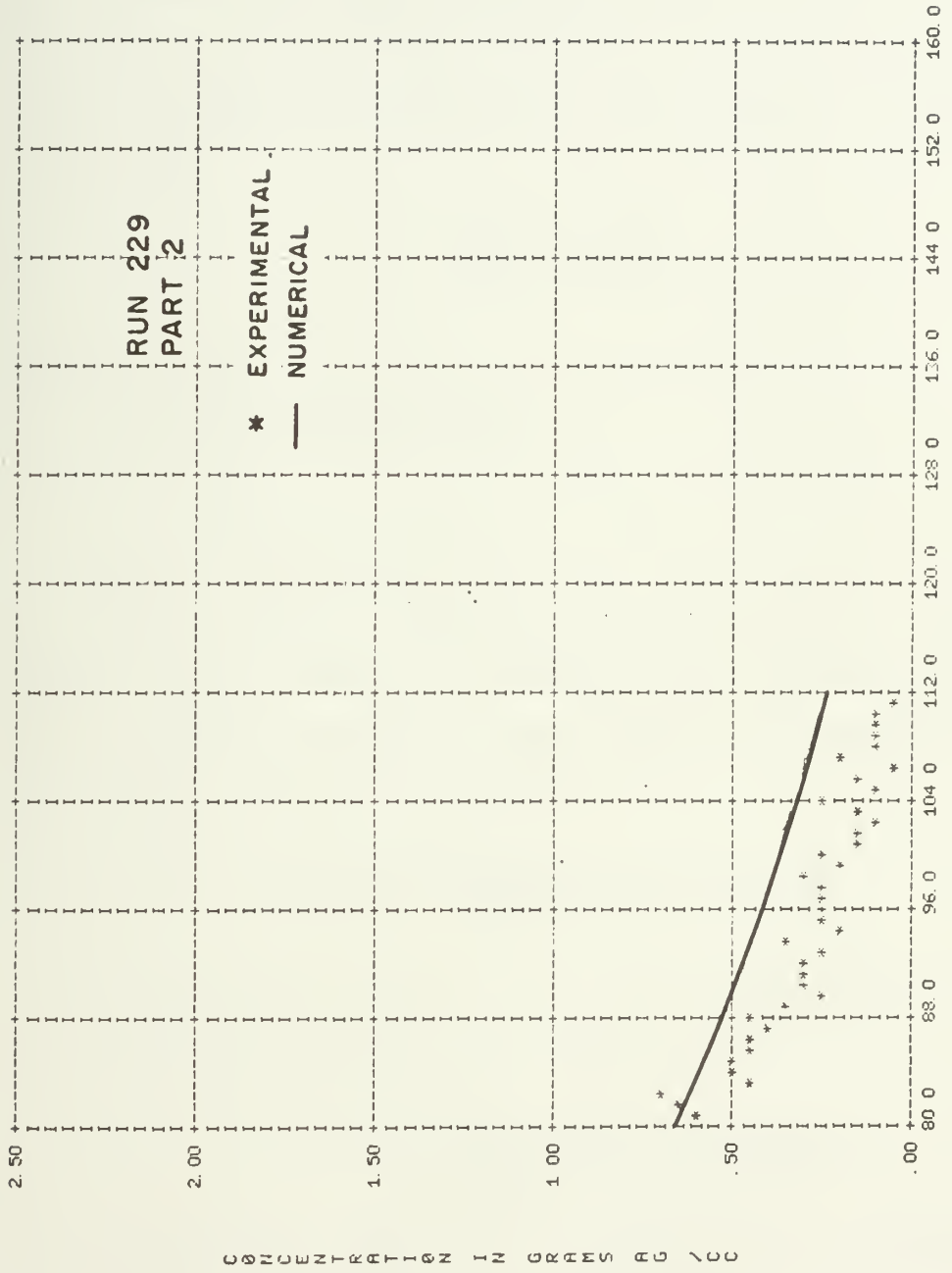

Figure 23 (Cont'd.)

chemical diffusivity as a function of temperature, the following analytical procedure was used.

In the case of the thin film incremental couples, it was assumed that Fick's second law for one dimensional diffusion is a valid approximation to the measurement of the rate of change of concentration with respect to time, and is written;

$$\frac{\partial C}{\partial t} = D \frac{\partial^2 C}{\partial x^2} \tag{16}$$

where $D \neq D(C)$; $D \neq D(x)$

C = mass concentration

t = time

x = distance

The solution to equation (16), if we have a thin (with respect to the lateral direction) strip centered at $x = 0$, with an initial thickness (with respect to the lateral direction) δ and concentration C_1 is

$$C(x,t) = \frac{C_1(0,0)\delta}{2\sqrt{\pi Dt}} \exp\left(-\frac{x^2}{4Dt}\right) \tag{17}$$

A thin strip centered at $x = \delta$, with an initial thickness δ and concentration C_2, gives

$$C(x,t) = \frac{C_2(\delta,0)\delta}{2\sqrt{\pi Dt}} \exp\left(-\frac{(x-\delta)^2}{4Dt}\right) \tag{18}$$

For an arbitrary collection of thin strips of thickness δ, for example, and arbitrary initial profile

$$C(x,t) = \sum_{n=-\infty}^{+\infty} C_n(x,t) = \sum_{n=-\infty}^{+\infty} \frac{C_n(n\delta,0)\delta}{2\sqrt{\pi Dt}} \exp\left[-\frac{(x-n\delta)^2}{4Dt}\right] \qquad (19)$$

The thin film incremental couple was assumed to represent a collection of thin strips of lateral thickness δ, and perpendicular thickness t (measured film thickness). The lateral strip thickness δ was chosen to be 0.8 microns, the distance between experimental data points. For the case of the initial concentration profile of Figure 16, the concentration of each thin strip was determined by the following relationship

$$C_n(n\delta,0) = \left[C_n(n\delta,0) + C_{n+1}((n+1)\delta,0)\right]/2 \qquad (20)$$

or the average concentration between two successive experimental concentration data points.

A computer program was written to numerically solve equation (19), for time = 24 hours, and a series of expected values of D, using the experimental data points of the initial concentration profile, and is shown in Appendix E.

On the basis of the numerical results of the computer solution to equation (19) the linear least squares slope of the numerically solved concentration profile, between the values of 1.56 and 0.56 grams Ag/cc, was chosen as the test parameter to compare the experimental profiles of Figures 17 through 23.

The linear least squares slope was determined using the statistical procedures of Volk [39], and included a test for the standard error of the estimate, sum squares deviation of y (concentration), coefficient of correction, and variance of slope. The statistical procedures are written into both the computer plotting program for the experimental profiles, (Appendix D), and the computer program which solves equation (19) (Appendix E).

Table 4 summarizes the statistical calculations for the annealed profiles and compares them with the numerical solutions of equation (19).

From the comparison of slopes of the annealed profiles with the numerical slopes of the solution of equation (19), values of D were determined. The concentration profiles generated from the numerical solution of Run 227 using equation (19) are drawn for the appropriate value of D on each experimental concentration profile shown in Figures 18-23. Figure 24 shows a plot of ln D versus 1/T for the 24 hour anneals at 200, 250, 300, 350 and 416°C. The experimental data fit the equation

$$D = 1.9 \times 10^{-7} \exp\left(-\frac{10,900}{RT}\right) cm^2 sec^{-1} \qquad (21)$$

In addition, the values of D, for the 12 and 48 hour annealed profiles at 416°C, are reported in Table 4. These values were determined in a manner similar to the 24 hour anneal, with the slope of their respective concentration profiles between 1.56 and 0.56 grams Ag/cc compared with

Table 4. Summary of the Statistical Calculations of the Incremental Thin Film Couples.

Run	Time of Anneal (hours)	Temperature of Anneal (°C)	$\frac{1000}{T}$ ($°K^{-1}$)	Slope	Standard Error of the Estimate
225	24	300	1.745	-.0526	.0644
226	24	350	1.605	-.0392	.0876
227	0	25	—	-.2858	.0238
228	24	416	1.451	-.0226	.0786
229	48	416	1.451	-.01885	.0818
230	24	250	1.912	-.0834	.0605
231	12	416	1.451	-.0355	.0412
232	24	200	2.114	-.1407	.0227

Run	Coefficient of Correlation	Variance of Slope	Numerical D Based on Exp. Slope (cm^2/sec)	Lower Estimate of D	Upper Estimate of D
225	.9815	.0020	1.3×10^{-11}	1.1×10^{-11}	1.6×10^{-11}
226	.9622	.0020	2.4×10^{-11}	1.9×10^{-11}	3.2×10^{-11}
227	.9920	.0210	——	——	——
228	.9643	.0009	7.4×10^{-11}	4.9×10^{-11}	1.1×10^{-10}
229	.9535	.0008	5.3×10^{-11}	4.0×10^{-11}	9.3×10^{-11}
230	.9756	.0050	5.2×10^{-12}	4.6×10^{-12}	5.9×10^{-11}
231	.9879	.0010	5.9×10^{-11}	4.2×10^{-11}	9.7×10^{-11}
232	.9970	.0037	1.8×10^{-12}	1.6×10^{-12}	1.9×10^{-12}

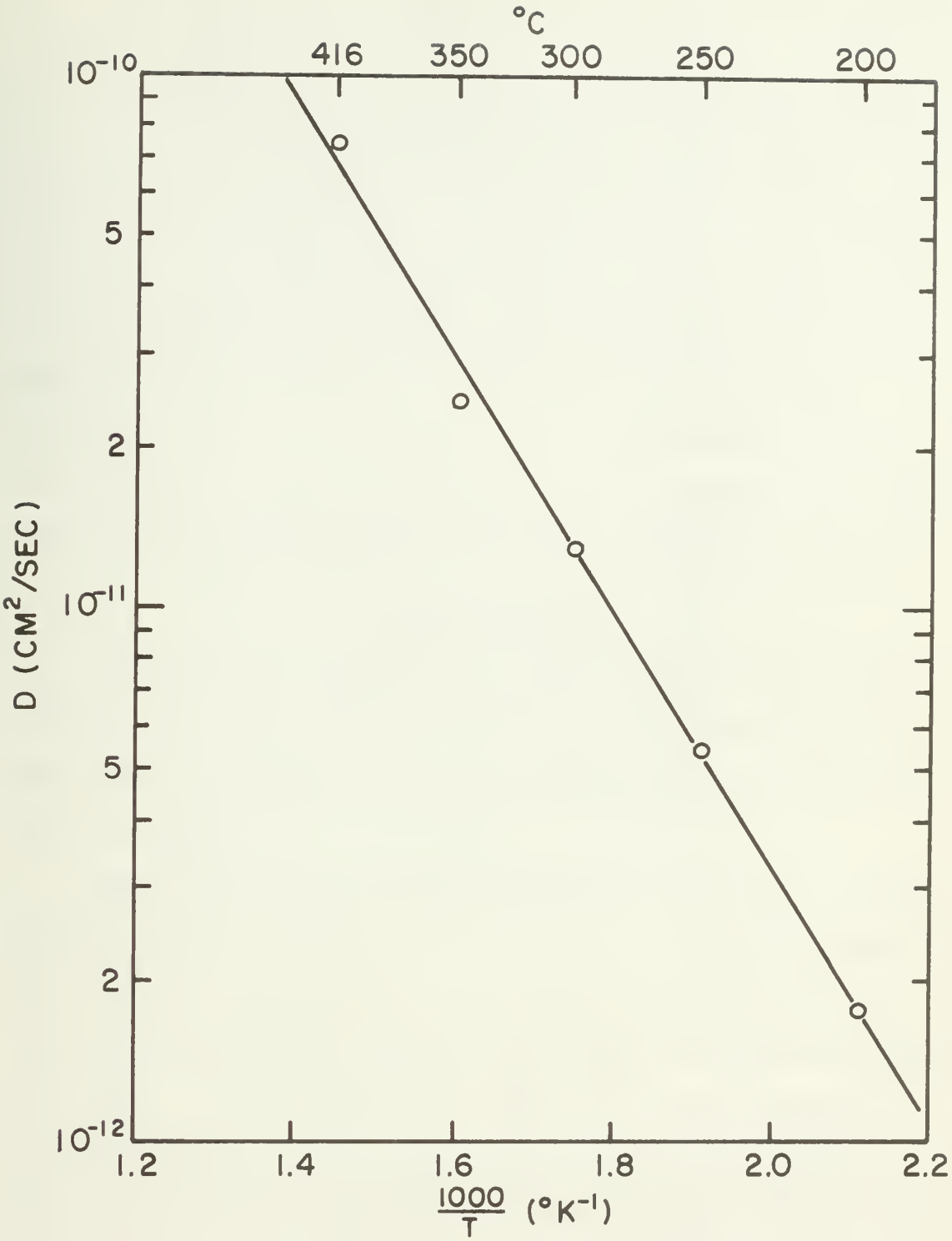

Figure 24

Plot of Ln D versus 1/T for the Incremental Thin Film Couples Annealed for 24 Hours.

the numerical solution with the corresponding times entered into equation (19).

Grain size determinations, using the transmission mode of the electron microscope, were made on each couple. The grain size varied between 1,000 and 2,000 Å on all couples observed. No variation across each couple, including the diffusion zone was observed. Figure 25 shows photomicrographs of the grain distribution in the 200 and 350°C couples. Figures 26 through 28 are photographs of the surfaces of selected incremental couples showing the change in surface structure with increasing deposition temperature.

Ag-Au Couples

Table 5 is a summary of the experimental test conditions of Runs 201 - 223. Each run involved the deposition of a pure gold film layered side by side with a silver film of equal thickness.

Runs 202 through 212 have comments in Table 5, listing reasons for the author's inability to use them for quantitative results. The problem occurring in the initial runs (202 - 206) was film breakup (dewetting) of the gold side of the couple. Along with this, there was some interesting particle shaping of the resultant discrete gold islands observed, such as smooth equilateral triangles, like those observed [40] in epitaxial gold films on [111] surfaces of M_0S_2, and particle shapes observed by Sundquist [41].

A.

B.

Figure 25

Transmission Electron Micrograph of Section of the Surface of Unsupported Thin Film. 23,000×

A. Gold Side of Incremental Thin Film Couple Annealed at 200°C for 24 Hours.

B. 80%Au-20%Ag Side of Incremental Thin Film Couple Annealed at 350°C for 24 Hours.

Figure 26

Scanning Electron Photograph of the Surface of the Unannealed Incremental Thin Film. Couple (Run 227) Showing Interface Region Film at 45° Tilt to the Electron Beam 10,000×.

Figure 27

Scanning Electron Photograph of the Surface of the Incremental Thin Film Couple Annealed at 250°C for 24 Hours, Showing Interface Region. Film at 45° Tilt to the Electron Beam. 10,000×.

Figure 28

Scanning Electron Photograph of the Surface of the Incremental Thin Film Couple Annealed at 416°C for 24 Hours, Showing Interface Region. Film at 45° Tilt to the Electron Beam. 10,000×.

Table 5. Summary of Experimental Conditions of Runs 201 through 223. (Ag-Au) Couples

Run	Temperature of Anneal* (°C)	Time of Anneal (hrs)	Film Thickness (Å)†	Comments
201	25	0.0	1000‡	used as time = 0 profile for Ag-Au couples.
202	675	5.0	1000‡	excessive breakup (dewetting) of gold portion of couple
203	575	16.00	1000‡	same as 202
204	500	2.0	1000‡	partial dewetting of gold side; no interface contact
205	675	0.0	1080	excessive surface roughness of gold and silver; partial dewetting
206	500	0.0	1000‡	same as 205
207	428	0.0	1000‡	no interface contact
208	416	24.0	1550	wide region of mixing
209	416	48.0	1500‡	no interface contact
210	416	48.0	1500‡	same as 209
211	416	48.0	1500‡	same as 209
212	416	48.0	1500‡	same as 209
213	416	48.0	1000	run 201 annealed
214	416	96.0	1000	run 201 annealed; dewetting of gold
215	416	72.0	1000	run 201 annealed
216	416	24.0	1520	
217	416	48.0	1540	
218	416	12.0	1510	
219	416	2.0	1490	
220	300	48.0	1560	
221	300	24.0	1500‡	no interface contact
222	300	24.0	1470	
223	300	12.0	1490	

* ± 1°C.
† ± 50 Å
‡ not measured on Dektac

Three (3) runs, 213, 214 and 215 were made, using sections of the 1,000 Å unannealed couple (Run 201), at 416°C for times of 48, 72 and 96 hours. The formation of a porous zone, running parallel to, and on the silver side of the interface, was observed in the couples annealed for 48 and 72 hours. In addition, a zone of protrusions was observed on the gold side of the interface. The porous zone was so extensive that complete film separation occurred. The width of the porous zone was slightly larger on the 72 hour couple. In the couple annealed for 96 hours, the film separation due to the porous zone was evident. However, dewetting was observed on the gold side of the film, with particle shaping like that described above for films deposited at higher temperature. The silver side of the couple also exhibited extensive pitting, and investigation on the scanning electron microscope revealed a high degree of surface roughness. Subsequently, no quantitative study of diffusion was undertaken for these runs.

Runs 216 through 219 involved the deposition of 1,500 Å thin film couples at 416°C, for annealing times of 2, 12, 24 and 48 hours. Again, the formation of the porous zone and surface protrusions were observed on the silver and gold side of the original interface, respectively. Figures 29 through 32 show photomicrographs of the respective interface region of the four (4) couples. Figure 33 is a scanning electron photograph of the interface region showing the porous zone, and the associated surface protrusions.

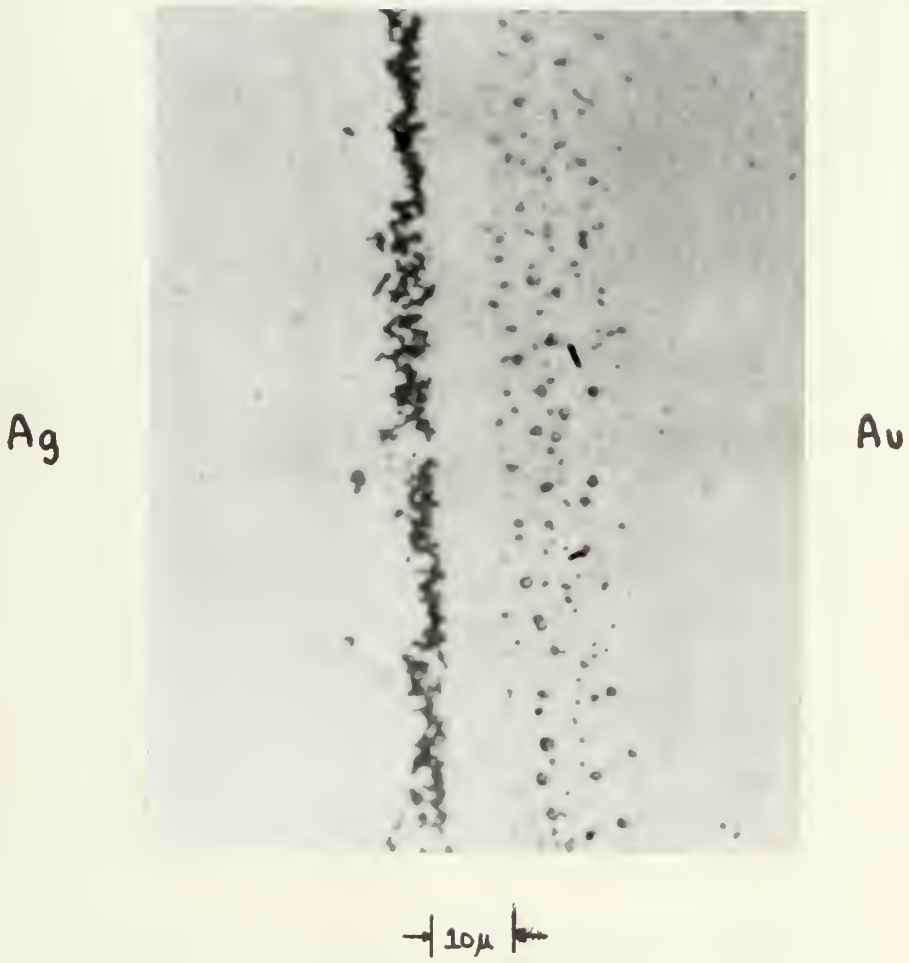

Figure 29

Optical Microscope Photograph of Interface Region of Ag-Au Thin Film Couple Annealed at 416°C for 2 Hours. 1080×.

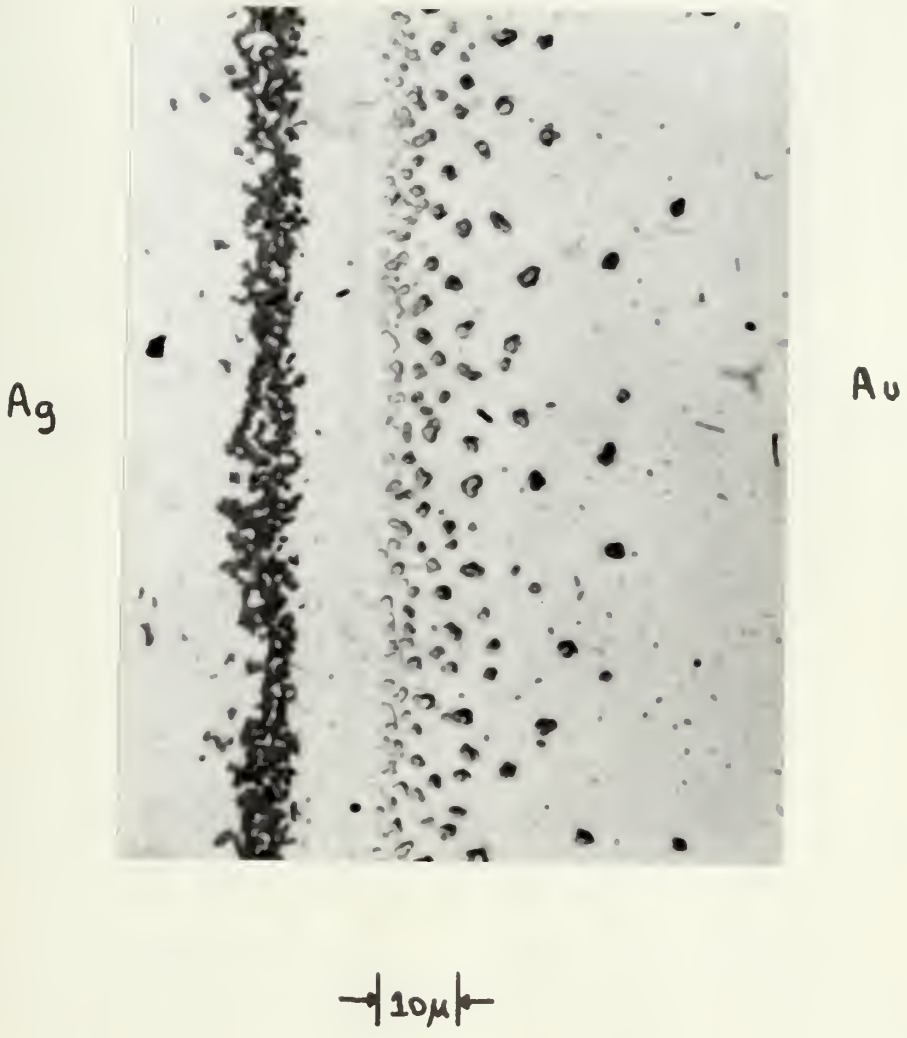

Figure 30

Optical Microscope Photograph of Interface Region of Ag-Au Thin Film Couple Annealed at 416°C for 12 Hours. 1080×.

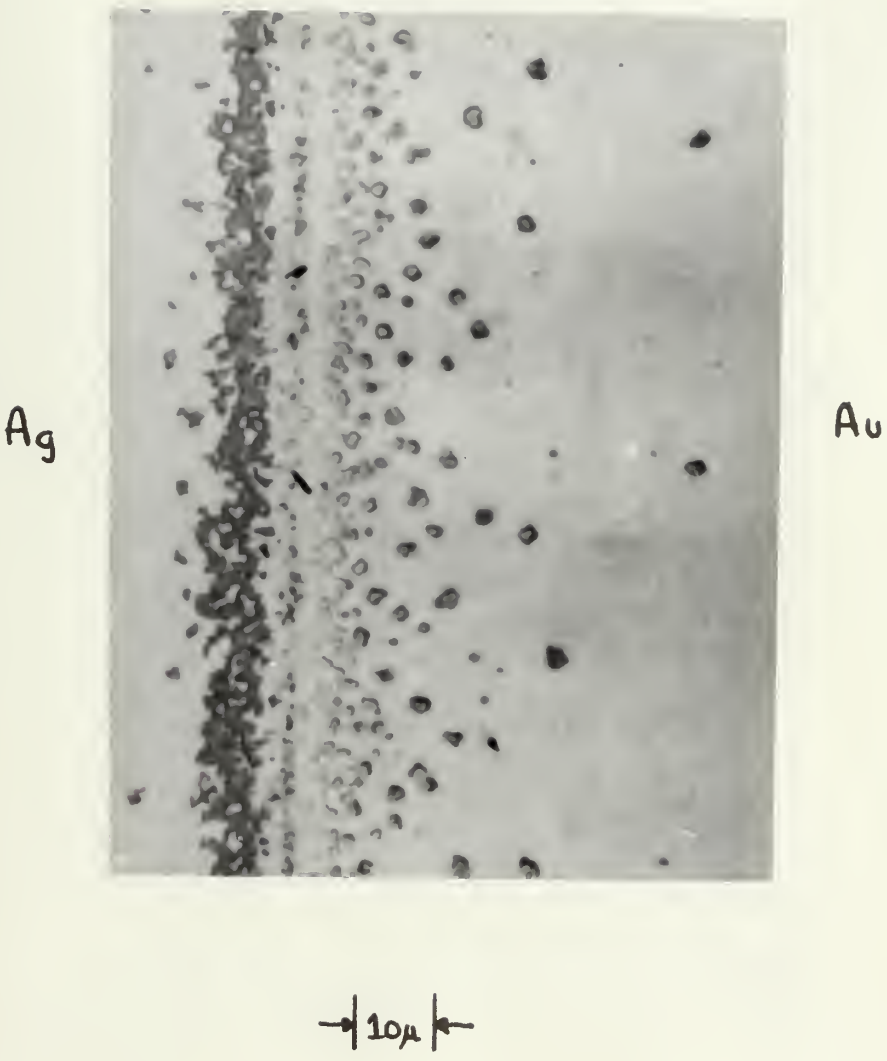

Figure 31

Optical Microscope Photograph of Interface Region of Ag-Au Thin Film Couple Annealed at 416°C for 24 Hours. 1080×.

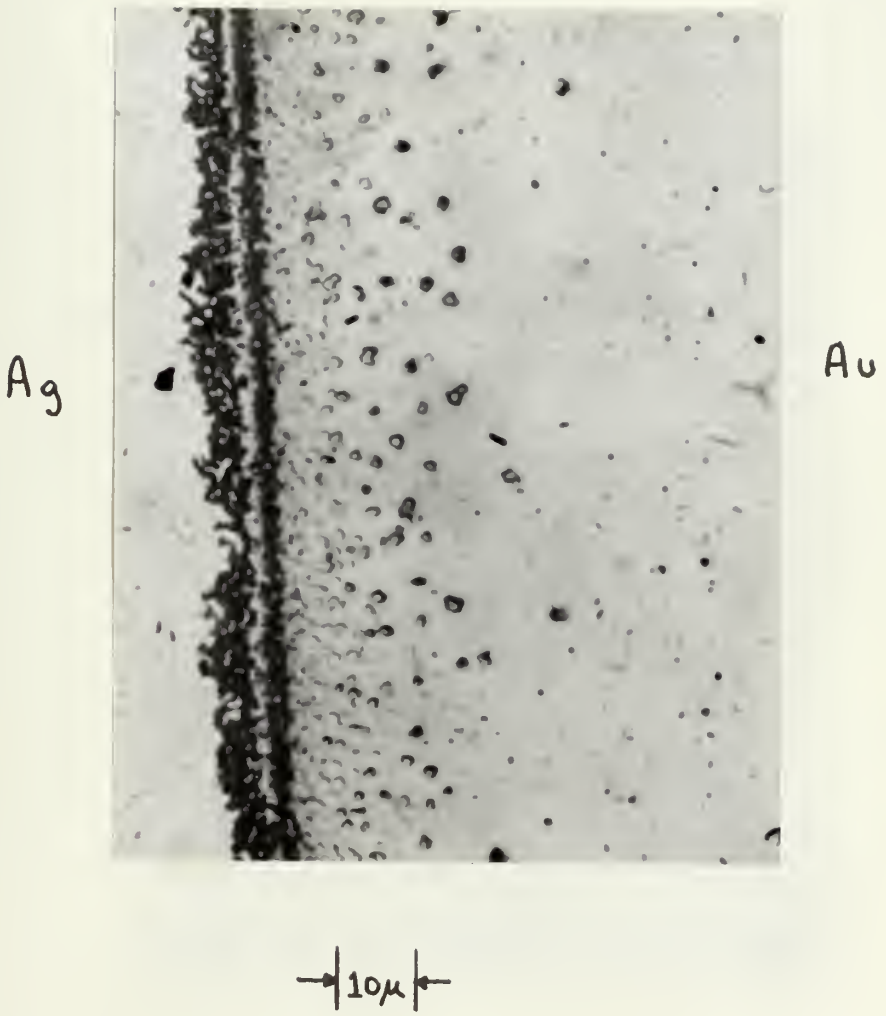

Figure 32

Optical Microscope Photograph of Interface Region of Ag-Au Thin Film Couple Annealed at 416°C for 48 Hours. 1080×.

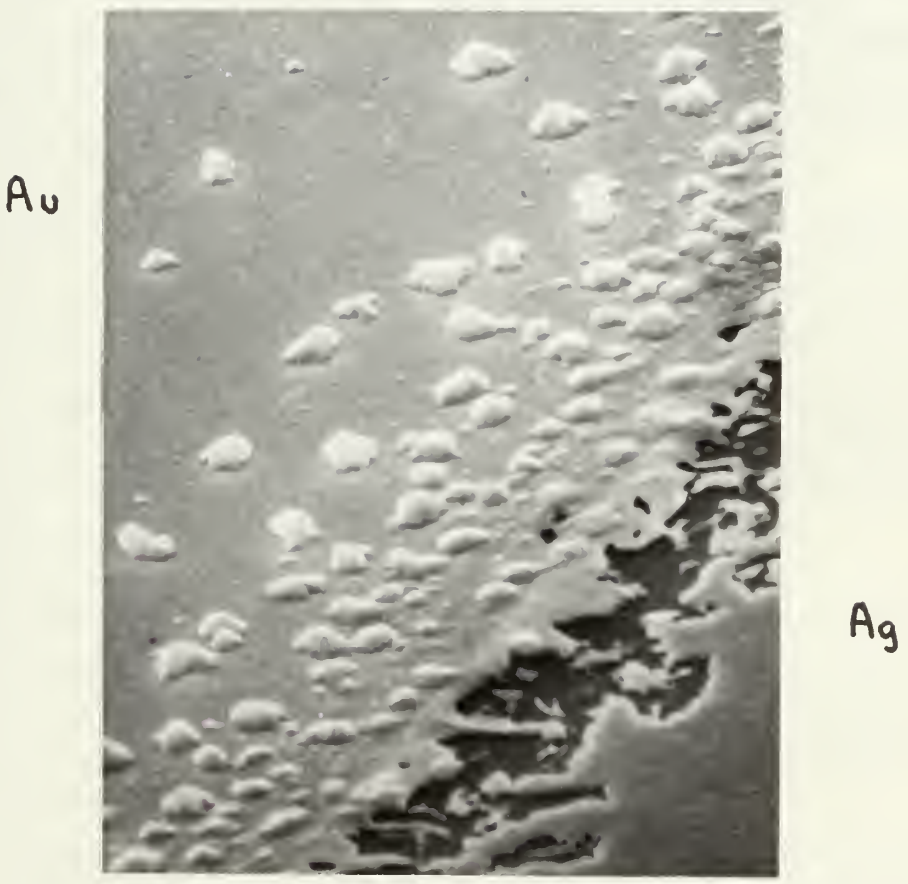

Figure 33

Scanning Electron Photograph of Interface Region of Ag-Au Thin Film Couple Annealed at 416°C for 24 Hours. Film at 45° Tilt to the Electron Beam. 3,000×.

An investigation of the chemical composition of the surface protrusions was undertaken by measuring characteristic x-ray lines generated from the electron beam of the scanning electron microprobe. For a counting time of 200 seconds, the counts of the Lα lines of the silver and gold remained constant with the electron beam, on and off, 4 different surface protrusions. The silicon counts decreased to one-half their original value when the electron beam was on a surface protrusion.

Characteristic x-ray measurements were also taken for Runs 216 - 219 as a function of lateral distance on the electron microprobe. A computer program similar to that used for the incremental couples, converted the intensity counts to units of mass concentration. The direct computer output of the couples are shown in Figures 34-37.

Because of the formation of the porous zone and associated protrusions, there was film thickness variation as a function of lateral distance, thus the concentration-distance profiles were suspect.

A scanning electron microprobe investigation of the couples, however, indicated the presence of silver on the gold side of the porous zone extending away from the interface approximately the same distance as indicated by the concentration-distance profiles. No counts of gold were observed on the silver side of the porous zone.

Figure 34

Concentration versus Relative Distance for Ag-Au Thin Film Couple

Annealed at 416°C for 2 Hours.

Concentration "Pulse" is shown Symmetrically about Edge of Porous Zone.

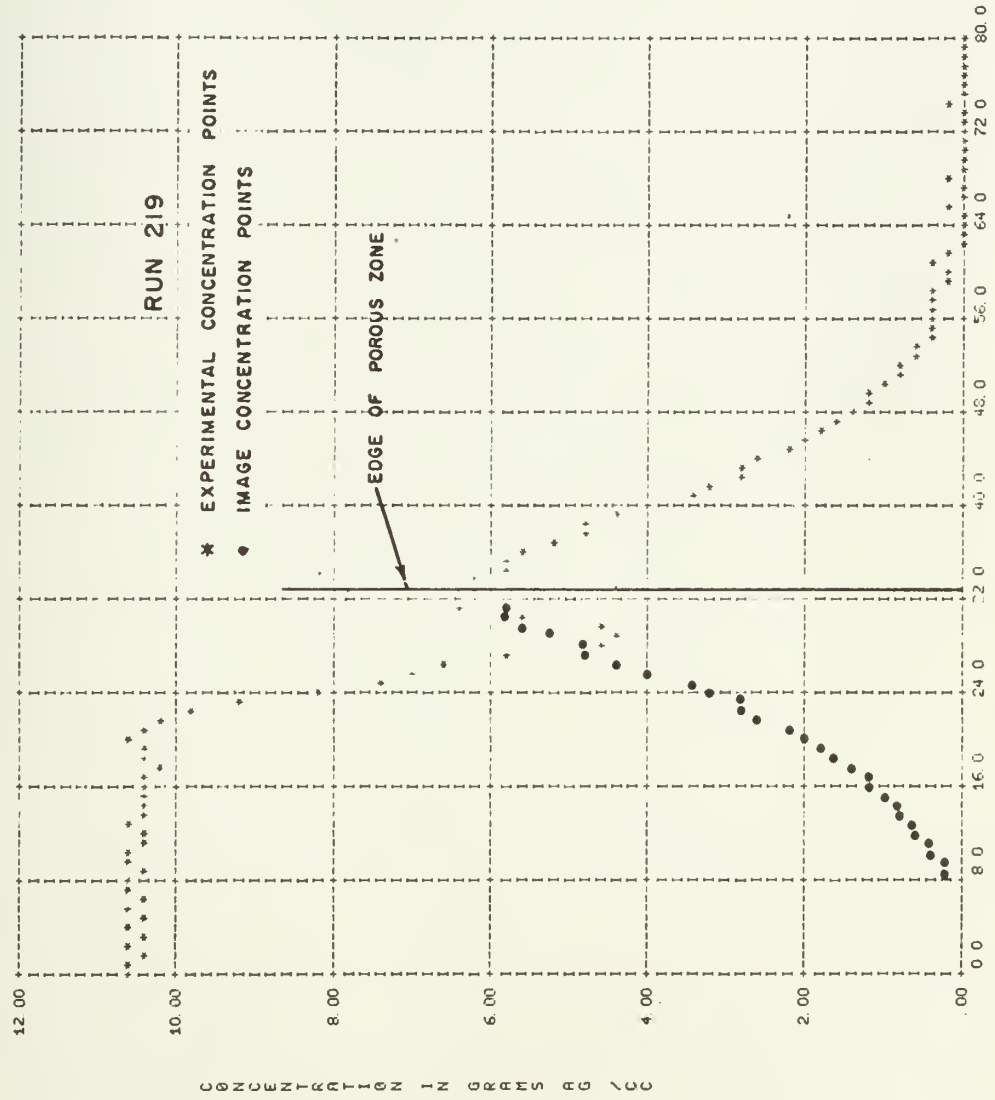
RUN 219
* EXPERIMENTAL CONCENTRATION POINTS
• IMAGE CONCENTRATION POINTS
EDGE OF POROUS ZONE
CONCENTRATION IN GRAMS AG /CC
RELATIVE DISTANCE (MICRONS)
12.00
10.00
8.00
6.00
4.00
2.00
.00
0.0
8.0
16.0
24.0
32.0
40.0
48.0
56.0
64.0
72.0
80.0

Figure 34

Figure 35

Comparison of Numerical Solution of Concentration "Pulse" with Experiment

Concentration Profile for Ag-Au Couple Annealed at 416°C for 12 Hours

(t' = 10 hours)

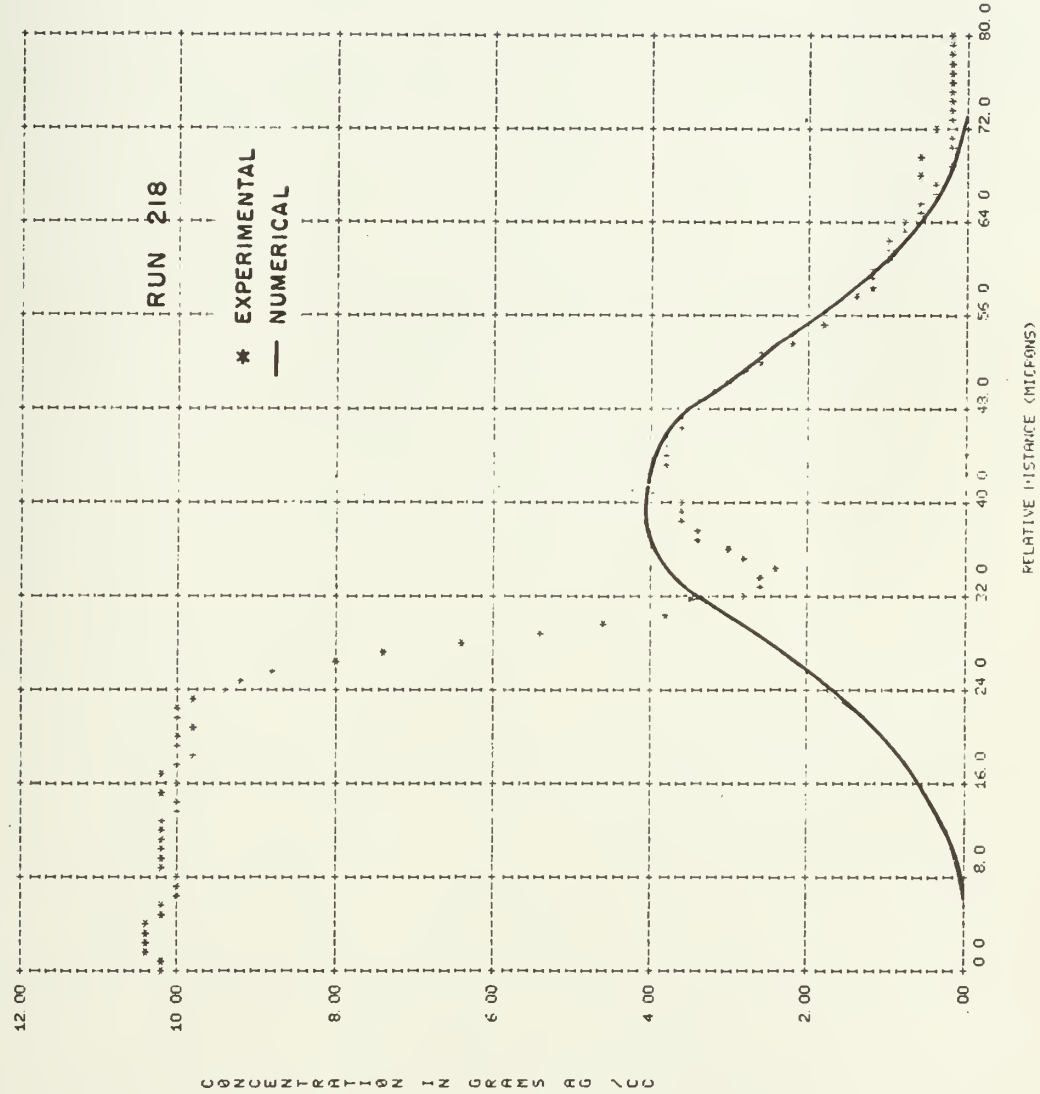
RUN 218
* EXPERIMENTAL
— NUMERICAL
CONCENTRATION IN GRAMS AG /CC
12.00
10.00
8.00
6.00
4.00
2.00
.00
0.0
8.0
16.0
24.0
32.0
40.0
48.0
56.0
64.0
72.0
80.0
RELATIVE DISTANCE (MICRONS)

Figure 35

Figure 36

Comparison of Numerical Solution of Concentration "Pulse" with Experimental Concentration Profile of Ag-Au Couple Annealed at 416°C for 24 Hours (t' = 22 hours)

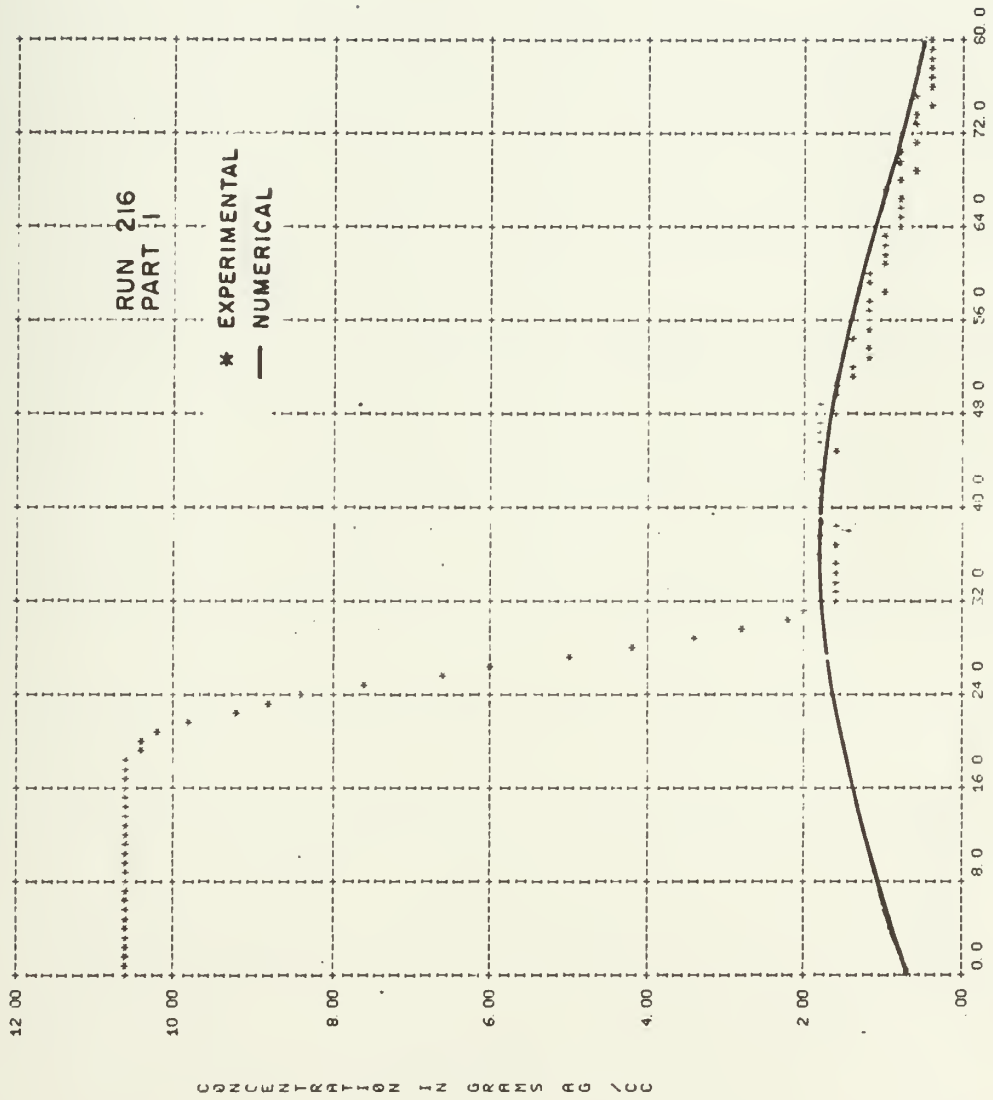
RUN 216
PART 1
* EXPERIMENTAL
— NUMERICAL
CONCENTRATION IN GRAMS AG /CC
12.00
10.00
8.00
6.00
4.00
2.00
.00
0.0
8.0
16.0
24.0
32.0
40.0
48.0
56.0
64.0
72.0
80.0
RELATIVE DISTANCE (MICRONS)

Figure 36

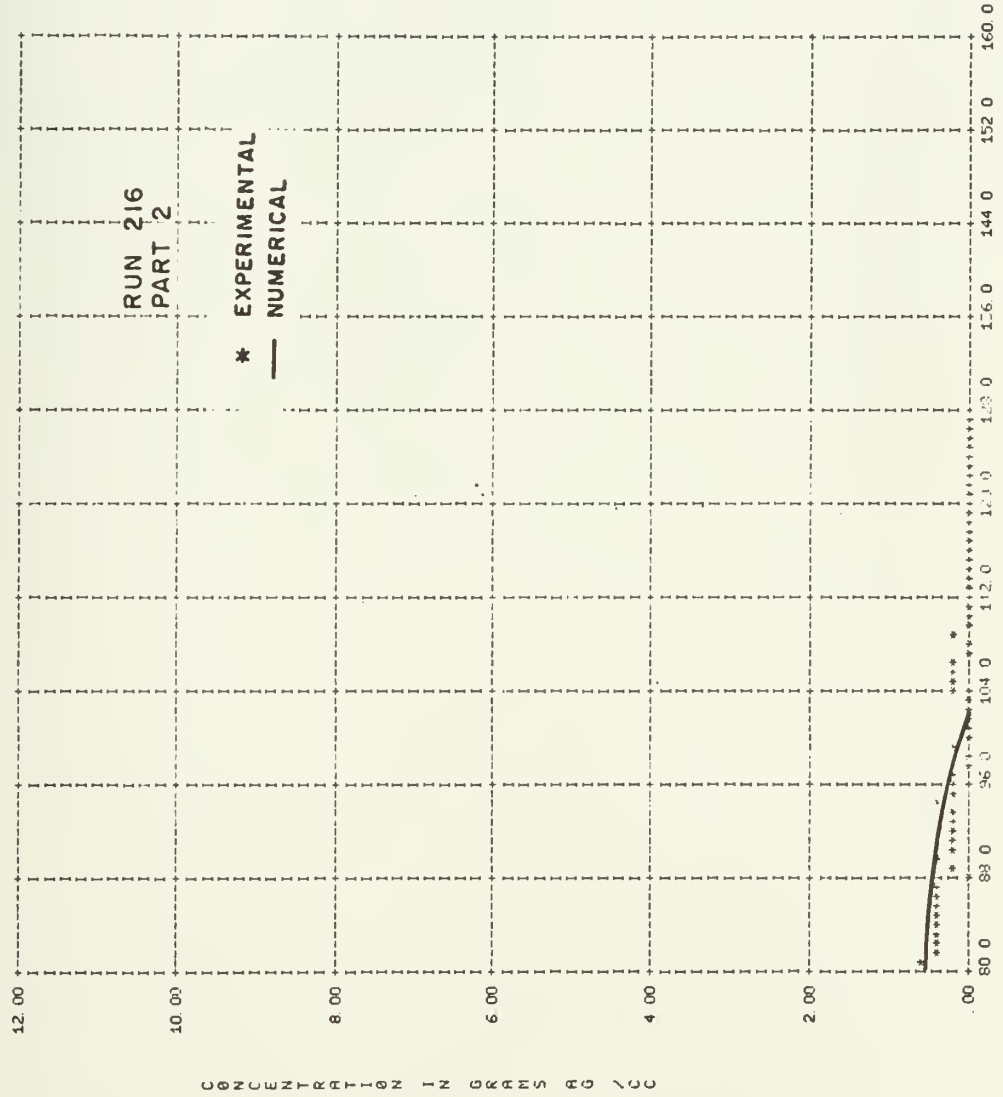

Figure 36 (Cont'd.)

Figure 37

Comparison of Numerical Solution of Concentration "Pulse" with Experimental Concentration Profile of Ag-Au Couple Annealed at 416°C for 48 Hours (t' = 46 hours)

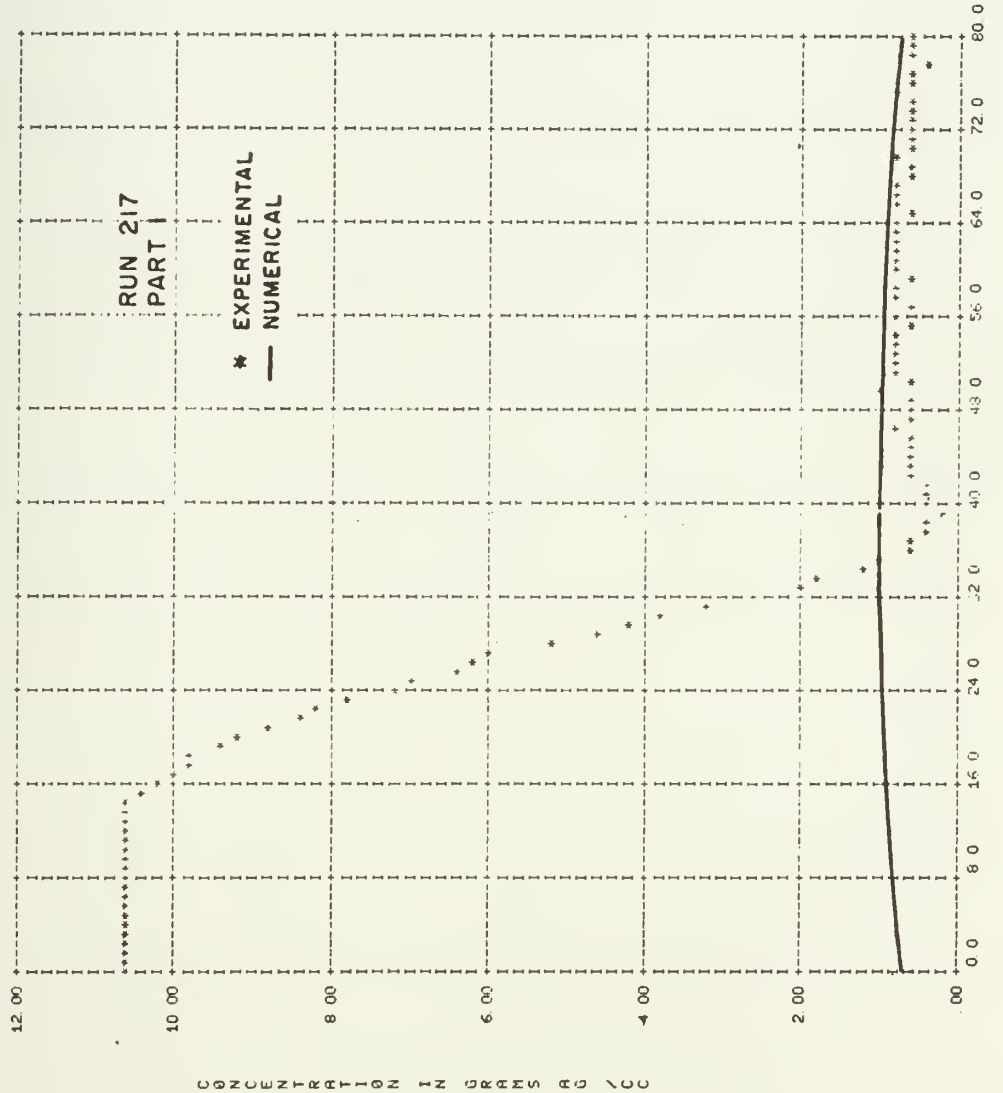
RUN 217
PART I
* EXPERIMENTAL
— NUMERICAL
CONCENTRATION IN GRAMS AG /CC
12.00
10.00
8.00
6.00
4.00
2.00
.00
0.0
8.0
16.0
24.0
32.0
40.0
48.0
56.0
64.0
72.0
80.0
RELATIVE DISTANCE (MICRONS)

Figure 37

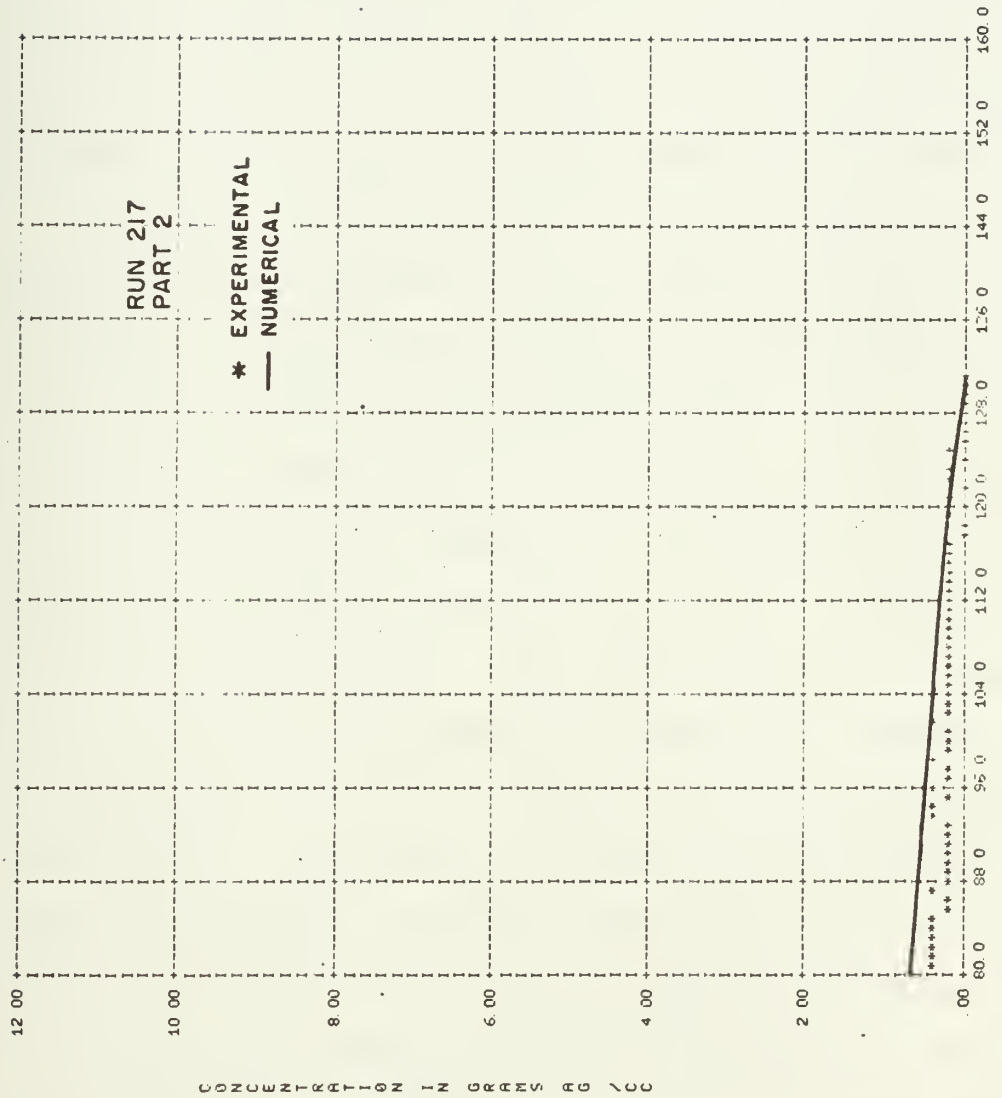

Figure 37 (Cont'd.)

The dip in the concentration value observed in the concentration-distance profiles was taken as a representative of the center of the porous zone. A computation of the area under the concentration profile from the center of the dip on into the gold region (increasing relative distance) was made on each profile. The area was determined using a computer program written to numerically integrate, employing Simpson's rule. The results are summarized in Table 6.

A computer program similar to that of Appendix E was written to treat the peak in concentration observed in the 4 couples. Run 219 (Figure 34), the couple annealed for 2 hours, was treated as the initial profile (time = 0) and the values of concentration on the gold side of the porous zone was fed into the computer program along with a complimentary set of image concentration values to make the initial profile an even function. The reduction in peak height of the 12, 24 and 48 hour annealed couples was compared with the numerical solution for times of 10, 22 and 46 hours respectively. The numerical solution to the concentration "pulse" of Run 219 is drawn on each concentration profile for an appropriate value of D. D values of 1, 5 and $9\times10^{-11}cm^2/sec$ fit the experimental profiles for the 12, 24 and 48 hour anneal, respectively (Figures 35-37).

Runs 220 - 223 were 1,500 Å thick thin film couples of Ag and Au annealed at 300°C for 12, 24 and 48 hours. The formation of a porous zone and associated surface protrusions

Table 6. Comparison of Area under Concentration Curves from the Edge of Porous Zone into the Pure Gold Region of the Couple. For Runs 216-219, Annealed at 416°C

Run	Microprobe Scan No.	Time of Anneal (hours)	Area (conc. microns)	Average Area
219	1	2	61.9	58.4
219	2	2	54.8	
218	1	12	62.1	60.2
218	2	12	58.4	
216	1	24	54.0	51.7
216	2	24	49.3	
217	1	48	40.1	37.7
217	2	48	35.3	

were again evident. The width of the porous zone of the 12 hour annealed couple was similar to that of the 2 hour annealed couple at 416°C. The porous zone enlarged with time, and film separation was evident in the couple annealed for 48 hours (Run 220). X-ray measurements as a function of lateral distance were made on the electron microprobe and the data were converted to units of mass concentration as described above. However, the porous zone of the 12 hour annealed sample was so small in extent that the dip in concentration was not evident. Therefore, the semi-quantitative technique to determine the rate of silver penetration, as described above, was not attempted.

DISCUSSION

Thin Film Standards

The linearity (high degree of correlation) observed between the microprobe intensity and film thickness for all the data exhibited in Tables 1 and 2 suggests that the thin film approximation, intensity is proportional to mass thickness, is a valid assumption throughout the entire composition range of the gold-silver system, for the film thickness studied. The reader is cautioned, however, that the numerical measurements are only valid for gold and silver films on a silicon substrate with a 1,500 Å oxidized layer on the surface.

The statistical equations used in the analysis of thin film standards, and subsequent work on thin film couples, are shown in Appendix F.

The maximum deviation from linearity occurred with the 2,000 Å films as should be expected, especially in the case of pure gold films where I/I_{bulk} was approximately 0.6. The maximum relative error, .25, in the empirical conversion parameter, was observed in the measurements taken off the silver spectrometer for films between 500 and 2,000 Å. Because of the small relative error, one conversion parameter was used. The parameter was determined from a linear

least squares fit of all the data, representing the relationship between measured relative intensity and weight fraction composition for films of thickness between 500 and 2,000 Å. Again, the largest deviation from the straight line fit occurred for the 2,000 Å films of high gold composition, where the thin film approximation became suspect.

The relation between an error in the empirical conversion parameter and errors in the calculated composition value is given by the usual expression

$$\Delta C = \frac{dC}{da} da \tag{22}$$

and from equation (2)

$$\frac{dC}{da} = C(1-C)/a. \tag{23}$$

The error in composition is

$$\Delta C = C(1-C)\Delta a/a \tag{24}$$

The maximum absolute error in composition is one-fourth ($\frac{1}{4}$) of the relative error in the conversion parameter, or (.25)(.25) which is approximately 6 weight %.

This, however, is based on the assumption that the composition of the standards is known to within negligible limits of the error of the calculated value.

The determination of the composition of the thin film standards used in the experimental work of this author was based on the assumption that the thin film density in both the pure and alloy states was that of the reported bulk value

discussed in the Background and Literature Survey section.

Hartmann [42] obtained bulk values for Au and Ag at thicknesses down to 200 Å. However, Blois and Reiser [43] found the density of Ag films to approach bulk values at a thickness of 1,200 Å. The data of [43] are suspect [57], for silver, which readily forms a surface oxide layer, lowering the effective density of the film.

This author, in the initial stages of determining the orientation relationship between the mass deposited on the monitoring crystals and that of the substrate, made three determinations each between the frequency shift of the crystal and measured thickness (Dektac) of pure gold and silver films. Using the relationship,

$$\Delta f = \beta \rho t \quad , \tag{25}$$

where Δf = frequency shift of the crystal

t = film thickness

β = substrate-crystal-source orientation parameter,

ρ = film density

a linear relationship was observed between Δf and the measured value of film thickness. Solving equation (25) for ρ_{Ag} and ρ_{Au} respectively, a bulk value was obtained within the relative error of the measured film thickness. If the standards are assumed to be of bulk density, then the major source of error is the measurement of film thickness, ± 50 Å. The error in composition can be written

$$\Delta C(\text{atomic } \%) = \frac{\Delta t_{Ag}/t_{Ag}}{\frac{\Delta t_{Ag}}{t_{Ag}} + \frac{\Delta t_{Au}}{t_{Au}}} \qquad (26)$$

which has a maximum value of ± 10 atomic % for film thickness of 500 Å and at each extreme of the composition range.

Ag-Au Couples

The experimental observations of film breakup on the gold side of the thin film couple suggest that the mechanism of atomic reorientation manifests itself as a function of time and temperature, and can be attributed to an annealing effect. The agglomeration of the gold side of the couple observed in Runs 202 - 206, at substrate temperatures above 500°C, was only observed at the conclusion of the anneal. The initial condition of the film, immediately after film deposition was in doubt and the observed effects, when compared to that of Run 201, could only be attributed to the substrate temperature. However, in the series of runs at 416°C (Runs 213 - 215) the 1,000 Å film deposited at room temperature (Run 201) was used, and the following anneal led to agglomeration of the gold after 96 hours (Run 214).

If a polycrystalline material is annealed, grooves develop at the intersection of the grain boundaries with the metal-vapor surface. If it is assumed that the grain boundaries do not move during annealing, then it can be expected that the groove depth (d) deepens with time. Mullins' [44] well known analysis of grain boundary grooving kinetics was

applied to the thin films of the present work, thus

$$d = \frac{(0.486)\gamma_B}{\gamma_S}\left[\frac{D_s\gamma_S\Omega^2 N t}{kT}\right]^{\frac{1}{4}} \qquad (27)$$

where d = depth of groove

γ_B = specific free energy of the grain boundary

γ_S = specific free energy of the surface

D_s = surface diffusion coefficient

k = Boltzmann's constant

T = temperature of anneal (°K)

t = time of anneal

N = number of surface atoms/unit area

Ω = volume per atom

In order to relate the experimental observations of the gold film breakup, a two stage model was proposed. In the initial stage there would be groove deepening to the substrate, the depth of the groove equal to the original film thickness. Secondly, the hole grows, with critical size agglomerates (adjacent to the holes) growing at the expense of the surrounding metal.

If equation (27) is evaluated at 416°C, (temperature of anneal of couple where gold agglomeration occurred after 96 hours) using the following values,

γ_S = 1450 from [49]

γ_B = 450 from [49]

$\Omega = 1.7 \times 10^{-23}$ cm^3

$N = 1.2 \times 1.15$ cm^{-2}

$D_S = 5 \times 10^{-8}$ cm^2/sec for Au at 416°C from [51]

$D_S = 6 \times 10^{-11}$ cm^2/sec for Ag at 416°C from [51]

The depth of the groove would equal 1,000 Å (film thickness) for annealing times of 62 and 2.5×10^4 hours for gold and silver respectively.

In the case of gold, we would expect groove deepening to the substrate after 62 hours. Following this, the anneal enables the film substrate system to lower its free energy by lowering its interfacial free energy. The motive force for the growth of an existing hole by surface diffusion is the surface tension vector sum of the film-substrate, substrate-vapor and film-vapor interfaces. The flow of migrating atoms is due to the difference in chemical potential at regions of differing curvature.

Presland et al., [45 and 46] in a series of two articles applied the theories of Mullins [44] to his experimental observations in annealed thin films of silver. He showed that following an induction period (hole deepening to the substrate with subsequent hillock growth) that further hillock growth followed, with critical size agglomerates growing at the expense of surrounding areas. The continuing hole growth resulted in a decrease in metal-substrate interfacial area, resulting in the separation of agglomerates (film breakup).

Brandon and Bradshaw [47] showed that the surface self diffusion coefficient of silver is increased in the presence of oxygen. Presland could only produce agglomeration in his

high vacuum deposited silver films when the silver vapor-metal interface was exposed to oxygen pressures greater than 10^{-3}torr. Below $p_{O_2} = 10^{-3}$torr, he reported groove deepening with subsequent hillock growth. However, the catchment area for the critical size agglomerates increased rapidly with decreasing p_{O_2}, suggesting changes in surface tension and the surface self diffusion coefficient with oxygen partial pressure. In comparison, gold agglomeration has been observed [48] in unsupported thin films in high vacuum.

The equilibrium shape of a particle on a substrate is determined by the vector sum of the interfacial free energies of the film, vapor, substrate system. If the observations of [46 and 47] are assumed to be operative for the gold film, then in conjunction with the sufficient groove deepening, as predicted by equation (27), the vector sum of the interfacial free energies is in accord to predict hole growth and subsequent agglomerates.

In the case of silver, the reduction of the film-vapor interfacial free energy, due to the presence of oxygen on the free surface of the silver as suggested by Presland [45, 46], would not be sufficient cause for hole growth.

More likely, the increase in the surface self diffusion coefficient due to oxygen pressure would reduce the time necessary for groove deepening to the substrate. Following groove deepening, a reduction in the substrate-vapor interfacial free energy due to oxygen pressure would be favorable for hole growth followed by film agglomeration.

The observed faceting on the gold film agglomerates could be attributed to the reported [41] surface anisotropy of gold. Gjostein [50], who provided some of the impetus for the studies of [45 and 46] in an earlier paper [51], is currently developing a manuscript to possibly improve on the studies of [45, 46 and 47] and should provide interesting reading when released.

To avoid the agglomeration of the gold film, further runs (216-223) were made at temperatures below 500°C and for annealing times only up to 48 hours. In each of these runs the porosity observations of bulk investigators with pure silver and gold sandwich couples were similarly reproduced in the thin film couples. The porosity increased with time and temperature of anneal. However, in contrast to the bulk counterpart, physical separation of the films occurred in the lateral direction.

The physical separation of the two regions of the film leads to thickness variations of the couple around the porous zone. The concentration profiles of Figures 34 to 37 were determined by assuming a uniform thickness across the diffusion zone. Therefore, in the region of the porous zone, the concentration profile is in error.

Secondly, the physical separation of the couple severely limits the atomic mobility of the two species. When this occurs, the quantity of gold and silver which had previously diffused into the silver and gold respectively, remains fixed

with time. The observation of the similarity of the areas under the concentration profiles of the 2, 12, 24 and 48 hour anneals confirms this conclusion. The smaller area observed in the 48 hour anneal (Run 217) can be attributed to the inability of the electron microprobe to detect the small concentration of Ag above background at distances far from the porous zone, and the corresponding increase in error of the empirical conversion parameter with low values of solute concentration.

The mass of silver remaining fixed with respect to time, after the formation of the porous zone, creates a set of boundary conditions different from that of an initial t = 0 profile. The series of photographs of the four anneals shown in Figures 29-32 indicate that physical separation of the couple is almost complete after the 2 hour anneal (Figure 29). On either side of the porous zone the film thickness is uniform, therefore the concentration profile of the 2 hour anneal can be taken to represent the new initial profile (t' = 0) and the 12, 24 and 48 hour anneals to represent values of t' = 10, 22 and 46 hours respectively.

The thin strip approximation was applied to the concentration "pulse" of silver observed on the gold side of porous zone of the t' = 0 profile. The center of the "pulse peak" indicated on Figure 34 was taken to represent the edge of the porous zone shown in Figure 29.

The exact solution [52] to the initial (t' = 0) concentration profile would be to represent the profile by f(x) and solve using a heat flow analogy. The porous zone would represent an impenetrable barrier (insulating medium). A numerical approximation to the exact solution was used, incorporating the thin strip approximation. The concentration "pulse" was made into an even function by reading into a computer program the image concentration values as shown in Figure 34. The thin strip approximation predicts a reduction in peak height with points of constant concentration moving laterally parabolically with time. The resultant fit to the t' = 10, 22 and 46 hour profiles shown in Figures 35 to 37 lends validity to the above approximation.

The reduction in D as the time of anneal increases can again be attributed to the errors in detecting small solute (Ag) concentration values and the rising error in the conversion parameter with decreasing solute concentration. Also, the errors in the thin strip approximation decrease as $\sqrt{Dt}$ increases relative to the assumed (0.8 microns) strip thickness (lateral direction). The value of D therefore, is probably somewhere between the results for the t' = 10 and 22 hour anneals. Averaging the two results gives a D of 7×10^{-11} $cm^2/sec.$ which closely represents what was reported for the incremental couples at 416°C.

An interesting observation was that of the secondary zone of porosity observed in the photographs for the 24 and

48 hour anneals (Figures 31 and 32). This could possibly be attributed to the new set of boundary conditions operative after the 2 hour anneal. The mass flow of silver in the t' framework could be viewed as a thin film of gold layered side by side of an alloy film of say 50 atomic % silver with only a 30 micron extent ($\frac{1}{2}$ width of concentration "pulse") in the lateral direction. The new set of boundary conditions would also shift the position of the original interface and the corresponding position of the maximum vacancy flux gradient [53].

This reasoning implies that the vacancy flux gradient must be a strong driving force for the nucleation of voids by an assimulation of excess vacancies. On the basis of energy considerations it would appear logical for the vacancies accumulating in the subsequent mass depletion zone to continue to annihilate themselves on the already formed voids in the original porous zone.

The x-ray investigation on the scanning electron microscope of the surface morphology on the gold side of the diffusion zone confirmed the suspicion that the morphology represented positions of increased film thickness or surface protrusions.

As with the porosity formation, no in-depth investigation of the formation mechanism of these surface protrusions, or if the reader will allow, surface hillocks, was undertaken, for it was not the purpose of this work.

However, some speculations will be made from the previous work of bulk investigators in the Ag-Au system and those studying thin film annealing phenomenon.

Several investigators, [54, 55 and 56], studying thin film annealing phenomenon have reported hillock growth in thin films, including Au, and attributed it to a mechanism of stress reduction. The driving force in their studies was the differential stress between the film and substrate, developed by the ΔT between the deposition and annealing temperature. In the present work, deposition at the annealing temperature (excepting Runs 212 - 215) eliminated this as a driving force. However, Barnes [30] and Balluffi [32] reported strain in the diffusion zone of bulk sandwich couples of the Cu-Ni and Ag-Au systems respectively. The reduction of strain in the diffusion zone and/or dislocation climb creating planes of vacancies similar to that proposed by Ruth [35] in the silver-gold system, could account for the observed hillock growth.

Incremental Couples (80 Au-Au)

As in the bulk studies of Johnson [38] with sandwich couples with small initial concentration differences, no porosity or hillock formation was observed in the diffusion zone of thin film couples with an initial 20 atomic % concentration difference.

The transmission electron microscope studies of the couples' grain size led to the conclusion that the grain size (1,000 - 2,000 Å) of the films was independent of the annealing temperature, and film composition over the working range of the couples. The grain size of Ag films deposited at room temperature has been reported to be as low as 50 Å. However, with the high deposition temperature of the present study, the grain size is expected to be larger, due to the increasing surface mobility of adatoms and clusters during deposition.

The surface roughness, which was uniform over each individual couple, increased with annealing temperature as was shown in Figures 26 to 28. As the surface mobility of adatoms increases (higher substrate temperatures), the condensation can occur preferentially at the surface concavites, and thus tend to smooth the surface. However, as was reported [41] with gold and experimentally observed in the present study, anisotropy of the surface energy will cause the condensate to grow preferentially along certain crystal faces, enhancing the resultant surface roughness. This is strongly evident in the couple annealed at 416°C shown in Figure 28.

In each of the concentration profiles, the variance in the slope was within .005. The value of .005 was within the statistical error of each slope. The error was determined from the experimentally observed variation in slope between successive scans of the microprobe across the diffusion zone

on different portions of the couple. The three values of D determined at 416°C for annealing times of 12, 24 and 48 hours lent credence to the use of the thin film approximation which predicts parabolic movement of atomic planes of constant composition with time.

The values of D determined for the 24 hour anneals at temperatures of 200, 250, 300, 350 and 416°C exhibited linearity on a ln D versus 1/T plot with correlation 0.99. This indicated a single atomic transport mechanism to be dominant over the working temperature range of the couples. The value of activation energy was almost $\frac{1}{4}$ of that reported for bulk diffusion in Ag-Au couples.

In the thin film couple, three possible atomic transport mechanisms are considered to be operative: Transport of matter along the grain boundaries and the substrate-film interface, through the crystal lattice, and along the film-vapor interface. The apparent diffusivity can be written as

$$D_{app} = D_{GB}\, g + D_L(1-g-s) + D_S\, s \qquad (28)$$

where D_{GB} = grain boundary diffusion coefficient

D_L = lattice diffusion coefficient

D_S = surface diffusion coefficient

g = fraction of time a diffusing atom spends on a grain boundary or along the substrate-film interface

s = fraction of time a diffusing atom spends on the surface.

For the case of a binary alloy, all atoms are not equivalent so the total time a diffusing atom spends on a grain boundary or surface is equal to fractional number of sites which are in or on each respectively, times its atomic fraction.

To estimate g, consider a sample made up of "spheres" that touch each other completely. The total number of atoms in a "sphere" is $4/3\pi r^3/\Omega$, where Ω equals the atomic volume. The total number of atoms in the grain boundary equals $4\pi r^2/\Omega^{2/3}$. Therefore,

$$g = (\text{atm. frac.})\left(\frac{4\pi r^2}{\Omega^{2/3}}\right)\left(\frac{3\Omega}{4\pi r^3}\right) = (\text{atm. frac.})\left(\frac{3\Omega^{1/3}}{r}\right)$$

for $\Omega^{1/3} = 2.2$ Å

$r = 1{,}000$ Å

atm. frac. $= 0.1$

Therefore $g = 10^{-3}$

To estimate s, consider a surface monolayer of thickness 2 Å. For a film thickness of 1,500 Å and atomic fraction 0.1, $s = 10^{-4}$.

We can rewrite equation (28) as

$$D_{app} = 10^{-3}\ D_{GB} + D_L + 10^{-4}\ D_s \qquad (29)$$

The activation energy for chemical diffusion through the lattice is approximately 40 kcal/mole, which is not in accord with the activation energy reported in this study. Over the temperature range of this present work the contribution to

the apparent diffusivity using the bulk value of diffusivity reported by Johnson [38] is negligible.

If surface diffusion is assumed to be dominant, then a similar discrepancy exists between the reported activation energies for surface diffusion and those of the present work. If we consider the terrace ledge kink model of a solid-vapor interface developed by Kossel [59], then the activated process for transport along a (111) FCC surface involves two steps.

The activation energy is considered to be the sum of two contributions, a change in enthalpy necessary for formation of the diffusing species and secondly, the change in enthalpy necessary for motion. The adatom in general carries the surface flux. It is the most weakly bonded atom to the surface, and on a FCC surface is characterized by 3 nearest neighbor bonds. An adatom is formed by an atom escaping from a kink site in a monatomic ledge (6 nearest neighbor bonds) to a site at the ledge (5 nearest neighbor bonds) and then to an adatom site. This involves the breaking of 3 bonds. The motion of an adatom involves the breaking of one bond. The activation energy therefore, can be looked upon as a process involving the breaking of 4 nearest neighbor bonds. The heat of sublimation of a FCC metal is the enthalpy change when a mole of atoms each atom breaking 6 bonds, escapes to the vapor state. Therefore, we can estimate the activation energy per mole of atoms as $2/3\ \Delta H_{sublimation}$. For gold and

silver, the heat of sublimation is approximately 80 and 60 kcal/mole respectively. This high value of activation energy is in accord with what has been reported for gold and silver where $T/T_{melt.pt.}$ is greater than 0.77.

It has been suggested by Gjostein [51] that for studies at low temperatures (T/Tm < 0.77) the activation energy is approximately one-fourth the heat of sublimation. One study [60] of grain boundary grooving in gold reported an activation energy of 17 kcal/mole for T/Tm = 0.57.

In order to be in accord with the presently accepted terrace ledge kink model, it must be postulated that the surface is covered with a large fraction of growth sites available for surface transport. The activation energy can then be assumed to involve the breaking of one bond. This model is for the most part unsubstantiated and sufficient experimental work has not been done in the present study to support or challenge this model.

If we consider grain boundary diffusion to be the dominant mechanism, then we again are faced with interpreting the low value of activation energy experimentally observed (10,900 cal/mole). Hoffman and Turnbull [36] reported an activation of 20,200 cal/mole for a study of grain boundary diffusion of radioactive silver in a silver bi-crystal. If we just take into account the grain size of the film, the ratio of D_{app}/D_{GB} equals 0.01, 0.15 and 0.40 for temperatures of 200, 300 and 416°C respectively. Let us assume the results of

Hoffman and Turnbull [36] as representative of a lower limit on the degree of disorder in a grain boundary. An upper limit would be to consider the grain boundary as in the liquid state. Activation energies for liquid self diffusion in silver have been reported [58] between 7 and 8 kcal/mole. The ratios of the apparent diffusivity to diffusion down "liquid" (highly disordered) grain boundaries are greater than 1 for all annealing temperatures. If we assumed that the grain boundaries between the grains in the thin film couples are highly disordered as the photographs of the film grain structure in Figure 25 and Figures 26 through 28 of the film surface suggest, then we would expect that the activated energy for transport along the grain boundaries to be between the upper and lower limit discussed above.

CONCLUSIONS AND RECOMMENDATIONS

Conclusions

The study of lateral diffusion in thin film couples of gold and silver can be investigated using one of the non-steady state solutions to Fick's second law. The thin strip approximation, which in the limit of strip thickness = 0, is more commonly applied to a pair of semi-infinite solids can also be applied to a thin film of constant thickness where the initial profile is experimentally determined.

The use of Zeibold's empirical conversion parameter, more commonly applied to the determination of composition in the bulk, is valid for thin films of the gold-silver system up to 2000 Å in thickness. Up to 2000 Å the thin film approximation that intensity is proportional to mass thickness is valid in the gold-silver system.

Studies of lateral diffusion in Ag-Au couples exhibit surface morphology changes similar to that reported in bulk couples. The mechanism, operative in the thin film diffusion couple giving rise to the formation of a zone of porosity and protrusions on the silver and gold sides of the interface of the couple respectively, can be attributed to the conclusions reported by bulk investigators. The maintenance of continuity of the silver and breakup of the gold sides of the thin film

couple follows the predictions of Mullin's theory of grain boundary grooving.

The use of incremental couples with small initial concentration differences eliminates the formation of porosity and hillocks as experimentally observed in the bulk studies of Johnson. The maintenance of continuity in film thickness across the diffusion zone allows the determination of diffusivity as a function of temperature. Using the standard rate equation for an activated process the apparent diffusivity was written as $D = 1.9 \times 10^{-7} \exp\left(\frac{-10,900}{RT}\right)$ $cm^2 sec^{-1}$ where $D_0 = 1.9 \times 10^{-7}$ and the activation energy is 10.9 kcal/mole. In addition a value of diffusivity was determined on the Ag-Au couple which had film separation by considering the porous zone as creating a new set of boundary conditions for the experimentally determined initial profile. The value of diffusivity was in accord with that observed in the incremental couples.

A comparison of the possible transport mechanisms operative in the thin film couples between 200 and 416°C suggests that grain boundary diffusion is the dominant mechanism. In order to resolve the low value of activation energy reported in both the incremental couple and the Ag-Au couples an assumption that the grain boundaries were highly disordered must be made.

Recommendations

In order to make a stronger case for the mechanism of grain boundary diffusion, incremental couples should be made with varying rates of deposition in order to vary the resultant grain size. Larger grains with a rising value of activation energy in accordance with the previously reported bulk values of grain boundary diffusion would lend more credence to the disorder assumption made in this study.

A study of incremental couples with larger concentration differences could prove interesting. The magnitude of the initial concentration difference necessary to cause the formation of porosity could produce some interesting conclusions as to the operative driving force for the formation of the porosity and hillocks.

Because of the small amounts of material present in thin films and short annealing times, a study of lateral diffusion using the scanning electron microprobe could prove valuable. The small beam size would allow greater resolution, in the lateral direction, and in the relationships of surface morphology to chemical composition, than in the electron microprobe.

A followup study on the application of the empirical conversion parameter of Zeibold to other thin film systems could prove to be a valuable tool in film composition determinations.

The study of non-miscible systems using the experimental deposition technique of the present work should prove superior to the overlap technique used in previous work. The elimination of the overlap region removes the necessity for diffusion normal to the substrate to homogenize the overlap region and more closely approximates the initial conditions of the bulk sandwich couple. The method of deposition used in the formation of the incremental couples could be applied to the study of diffusion in non-miscible systems in single phase regions.

REFERENCES

REFERENCES

1. Weaver, C., 1959, Advanced Physics, Vol. 8, pp. 375-437.

2. Weaver, C., 1971, Physics of Thin Films, Vol. 6, Academic Press, New York, pp. 301-346.

3. Monch, G. C., 1952, Wiss. Z., Martin-Luther University, Halle-Wittenberg, Vol. 2, p. 601; Ann. Phys., LPZ., Vol. 12, p. 175; 1954 a, ibid., Vol. 14, p. 367; 1954 b, ibid., Vol. 14, pp. 377-383.

4. Pines, B. YA., Grebennik, I. P., Bazyura, R. I., and Zozulya, G. V., 1967, Phys. Stat. Sol., Vol. 20, pp. 213-223.

5. Johnson, D. B., and Brown, L. C., 1969, J. Appl. Phys., Vol. 40, pp. 149-152; ibid., Vol. 40, pp. 1711-1714.

6. Smallen, R. P., 1969, Thin Film Diffusion in the Gold-Copper System, Master of Science Dissertation submitted to Material Science and Metallurgical Engineering Department, Purdue University, (unpublished) October 22, 1969.

7. Elliot, R. P., 1965, Constitution of Binary Alloys-First Supplement, McGraw-Hill, New York, pp. 201-203.

8. Watkins, W. A., 1969, A History of the Bismuth Tellurium Phase System, unpublished literature survey, prepared for Vest, R. W., School of Material Science, Purdue University, May 19, 1969.

9. Watkins, W. A., 1970, Thin Film Diffusion in the Bismuth Tellurium System, Master of Science Dissertation submitted to Material Science and Metallurgical Engineering Department, Purdue University, (unpublished) January 21, 1970.

10. Honig, R. E., and Kramer, D. A., Physics of Thin Films, Vol. 5, Academic Press, New York, pp. 505-531.

11. Anderson, R. M., and Neudeck, G. W., 1971, J. Vac. Sci. and Tech., Vol. 8, pp. 454-457.

12. Dektak, Made by Sloan Instrument Company.

13. Robbie, C. J., and Stoddart, C. T. H., 1968, J. of Sci. Inst. (J. of Phys. E.), Vol. 1, pp. 56-57.

14. Campbell, W. J., 1963, Symposium on X-Ray and Electron Probe Analysis, American Society for Testing and Materials, Philadelphia, pp. 48-69.

15. Holliday, J. S., and Sternclass, E. J., 1957, J. Appl. Phys., Vol. 28, p. 1191.

16. Birks, L. S., 1963, Symposium on X-Ray and Electron Probe Analysis, American Society for Testing and Materials, Philadelphia, pp. 151-162.

17. Castaing, R., 1951, Ph.D. Thesis, Paris University, O.N.E.R.A. Publ. No. 55.

18. Ziebold, T. O., and Ogilvie, R. E., 1964, Analytical Chem., Vol. 36, pp. 322-327.

19. Hutchins, C. A., 1966, The Electron Probe, (McKinley, Heinrich, Wittrey ed.), John Wiley and Sons, New York, pp. 390-404.

20. Sachs, and Werts, J., 1930, Z. Phys., Vol. 60, p. 481.

21. Hund, F., and Tragner, E., 1952, Natur. Wiss., Vol. 39, p. 63.

22. Barrett, C., and Massalski, T. B., 1967, Structure of Metals, McGraw-Hill, New York, p. 189.

23. Fraenkel, W., and Houeben, H., 1921, Ztsch. Anorg. Allg. Chem., Vol. 116, p. 1.

24. Weiss, H., and Henry, P., 1922, Compt. Rend., Vol. 175, p. 1402.

25. Jost, W., 1930, Ztsch. Physik Chem., Vol. B9, p. 63.

26. Mallard, W. C., Gardner, A. B., Bass, R. F., and Slifkin, L. M., 1963, Phys. Rev., Vol. 129, pp. 617-625.

27. Balluffi, R. W., and Seigle, L. L., 1954, Jour. App. Phys., Vol. 25, pp. 607-614.

28. Seitz, W., and Kotterman, A., 1952, Angew. Chem., Vol. 64, p. 379.

29. Balluffi, R. W., and Alexander, B. H., 1952, Jour. App. Phys., Vol. 23, pp. 953-956.

30. Barnes, R. S., 1952, Proc. Phys. Soc., Vol. 65B, pp. 512-525.

31. Huntingdon, H. B., and Seitz, F., 1942, Phys. Rev., Vol. 61, p. 315.

32. Balluffi, R. W., 1954, Acta. Met., Vol. 2, pp. 194-202.

33. Barnes, R. S., and Mazey, P. J., 1958, Acta. Met., Vol. 6, pp. 1-7.

34. Seitz, F., 1953, Acta. Met., Vol. 1, pp. 355-369.

35. Ruth, V., 1963, Trans. Met. Soc. AIME, Vol. 227, p. 778.

36. Hoffman, R. E., and Turnbull, D., 1951, Jour. App. Phys., Vol. 22, pp. 634-639.

37. Manning, J. R., 1967, Acta. Met., Vol. 15, pp. 817-826.

38. Johnson, W. A., 1942, Trans. AIME, Vol. 147, p. 331.

39. Volk, W., 1958, Applied Statistics for Engineers, McGraw-Hill, New York, pp. 224-295.

40. Pashley, D. W., 1956, Advanc. Phys., Vol. 5, p. 173.

41. Sundquist, 1964, Acta. Met., Vol. 12, pp. 67-86.

42. Hartmann, T. E., 1965, J. Vac. Sci. Tech., Vol. 2, p. 239.

43. Blois, M. S. and Reiser, L. M., 1969, J. Appl. Phys., Vol. 25, p. 338.

44. Mullins, W. W., 1957, J. Appl. Phys., Vol. 28, pp. 333-339.

45. Presland, A. E. B., Price, G. L. and Trimm, D. L., 1972, Surf. Sci., Vol. 29, pp. 424-434.

46. Presland, A. E. B., Price, G. L. and Trimm, D. L., 1972, Surf. Sci., Vol. 29, pp. 435-446.

47. Brandon, R. H., and Bradshaw, F. J., 1966, Royal Aircraft Establishment Research Report No. 66095.

48. Gimpl, M. L., McMaster, A. D., and Fuschild, N., 1964, J. Appl. Phys., Vol. 35, p. 3572.

49. Elliot, J. F., and Gleiser, M., 1960, Thermochemistry for Steel Making, Addison Wesley, London, pp. 8-12.

50. Private Communication.

51. Gjostein, N. A., 1967, Surfaces and Interfaces, Eds. Burke, T. T., Reed, N. L., and Weiss, V., Syracuse Univ. Press, New York.

52. Carslaw, H. S. and Jeager, J. C., 1959, Conduction of Heat in Solids, Claredon Press, Oxford.

53. Shewmon, P. G., 1963, Diffusion in Solids, McGraw-Hill, New York, p. 128.

54. Pennebaker, W. B., 1969, Jour. App. Phys., Vol. 40, pp. 394-400.

55. Lahiri, S. K., 1970, Jour. App. Phys., Vol. 41, pp. 3172-3176.

56. Murbach, H. P., and Wilman, H., 1953, Proc. Phys. Soc., Vol. 46, pp. 905-910.

57. Chopra, K. L., 1969, Thin Film Phenomena, McGraw-Hill, New York, p. 189.

58. Smithells, C. J., 1967, Metals Reference Book, Vol. 2, 4th Edition, Butterworths and Co., London, pp. 682-683.

59. Kossell, W., 1927, Nach. Ges. Wiss., Gottingen, p. 135.

60. Geguzin, Ya. E., Koualev, C. N., and Ovcharenko, N. N., 1964, Sov. Phys. Sol. St., Vol. 5, pp. 2627-2633.

APPENDICES

APPENDIX A

A STUDY OF LATERAL DIFFUSION IN THIN FILM COUPLES OF BISMUTH AND TELLURIUM

APPENDIX A

A STUDY OF LATERAL DIFFUSION IN THIN FILM COUPLES OF BISMUTH AND TELLURIUM

This author's initial investigation of lateral thin film diffusion took place in the bismuth-tellurium system. The separation between the razor blade and the substrate was achieved using a differential screw driving mechanism [9]. The adjustment was done manually and resulted in regions of mixing on the order of 10^{-5} meters.

All Bi-Te thin film couples were 1,000 Å thick and deposited at room temperature. The anneals were carried out in two separate environments. Vycor encapsulated tubes at a residual gas pressure of approximately 50 microns were used for anneals at 1, 3, 10, 30 and 96 hours. In addition, anneals in high vacuum at pressures less than 10^{-7}torr were carried out for times of 1, 3, 10, and 30 hours.

The initial profile was determined on the electron microprobe, on an unannealed thin film couple. The region of mixing was 84 microns. From optical observation, and the electron microprobe intensity data, 71.5 and 12.5 microns were attributed to the bismuth and tellurium overlap region respectively. The interface (position of razor blade) separated the two overlap regions.

In the series of anneals in the vycor tubes, the following observations were made: A peak in tellurium intensity was observed to move through the region of mixing towards the pure bismuth side of the couple into the tellurium overlap region. The anneal at 10 hours signaled the completion of the shift of the tellurium "pulse," which now was entirely in the original tellurium overlap region. In the bismuth overlap region (tellurium side of original interface) a reduction of tellurium on the pure tellurium side of the couple was observed, followed with an increase in tellurium over the entire bismuth side of the couple. The pure tellurium film thickness originally at 1,000 Å was reduced to 200 Å.

The observations of the couples annealed in high vacuum were the same for 1, 3 and 10 hours. However, the 30 hours anneal exhibited no significant decrease in tellurium thickness on the pure tellurium side of the couple or subsequent increase in tellurium intensity over the bismuth side of the couple.

The bismuth intensity profile remained immobile for all annealing times in both environments. X-ray fluorescent analysis using Cu Kα radiation confirmed the presence of the intermetallic compound Bi_2Te_3 in the region of mixing for annealing times greater than or equal to 3 hours. After 10 hours no further growth of the intermetallic compound was observed.

The mean free path of ambient gas atoms at 50 microns is 0.5 cm. The rate of free evaporation of tellurium and bismuth at 200°C is 0.2 and 2×10^{-5} monolayers/sec., respectively. Therefore, mass transport by the vapor phase is a probable mechanism in the couples encapsulated in the vycor tubing. This would explain the increase and decrease in counts of tellurium over the bismuth and tellurium sides of the couple for the 30 and 96 hour anneals in the vycor capsules.

The formation of the intermetallic compound occurs in both environments, ruling out a vapor transport mechanism, especially unlikely in high vacuum at 10^{-7}torr where the mean free path is 450 meters.

The relative immobility of the bismuth profile, and the moving tellurium "pulse" for the anneals at 1, 3, and 10 hours in both environments led the author to conclude that the tellurium was the only active (within the time frame of the author's study) species in the mass transport process.

Let us consider the region of mixing to be made up of a series of thin strips side by side in the lateral direction. Because of the simultaneous deposition process, each strip will be homogeneous in composition in the direction normal to the substrate. The variation in strip composition in the lateral direction should be from pure tellurium to pure bismuth across the region of mixing starting from the pure tellurium side of the region. Therefore, one strip in

original region of mixing should be of the stoichiometric composition of the intermetallic compound Bi_2Te_3. If we arbitrarily assign the mass ratio of bismuth to tellurium (m_{Bi}/m_{Te}) in this strip of stoichiometric Bi_2Te_3 equal to 1, then strips on either side would have a mass ratio < 1 and > 1 towards the pure tellurium and bismuth side respectively. Mass transport of tellurium in the direction of the pure bismuth side of the couple would increase and decrease the respective mass ratios towards 1, on the tellurium and bismuth sides of the initially stoichiometric strip. The region of mixing would now be a series of strips of Bi_2Te_3.

However, after the 10 hour anneal which signals the conclusions of the mass transport process, the region of mixing, and now zone of intermetallic compound, appears to remain stationary for further times. If the compound formation was diffusion controlled, a parabolic growth of this zone with respect to time, would be expected. Since some other time law is governing its process, it would appear to be an interface controlled process.

This, however, creates an anomaly in that mass transport was observed across this small strip of originally formed intermetallic which certainly had some sort of interface associated with it and yet the interfaces of the strips on each side of the region of mixing limit the intermetallic's growth to some small time power law.

A possible explanation for this behavior is that surface diffusion is the dominant mechanism. Instead of tellurium atoms moving across the interface, consider mass transport across the surface of this small strip of initially stoichiometric Bi_2Te_3. This causes tellurium accumulation on the bismuth side and mass depletion on the tellurium rich side of the strip. Followed by diffusion into the film perpendicular to the substrate, the stoichiometric strip will grow laterally. However, as the strip grows in lateral extent, the distance of tellurium surface transport would increase. If the rate of transport across the surface decreases as the extent of the strip grows, as is experimentally observed when the extent of tellurium transport is limited to the region of mixing, then the rate of formation of the intermetallic is fast initially falling at an unknown decreasing rate.

This strip as it grows would also provide a barrier to the tellurium moving away from the tellurium rich side of the region mixing, which at the same time, through tellurium depletion, is creating strips of intermetallic, even though very thin in thickness normal to the substrate.

With the intermetallic extending throughout the region of mixing, and now due to its extent in lateral dimension, and its respective interfaces, we would not expect and do not observe any growth with respect to time.

In summary, we can conclude that thin film couples of bismuth and tellurium form the intermetallic compound in the region of mixing and further growth of the intermetallic compound was not observed. Therefore, the intermetallic compound acts as a diffusion barrier and transport of bismuth and tellurium through the intermetallic is interface controlled following some small time power law which was not determined in this work. Due to the vapor pressure of tellurium, it is recommended that any further studies in the bismuth-tellurium system be done in a high vacuum condition and/or temperatures below 200°C.

APPENDIX B

EXPERIMENTAL RELATIONSHIPS USED FOR DEPOSITION OF ALLOY FILMS AND THIN FILM COUPLES

APPENDIX B

EXPERIMENTAL RELATIONSHIPS USED FOR DEPOSITION OF ALLOY FILMS AND THIN FILM COUPLES

Figure 38 shows the orientation relationship between the source, substrate and crystal monitor. The equations for evaporation from a small area (source) onto a parallel plane receiver had been previously reported [9]. The change in frequency (frequency shift) of the 5 MC crystal is related to the mass deposited on the crystal by equation (25) of the present work. The β variable represents the correction parameter that adjusts for the orientation relationships of Figure 38. Therefore, the t in equation (25) represents the thickness of the film. β consists of the following variables

$$\beta = \frac{1}{2}\left(\frac{R_1}{R_2}\right)^2 \frac{1}{\cos^2\Theta} \tag{30}$$

where $\frac{1}{2}$ is a constant of the crystal

R_1 = the substrate to source distance

R_2 = the crystal to source distance

Θ = angle between the source normal and the crystal monitor.

The thickness variation across the film is

$$\frac{t}{t_0} = \frac{1}{\left[1 + \left(\frac{r}{R_1}\right)^2\right]^2} \tag{31}$$

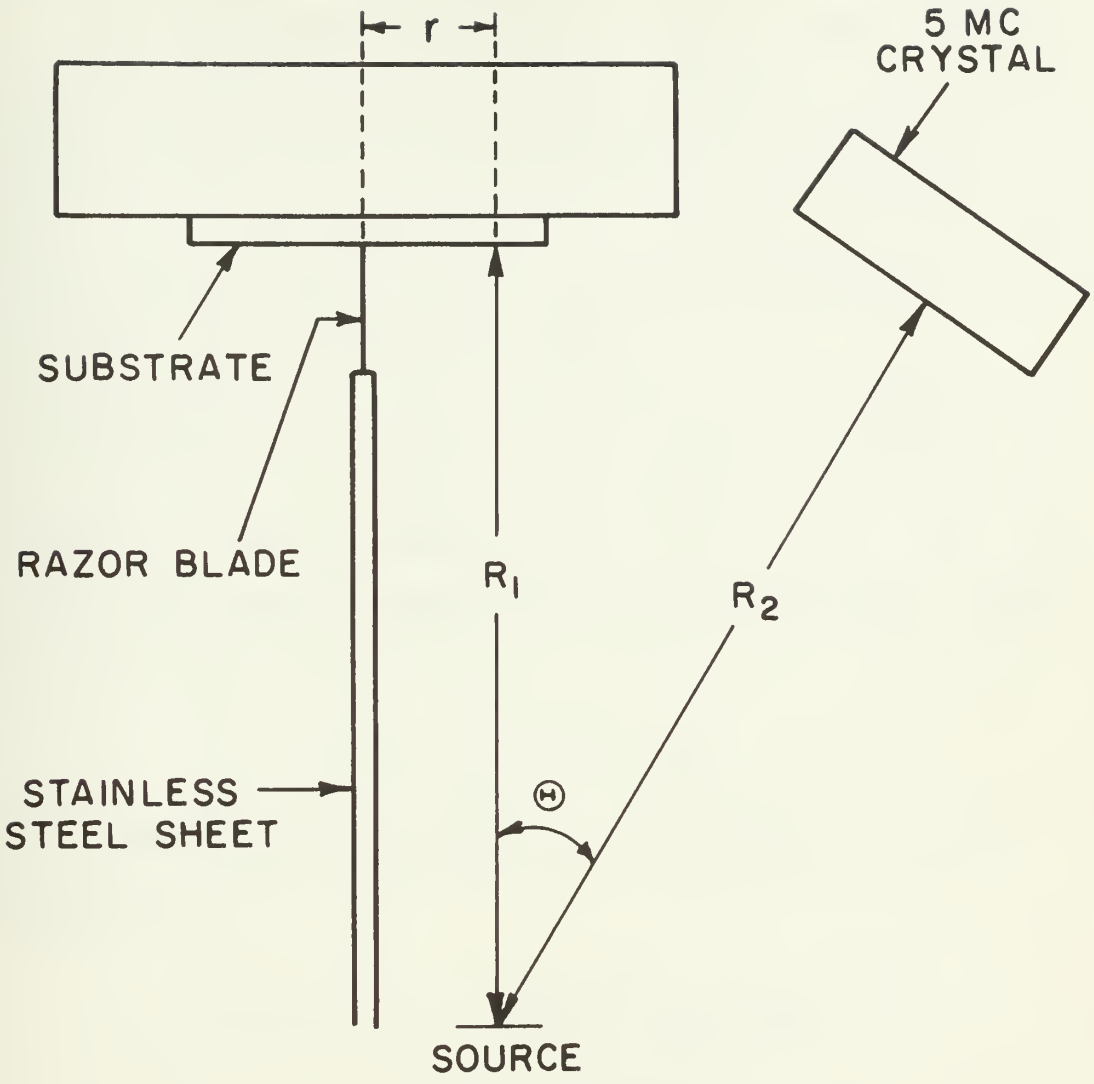

Figure 38

Orientation Relationships between the Source,

Substrate and Crystal Monitor

where t = thickness of film directly above source

t_0 = thickness of film at distance r from point on substrate directly above source.

Using equation (31) the maximum thickness variation for a 1,500 Å film using the values of r = 2 cm, R = 18 cm, used in the present study, is 38 Å, which is within the error of thickness measurement of the Dektac.

Alloy deposition was carried out by 1) assuming that the film density was that of the reported bulk value and 2) that the total thickness of the alloy film, t, was equal to the sum of the thickness of the two pure films. Therefore, let

$$t = t_{Au} + t_{Ag} \tag{32}$$

Let desired composition of film be X weight% Ag, (1-X) weight% Au.

$$X \text{ weight\% Ag} = \frac{\text{mass Ag}}{\text{mass Ag} + \text{mass Au}} \times 100$$

$$= \frac{\rho_{Ag}\, t_{Ag}\, A}{\rho_{Ag}\, t_{Ag}\, A + \rho_{Au}\, t_{Au}\, A} \tag{33}$$

where A = substrate area on which gold and silver is deposited.

Substituting equation (32) into equation (33) and solving for t_{Ag}

$$t_{Ag} = \frac{t\rho_{Au}(\text{w\% Ag})}{\rho_{Au}(\text{w\% Ag}) + \rho_{Ag}(\text{w\% Au})} \tag{34}$$

and

$$t_{Au} = t - t_{Ag} \tag{35}$$

APPENDIX C

COMPUTER PROGRAM USED IN ANALYZING DATA FOR THIN FILM STANDARDS

APPENDIX C

```
C
C
C     THIS IS A PROGRAM TO DETERMINE THE EMPIRICAL ZEIBOLD
C     CORRECTION PARAMETER FROM THE THIN FILM STANDARDS OF
C     THE SILVER-GOLD SYSTEM
C
C     A LINEAR LEAST SQUARES FIT IS DONE FOR EACH ALLOY
C     COMPOSITION MADE AS A FUNCTION OF FILM THICKNESS.
C
C     FROM THE RESULTANT EQUATIONS DATA IS EXTRAPOLATED FOR
C     FILM THICKNESSES OF 500,1000,1500, AND 2000 ANGSTOMS.
C
C     THE VALUES OF K AND C ARE DETERMINED AND A LINEAR
C     LEAST SQUARES FIT IS DONE FOR A PLOT OF 1-K/K VRS.
C     1-C/C, FOR EACH FILM THICKNESS.
C
C     FROM THE SLOPE THE ZEIBOLD CORRECTION PARAMETER IS
C     DETERMINED.
C
C     COMPOSITION FOR ALL THE DATA IS REPORTED IN ATOMIC
C     PERCENT SILVER
C
C     K IS THE BACKGROUND CORRECTED INTENSITY/BACKGROUND
C     CORRECTED PURE INTENSITY
C
C     C IS WEIGHT FRACTION COMPOSITION
C
C     BKGD1 IS THE BACKGROUND OF THE PURE ELEMENT
C
C     BKGD2 IS THE BACKGROUND OF THE ALLOY
C
C     INT IS THE TOTAL INTENSITY FROM THE MICROPROBE
C
C     THK IS THE FILM THICKNESS
C
C
      DIMENSION INT(10),THK(10),A0(10),A1(10),IPURE(5,5),IALLOY(10,10),K
     1A(10,10),C(10),X(10),Y(10,10)
      REAL KA,IPURE,IALLOY,INT
      B=0.0
      J=1
    1 IF(J.EQ.1) WRITE(6,112)
      IF(J.EQ.2) WRITE(6,113)
      DO10 L=1,7
      N=4
      IF(L.GT.1) N=5
      READ(5,100) COMP, (INT(I)  I=1,N)
      READ(5,101) (THK(I), I=1,N)
      IF(N.EQ.4.AND.J.EQ.1) GO TO 20
      IF(N.EQ.4.AND.J.EQ.2) GO TO 22
      GO TO 21
   20 WRITE(6,114)
      GO TO 23
   22 WRITE(6,115)
      GO TO 23
   21 WRITE(6,102) COMP
   23 WRITE(6,110)
      WRITE(6,103) (INT(I),THK(I), I=1,N)
      SUM1=0.0
      SUM2=0.0
      SUM3=0.0
      SUM4=0.0
      SUM5=0.0
      DO11 I=1,N
      XY=INT(I)*THK(I)
```

```
      YY=INT(I)*INT(I)
      XX=THK(I)*THK(I)
      SUM1=THK(I)+SUM1
      SUM2=INT(I)+SUM2
      SUM3=XY+SUM3
      SUM4=XX+SUM4
   11 SUM5=YY+SUM5
      AN=(SUM2*SUM4)-(SUM1*SUM3)
      AD=(N*SUM4)-(SUM1*SUM1)
      A1N=(N*SUM3)-(SUM1*SUM2)
      A0(L)=AN/AD
      A1(L)=A1N/AD
      WRITE(6,111)
      SYX1=SUM5-(A0(L)*SUM2)
      SYX2=(SYX1-(A1(L)*SUM3))/N
      SYX=SQRT(SYX2)
      SIG1=SUM5/N
      SIG2=(SUM2/N)*(SUM2/N)
      SY2=SIG1-SIG2
      SY=SQRT(SY2)
      CORR=SQRT(1.0-(SYX2/SY2))
      WRITE(6,107) A0(L),A1(L),SYX,SY,CORR
      IF(L EQ.1) GO TO 10
      IF(L GT.2) GO TO 12
      THICK=500.
      DO13 M=1,4
      BKGD1=A0(1) + (A1(1)*THICK)
      IPURE(2,M)=(A1(L)*THICK) + A0(L) - BKGD1
   13 THICK=THICK+500.
      GO TO 10
   12 THICK=500.
      IF(L.EQ.3) GO TO 10
      DO14 M=1.4
      BK=A0(3) + (A1(3)*THICK)
      IF(J.EQ.2) GO TO 40
      BKGD2=BK*(1.-COMP) + BKGD1*COMP
      GO TO 41
   40 BKGD2=BK*COMP + BKGD1*(1.-COMP)
   41 IALL0Y(L,M)=(A1(L)*THICK) + A0(L) - BKGD2
      KA(L,M)=IALL0Y(L,M)/IPURE(2,M)
      THICK=THICK+500.
   14 Y(L,M)=(1.0-KA(L,M))/KA(L,M)
      C1=1.0788*COMP
      C2=1.97*(1.-COMP)
      C(L)=C1/(C1+C2)
      IF(J.EQ.2) C(L)=1.0-C(L)
      X(L)=(1.0-C(L))/C(L)
   10 CONTINUE
      THICK=500.
      ALL1=0.0
      ALL2=0.0
      ALL3=0.0
      ALL4=0.0
      DO15 M=1,4
      WRITE(6,105) THICK
      THICK=THICK+500.
      WRITE(6,104)
      DO16 L=4,7
   16 WRITE(6,106) Y(L,M),X(L)
      SUM1=0.0
      SUM2=0.0
      SUM3=0.0
      SUM4=0.0
      DO18 L=4,7
      XX=X(L)*X(L)
```

```
      YY=Y(L,M)*Y(L,M)
      XY=X(L)*Y(L,M)
      SUM1=XX+SUM1
      SUM2=YY+SUM2
      SUM3=XY+SUM3
   18 SUM4=Y(L,M)+SUM4
      ALL1=ALL1+SUM1
      ALL2=ALL2+SUM2
      ALL3=ALL3+SUM3
      ALL4=ALL4+SUM4
      SL0PE=SUM3/SUM1
      SYX2=(SUM2-(SL0PE*SUM3))/4.
      SYX=S0RT(SYX2)
      SIG1=SUM2/4.
      SIG2=(SUM4/4. )*(SUM4/4. )
      SY2=SIG1-SIG2
      SY=S0RT(SY2)
      C0RR=S0RT(1. 0-(SYX2/SY2))
   15 WRITE(6,107) B,SL0PE,SYX,SY,C0RR
      SL0PE=ALL3/ALL1
      SYX2=(ALL2-(SL0PE*ALL3))/16.
      SYX=S0RT(SYX2)
      SIG1=ALL2/16.
      SIG2=(ALL4/16. )*(ALL4/16. )
      SY2=SIG1-SIG2
      SY=S0RT(SY2)
      C0RR=S0RT(1. 0-(SYX2/SY2))
      WRITE(6,108)
      WRITE(6,107) B,SL0PE,SYX,SY,C0RR
      IF(J EQ. 2) ST0P
      J=2
      G0 T0 1
  100 F0RMAT(F5. 1,5X,5F10. 5)
  101 F0RMAT(5F10. 5)
  102 F0RMAT(1H0,////,20X,'(AT0MIC FRACTI0N SILVER)',/,24X,'C0MP0SITI0N
     1= ',F5. 2)
  103 F0RMAT(2(20X,F13. 6))
  104 F0RMAT(1H0,17X'1-K/K',20X,'1-C/C')
  105 F0RMAT(1H0,////,20X,'FILM THICKNESS = ',F10. 2)
  106 F0RMAT(2(15X,F10. 6))
  107 F0RMAT(1H0,20X,'INTERCEPT (A0) = ',26X,F13. 5,//,21X,'SL0PE (A1) =
     1',30X,F13. 5,//,21X,'STANDARD ERR0R 0F THE ESTIMATE = ',10X,F13. 5,/
     2/,21X,'STANDARD DEVIATI0N 0F Y = ',17X,F13. 5,//,21X,'C0EFFICIENT 0
     3F C0RRELATI0N = ',14X,F13. 5)
  108 F0RMAT(1H0,////,15X,'LINEAR LEAST SQUARES FIT F0R ALL DATA')
  109 F0RMAT(1H1)
  110 F0RMAT(1H0,22X,'INTENSITY',22X,'FILM THICKNESS')
  111 F0RMAT(1H0,15X,'EQUATI0N 0F LINE IS.....INTENSITY = A0 + A1 X T
     1HICKNESS.....')
  112 F0RMAT(1H1,15X,'CALIBRATI0N DATA TAKEN 0FF THE SILVER SPECTR0METER
     1')
  113 F0RMAT(1H1,15X,'CALIBRATI0N DATA TAKEN 0FF THE G0LD SPECTR0METER')
  114 F0RMAT(1H0,15X,'BACKGR0UND INTENSITY 0F PURE SILVER FILMS')
  115 F0RMAT(1H0,15X,'BACKGR0UND INTENSITY 0F PURE G0LD FILMS')
      END
```

APPENDIX D

COMPUTER PLOTTING PROGRAM WHICH PLOTS CONCENTRATION VERSUS RELATIVE DISTANCE FROM MICROPROBE INTENSITY DATA OF THIN FILM COUPLES

APPENDIX D

```
C
C
C     THIS IS A PLOTTING PROGRAM WHICH FIRST DETERMINES THE
C     CONCENTRATION FROM THE INTENSITY OUT OF THE MICROPROBE
C     AND PLOTS CONCENTRATION VERSUS RELATIVE DISTANCE
C
C     BKGD1 IS THE BACKGROUND CORRECTION FOR THE PURE FILM
C
C     BKGD2 IS THE BACKGROUND CORRECTION FOR THE ALLOY FILM
C
C     ABAR IS THE JEIBOLD PARAMETER DETERMINED FROM INDEPENDANT
C     MEASUREMENTS OF  THIN FILM STANDERDS
C
C     PURET IS THE RAW INTENSITY OF THE PURE ELEMENT MEASURED
C     FROM THE MICROPROBE SPECTROMETER
C
C     ALY(I) IS THE RAW INTENSITY OF THE ALLOY THIN FILM MEASURED
C     DIRECTLY FROM THE MICROPROBE SPECTROMETER
C
C     ALDEN IS THE ALLOY DENSITY FOR THE SILVER - GOLD SYSTEM AND IS
C     COMPUTED ON THE BASIS OF AN ASSUMED LINEAR RELATIONSHIP BETWEEN
C     THE ALLOY DENSITY AND THE ATOMIC FRACTION OF THE PHASE SYSTEM
C
C
      DIMENSION ALY(500),CONC(500),DIST(500),CONC1(500),DIST1(500),CONC2
     1(500),DIST2(500),IMAGE(1500),CTEST(100),DTEST(100),NSCALE(5)
      REAL K,KA,KAA
      INTEGER RUN,Z,Y,G
      NSCALE(1)=1
      NSCALE(2)=0
      NSCALE(3)=2
      NSCALE(4)=0
      NSCALE(5)=1
      PI=3.14159
      DX=2.E-05
      CALL PLOT1(NSCALE,5,10,11,10)
    1 READ(5,100) RUN,N,ABAR,BKGD1,BKGD2,PURET,TIME,TEMP
      M=1
      G=0
      DO 2 I=1,N
      READ(5,103) ALY(I)
    2 DIST(I)=0.8*FLOAT(I-1)
      E=PURET-BKGD1
      I=1
    9 D=ALY(I)-BKGD2
      IF(D .LE. 0.0) GO TO 3
      K=D/E
      KA = (1.0-K)/(K*ABAR)
      KAA=1.0+KA
      C=1.0/KAA
      GO TO 4
    3 K=0.0
      C=0.0
      GO TO 4
    4 AG= C/1.07S8
      AU=(1 -C)/1.97
      ATMFR=AG/(AG+AU)
      ALDEN=19.415 - (8.843*ATMFR)
      CONC(I)=ALDEN*C
      IF(CONC(I).GT.1.56.OR.CONC(I).LT.0.56) GO TO 20
      G=G+1
      CTEST(G)=CONC(I)
      DTEST(G)=DIST(I)
   20 IF(I-111) 5,6,6
    6 CALL PLOT2(IMAGE,1500,88.0,0.0,2.5,0.0)
```

```
      CALL FLOAT(IM,DIST,CONC,I)
      WRITE(6,110)
      CALL PLOT(4.2,4.4,H                CONCENTRATION IN GRAMS AG /CC)
      WRITE(6,103)
      GO TO 15
    5 IF(I-N) 12,6,15
   12 I=I+1
      GO TO 9
   15 SUM1=0.0
      SUM2=0.0
      SUM3=0.0
      SUM4=0.0
      SUM5=0.0
      DO21 I=1,6
      XY=DTEST(I)*DTEST(I)
      XYY=DTEST(I)+DTEST(I)
      XX=DTEST(I)*DTEST(I)
      SUM1=DTEST(I)+SUM1
      SUM2=DTEST(I)+SUM2
      SUM3=XY+SUM3
      SUM4=XX+SUM4
   21 SUM5=XYY+SUM5
      AN=(SUM2*SUM4)-(SUM1*SUM3)
      AD=(FLOAT(G)*SUM4)-(SUM1*SUM1)
      A1N=(FLOAT(G)*SUM3)-(SUM1*SUM2)
      A0=AN/AD
      A1=A1N/AD
      SYX1=SUM5-(A0*SUM2)
      SYX2=(SYX1-(A1*SUM3))/FLOAT(G)
      SYX=SQRT(SYX2)
      SIG1=SUM5/FLOAT(G)
      SIG2=(SUM2/FLOAT(G))*(SUM2/FLOAT(G))
      SY2=SIG1-SIG2
      SY=SQRT(SY2)
      CORR=SQRT(1.0-(SYX2/SY2))
      WRITE(6,111) RUN,TIME,TEMP
      WRITE(6,112) A1,A0,SYX,SY,CORR
      GO TO 1
  100 FORMAT(I3,I3,4X,6F10.5)
  101 FORMAT(1H1,1X,'RUN NO.',5X,'ABAR = ',8X,'BKGD1 = ',7X,'BKGD2 = ',7
     1X,'PUREI = ',7X,'N = ',5X,'TIME = ',7X,'TEMP = ')
  102 FORMAT(1HO,I5,4X,F8.5,3(5X,F10.1),7X,I3,5X,F6.1,8X,F6.1)
  103 FORMAT(F13.5)
  104 FORMAT(1HO,4X,'ALLOY INTENSITY',5X,'KAG',9X,'WT  FRACT.',7X,'ATOM
     1FRACT.',5X,'ALLOY DENSITY',2X,'CONCENTRATION')
  105 FORMAT(6(5X,F10.5))
  106 FORMAT(1H1,5X,'DIFFUSION COEFFICIENT EQUALS ',1PE13.4)
  107 FORMAT(5(F10.5))
  108 FORMAT(1H1,5X,'CONCENTRATION      GRAMS/CC')
  109 FORMAT(1H ,'DIS.  RELATIVE DISTANCE  MILLIMETERS')
  110 FORMAT(1H1)
  111 FORMAT(1H ,20X,'RUN = ',I3,10X,'TIME = ',F6.1,10X,'TEMPERATURE OF
     1ANNEAL = ',F6.1)
  112 FORMAT(1H ,20X,'SLOPE = ',35X,F13.5,/,21X,'INTERCEPT OF CONCENTRAT
     1ION AXIS = ',11X,F13.5,/,21X,'STANDARD ERROR OF THE ESTIMATE = ',1
     20X,F13.5,/,21X,'STANDARD DEVIATION OF Y = ',17X,F13.5,/,21X,'COEFF
     3ICIENT OF CORRELATION = ',14X,F13.5)
  113 FORMAT(20X,2(10X,F8.2))
  114 FORMAT(1H1,20X,'G = ',I3)
      END
```

APPENDIX E

COMPUTER PROGRAM WHICH NUMERICALLY SOLVES EXPERIMENTAL DATA OF THE INITIAL CONCENTRATION PROFILE FOR GIVEN VALUE OF D AND TIME

APPENDIX E

```
C
C
C     THIS IS THE NUMERICAL TEST PROGRAM WHICH OPERATES ON THE
C     EXPERIMENTAL DATA OF RUN 227 USING THE THIN FILM SOLUTION
C
C     ABAR IS THE ZEIBOLD PARAMETER DETERMINED FROM INDEPENDANT
C     MEASUREMENTS OF THIN FILM STANDERDS
C
C     PUREI IS THE RAW INTENSITY OF THE PURE ELEMENT MEASURED
C     FROM THE MICROPROBE SPECTROMETER
C
C     ALY(I) IS THE RAW INTENSITY OF THE ALLOY THIN FILM MEASURED
C     DIRECTLY FROM THE MICROPROBE SPECTROMETER
C
C     BKGD1 IS THE BACKGROUND CORRECTION FOR THE PURE FILM
C
C     BKGD2 IS THE BACKGROUND CORRECTION FOR THE ALLOY FILM
C
C     ALDEN IS THE ALLOY DENSITY FOR THE SILVER - GOLD SYSTEM AND IS
C     COMPUTED ON THE BASIS OF AN ASSUMED LINEAR RELATIONSHIP BETWEEN
C     THE ALLOY DENSITY AND THE ATOMIC FRACTION OF THE PHASE SYSTEM
C
C     ATMFR IS THE ATOMIC FRACTION
C
C
C
      DIMENSION ALY(500),DIST(500),CONC(500),TCONC(500),CODELT(100),TCO
     1NC(100),IMAGE(1500),DIST1(100),TEST(100),NSCALE(5)
      REAL K,KA,KAA
      INTEGER W,RUN,Z,Y,O
      Y=0
      PI=3.14159
      DX=8.E-05
      NSCALE(1)=1
      NSCALE(2)=0
      NSCALE(3)=2
      NSCALE(4)=0
      NSCALE(5)=2
    1 READ(5,100) RUN,N,ABAR,BKGD1,BKGD2,PUREI,TIME,TEMP
      WRITE(6,101)
      WRITE(6,102) RUN,ABAR,BKGD1,BKGD2,PUREI,N,TIME,TEMP
      TIME=48.0
      DO 2 I=1,N
      READ(5,103) ALY(I)
    2 DIST(I)=0.04*FLOAT(I-1)
      E=PUREI-BKGD1
      I=1
      WRITE(6,104)
    9 D=ALY(I)-BKGD2
      IF(D .LE. 0.0) GO TO 3
      K=D/E
      IF(K.GE.1.0) GO TO 14
      KA = (1.0-K)/(1.+ABAR)
      KAA=1.0+KA
      C=1.0/KAA
      GO TO 4
    3 K=0.0
      C=0.0
      GO TO 4
   14 K=1.0
      C=1.0
    4 AG= C/1.0788
      AU=(1.-C)/1.97
      ATMFR=AG/(AG+AU)
      ALDEN=19.41G - (8.843*ATMFR)
```

```
      C0NC(I)=ALDEN+C
      WRITE(6,105) ALY(I),K,C,ATMFR,ALDEN,C0NC(I)
    5 T0C0NC(I)=C0NC(I)
    6 IF(I.EQ.N) G0 T0 8
      I=I+1
      G0 T0 9
    8 M=N-1
      D010 I=1,M
      C0DELT(I)=(T0C0NC(I)+T0C0NC(I+1))/2
   10 C0NTINUE
   99 DIFC=5.3E-11
   98 W=0
      RDT2=2.*SQRT(DIFC*3600.*TIME)
      DT4=DIFC*TIME*0.144E05
      R00TDT=SQRT(PI*DIFC*3600.*TIME)
      D0 12 Z=1,M
      SUM=0.0
      D013 L=1,M
      DELT=(FL0AT(Z)-FL0AT(L))*DX
      DELTSQ=DELT*DELT
      DIV=-(DELTSQ/DT4)
      E=EXP(DIV)
      PR0D=E*C0DELT(L)*DX
      SUM=SUM+PR0D
   13 C0NTINUE
      FUN=(FL0AT(Z-1)+DX)/RDT2
      TC0NC1=(2.12/2.)*ERFC(FUN)
      TC0NC2=SUM/(2.*R00TDT)
      TC0NC(Z)=TC0NC1+TC0NC2
      IF(TC0NC(Z).GT.1.56 0R.TC0NC(Z).LT.0.56) G0 T0 12
      W=W+1
      TEST(W)=TC0NC(Z)
      DIST1(W)=DIST(Z)
   12 C0NTINUE
      WRITE(6,106) DIFC
      WRITE(6,110) TIME
      CALL PL0T1(NSCALE,5,10,10,10)
      CALL PL0T2(IMAGE,1500,80.0,0.0,2.5,0.0)
      CALL PL0T3(1H*,DIST,TC0NC,Z)
      CALL PL0T4(42,42H                C0NCENTRATI0N IN GRAMS AG /CC)
      WRITE(6,109)
      Y=Y+1
      IF(Y.EQ.1) TIME=12.0
      IF(Y.EQ.2) ST0P
      DIFC=5.9E-11
      G0 T0 98
  100 F0RMAT(I5,I3,1X,6F10.5)
  101 F0RMAT(1H1,1X,'RUN N0.',5X,'ABAR = ',8X,'BKGD1 = ',7X,'BKGD2 = ',7
     1X,'PUPET = ',7X,'N = ',5X,'TIME = ',7X,'TEMP = ')
  102 F0RMAT(1H0,2X,I5,4X,F8.5,3(5X,F10.1),8X,I3,7X,F6.1,8X,F6.1)
  103 F0RMAT(F13.5)
  104 F0RMAT(1H0,4X,'ALL0Y INTENSITY',5X,'KAG',9X,'WT. FRACT.',7X,'AT0M
     1FRACT.',2X,'ALL0Y DENSITY',2X,'C0NCENTRATI0N')
  105 F0RMAT(6(5X,F10.5))
  106 F0RMAT(1H1,5X,'DIFFUSI0N C0EFFICIENT EQUALS ',1PE13.4)
  107 F0RMAT(5X,F10.5)
  108 F0RMAT(1H0,5X,'C0NCENTRATI0N'/5X,'   GRAMS/CC    ')
  109 F0RMAT(1H0,55X,'RELATIVE DISTANCE (MICR0NS)')
  110 F0RMAT(1H0,55X,'TIME = ',F4.1)
  111 F0RMAT(10X,F10.5,20X,F10.5)
  112 F0RMAT(1H0,5X,'TEST C0NCENTRATI0N',5X,'RELATIVE DISTANCE (MICR0NS)
     1')
  113 F0RMAT(1H0,20X,'SL0PE = ',35X,F13.5,//,21X,'INTERCEPT 0F C0NCENTRA
     1TI0N AXIS = ',09X,F13.5,//,21X,'STANDARD ERR0R 0F THE ESTIMATE = '
     2,10X,F13.5,//,21X,'STANDARD DEVIATI0N 0F Y = ',17X,F13.5,//,21X,'C
```

APPENDIX F

STATISTICAL RELATIONSHIPS USED IN THE PRESENT WORK

APPENDIX F

STATISTICAL RELATIONSHIPS USED IN THE PRESENT WORK

Consider curve of the type $Y = a_1X$. Assume that for the data point (Yi, Xi) each Yi is an observation from a normal population with a mean a_1 Xi and constant variance σ^2. Assuming that measurement of Y locates it within a small interval of extent ΔY, the probability of observing the value Yi is from the normal distribution:

$$S = \sum_{i=1}^{N} (Yi - a_1Xi)^2 \tag{36}$$

For S to be a minimum $\frac{\partial S}{\partial a_1} = 0$

$$\frac{\partial S}{\partial a_1} = - 2\Sigma YX + 2a_1\Sigma X^2 = 0$$

Therefore,

$$a_1 = \frac{\Sigma XY}{\Sigma X^2} \tag{37}$$

The variance about the regression line is estimated by the square of the standard error of the estimate

$$S^2_{YX} = \frac{\Sigma(Y - a_1X)^2}{N} = \frac{\Sigma Y^2 - a_1\Sigma YX}{N} \tag{38}$$

where N = the number of data points.

Lines drawn parallel to the regression line at vertical distance (Y) of $\pm S_{YX}$, $\pm 2S_{YX}$ and $\pm 3S_{YX}$ will enclose 68%, 95% and 99% of the data points. The value of S_{YX} gives a measure of the dispersion about the mean.

The coefficient of correlation is defined as

$$r = \left[1 - \frac{S_{YX}^2}{S_Y^2}\right]^{\frac{1}{2}} \tag{39}$$

where $$S_Y^2 = \frac{\Sigma Y^2}{N} - \left(\frac{\Sigma Y}{N}\right)^2$$

The coefficient of correlation is a confidence test on the linearity of the data. For example, if the coefficient of correlation equals 0.658 and 0.708 we can say with 98 and 99% certainty that there is linear correlation of the data.

If we consider a curve of the type $Y = a_0 + a_1X$, then following the procedures above we can derive the following relationships

$$a_0 = \frac{(\Sigma Y)(\Sigma X^2) - (\Sigma X)(\Sigma XY)}{N\Sigma X^2 - (\Sigma X)^2} \tag{40}$$

$$a_1 = \frac{N\Sigma XY - (\Sigma X)(\Sigma Y)}{N\Sigma X^2 - (\Sigma X)^2} \tag{41}$$

S_{YX}^2, the square of the standard error of the estimate equals

$$S_{YX}^2 = \frac{\Sigma Y^2 - a_0\Sigma Y - a_1\Sigma XY}{N} \tag{42}$$

The variance of slope, $$V = \left[\frac{S_{YX}^2}{\Sigma X^2 - \frac{(\Sigma X)^2}{N}} \right]^{\frac{1}{2}} \qquad (43)$$

The confidence band of the slope, say equal to b, is a fan shaped area converging on the mean value of X and Y with slopes $b \pm Vt$, where t is the probability level determined from an F test on the coefficient of correlation (equation 39).

VITA

VITA

The author was born in Elmira, New York on February 28, 1944. After several short moves, his family settled in Rochester, New York where he proceeded through his elementary and secondary education, graduating from Webster High School in June, 1961.

Upon graduation he entered the U. S. Navy. After completion of ET/A and ET/C schools, at Great Lakes Training Center, Great Lakes, Illinois, he was assigned as an Electronics Technician aboard the U.S.S. Hull (DD-945).

In June, 1965 he was selected for the NESEP program, and entered Purdue University in September of the same year. In January, 1970 he received his Bachelor of Science and Master of Science Degrees simultaneously, and thereupon was commissioned as an Ensign in the U. S. Navy.

The author married the former Sandy Lippa in September, 1962. They have three children, David, Sean and Katrice.

He is a member of the following honorary societies: Tau Beta Pi, Alpha Sigma Mu, Sigma Xi and Phi Kappa Phi. He is also a member of the American Society of Metals, the American Institute of Mining, Metallurgical and Petroleum Engineers, and the American Vacuum Society.

The author is a Third Degree Mason and a citizen of the United States of America.

Thesis
W2357 Watkins
A study of lateral diffusion in thin film couples of gold and silver.